Removal of PFOS using amphiphilic cyclodextrins coated onto polypropylene

Thomas Sandberg Nielsen

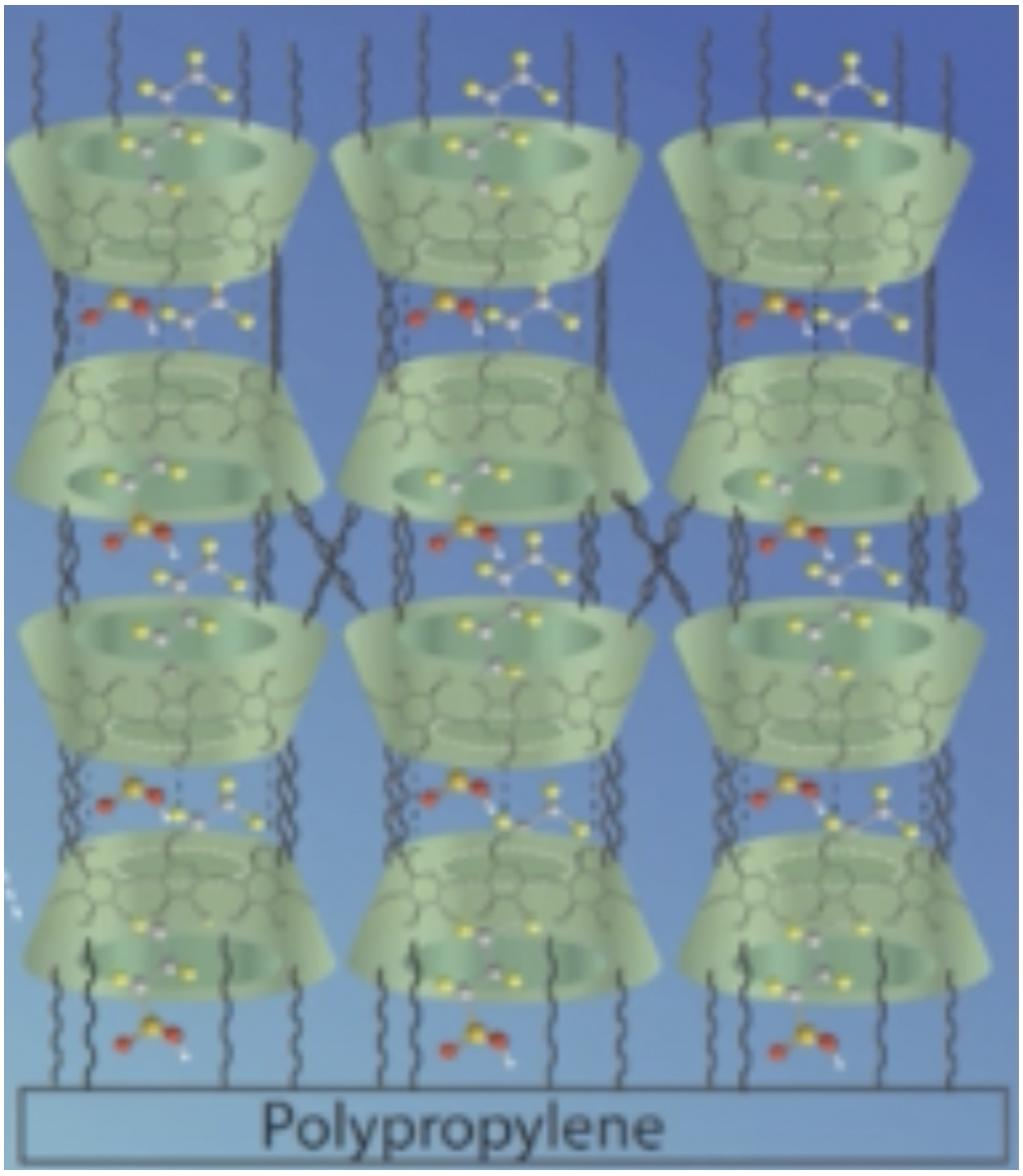

Chemistry Civil Engineer
Aalborg University
2. Juni 2025

Front page picture:[1]

AALBORG UNIVERSITY
STUDENT REPORT

The Faculty of Engineering and Science
Fibigerstræde 16
9220 Aalborg Øst
Denmark
https://www.engineering.aau.dk

Title:
Removal of PFOS using amphiphilic cyclodextrins coated onto polypropylene

Project period:

September 2024 - June 2025

Student:

Thomas Sandberg Nielsen

Supervisors:

Thorbjørn Terndrup Nielsen
Kasper Skovbølling Hedegaard

Page number: 108
Appendix: 8
Finished 02-06-2025

Abstract:

This project investigates the coating of amphiphilic cyclodextrins onto polyproypelene with the aim of removing PFOS from water. A series of ACDs with varying degrees of substitution were synthesised and characterised.
The effect of ethanol/water (E/W) ratios on coating behavior was examined, revealing that particle formation, and the transition from suspension to solution changed with increasing DS. Dynamic light scattering showed that more substituted ACDs solutions at higher ethanol concentrations, indicating increased hydrophobicity.
Contact angle measurements demonstrated that ACD coatings reduced the hydrophobicity of PP surfaces, with lower DS ACDs yielding more hydrophilic surfaces. An adsorption experiment using bisphenol A, confirmed the ability of the ACD-coated surfaces to participate in host–guest interactions, with uptake capacity increasing with DS. A PFOS removal experiment further validated the adsorption capacity of the coated PP sheets
^{1}H-NMR analysis was used to calculate the amount of coating and indicated differences in the amount of coating depending on the areal densitites of the PP sheets
The results suggest that ACD-coated PP sheets offer a promosing prospects for removal of PFAS.

Preface

This master thesis was written by Thomas Sandberg Nielsen at Section of Chemistry, the Department of Chemistry and Bioscience, Aalborg University.

I would like to thank the following persons:

Kasper Skovbølling Hedegaard, for supervision and practical help in the laboratory

Thorbjørn Terndrup Nielsen, for supervision

Peter Kjær Kristensen, for assistance during the coat examination with a SEM

Readers guide
The source references are numbered in order and are collected in a bibliography at the end of the report. The bibliography lists books with author, title, and publisher, while internet sources are listed with author, title, URL, and date visited. Figures, tables, and equations are numbered according to the respective chapter, for example, the first figure in chapter 3 has the number 3.1, the second figure number 3.2, and so on. Figure and table captions are found below and above their respective figures and tables respectively.

Thomas Sandberg Nielsen

tsni19@student.aau.dk

Abbreviation

Abbreviation	Description
ACD	Amphiphilic cyclodextrin
ACD1	ACD with DS of 3.1
ACD2	ACD with DS of 3.6
ACD3	ACD with DS of 4.9
ACD3.6	ACD with DS of 5.9
ACD3.1	ACD with DS of 6.6
AUC	Area under the curve
BPA	Bisphenol A
CD	Cyclodextrin
DLS	Dynamic light scattering
DS	Average degree of substitution
E/W	Ethanol/water ratio
FT-IR	Fourier-transform infrared spectroscopy
HCl	Hydrochloric acid
MALDI-TOF MS	Matrix-Assisted Laser Desorption/Ionization Time-of-Flight Mass Spectrometry
MS	Mass spectrometry
NaCl	Sodium chloride
PDI	Polydispersity index
PFAS	Per- and polyfluoroalkyl substances
PFOS	Perfluorooctanesulfonic acid
PP	Polypropylene
SEM	Scanning electron microscopy
TP	Transition point
UV	Ultraviolet

Table 0.1. List of abbreviations used in this thesis.

Contents

Introduction and problem analysis 1

Efficient removal of organic pollutants, which pose significant environmental and health risks, has long been a subject of interest. Among these pollutants are per- and polyfluoroalkyl substances (PFAS) which is a group of synthetic compounds composed of carbon chains linked to flourine atoms and a polar functional group with perfluorooctanesulfonic acid (PFOS) and perfluorooctanoic acid (PFOA) being the most invesigated of the fluorinated substances. They have been widely used in applications such as firefighting foams, non-stick cookware, and food packaging due to their thermal and chemical properties such as resistance to oil and water [2]. However, these properties are associated with environmental challenges and have also been linked to adverse health effects, even in very low concentrations 3. This is mainly due to the characteristic carbone fluorine bonds present in the structure which render the molecules persistent, bioacummulative, toxic and mobile [4]. Hence, degradation of PFAS is challenging and their release into groundwater and soil form wastewater treatment plants and industrial discharge is a major concern [5].

Several methods have been investigated to address this emerging issue such as advanced oxidation, reverse osmosis and filtration. However, these techniques result in low water recovery while demanding high energy input and high operational costs. Another method that has shown more efficient removal of PFAS is adsorption. The advantages of this process include its simple setup, ease of operation, and cost-effectiveness. Among these, activated carbon and ion exchange resins are the most widely used. A major disadvantage of the first method is the limited anion exchange capacity which significantly reduces its usability for adsorption of PFAS while the latter has shown less adequate removal of short-chain PFAS and slow adsorption kinetics [4].

An adsorbent that has displayed fast and high uptake capacity with respect to PFAS removal, are cyclodextrins (CDs). These compounds consist of a ring structure with a hydrophobic inside which is capable of encapsulating the PFAS molecules of the right size or at least parts of it through hydrophobic interactions [2]. The CDs can also be chemically modified to allow for other interactions such as electrostatic interactions between the PFAS molecules and the CDs [6].

To efficiently remove PFAS from groundwater, soil and other sources, it is crucial to understand the chemical nature of the cyclodextrins.

1.1 Cyclodextrins

CDs are cyclic oligosaccharides derived of glucose units that are connected by α-/(1,4) glycosidic linkages with the most abundant CDs being α-, β- and γ-CD consisting of six, seven and eight units, respectively[7]. The configuration of the CDs are shown in Figure 1.3.

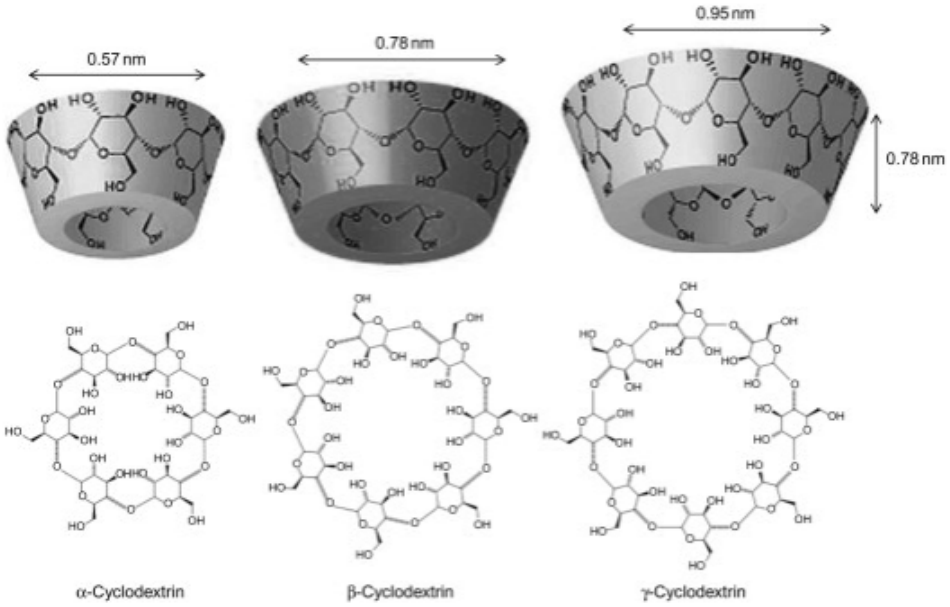

Figure 1.1. Structures of α, β, and γ-cyclodextrin and their dimensions. The image has been edited from[8].

The structure of CDs resemble a truncated cone with primary hydroxyl groups located at C-2 and C-3 on the narrow rim and secondary hydroxyl groups located at C-6 on the wide rim. The primary hydroxyl groups are relative flexible compared to the secondary hydroxyl groups resulting in a hydrophilic exterior and hydrophobic interior due to the abundance of C-atoms and glycosidic oxygen bonds in the cavity.

Due to the hydrophobic cavity, a CD is capable of forming inclusion complexes with hydrophobic molecules of the right size. This is denoted as a host-guest complex with the CD being the host and the molecule being the guest. Through this encapsulation the solubility of the hydrophobic molecule is increased, hence stabilising the guest compound [9].

The complexation phenomena is characteristic of each of these CDs with β- CD being the most commonly used CD due to its accessible and low price despite its low water solubility which is attributed to intramolecular hydrogen bonding.

Upon this interaction, an equilibrium is established between the inclusion complex and dissociation of these compounds. The shift of the equilibrium towards the complexation depends on several thermodynamic properties [10] Prior to encapsulation of hydrophobic molecules, multiple steps take place as shown in Figure. The overall complexation is shown

in Figure 1.2

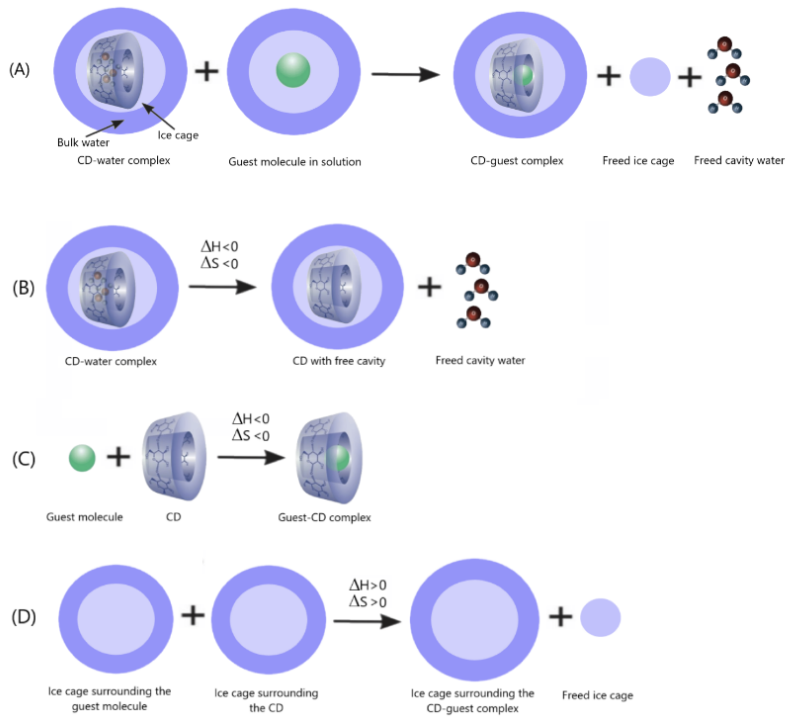

Figure 1.2. Overview of the complexation process (A) and the individual mechanisms, including release of water from the cavity (B), the inclusion complex formation (C), and shrinkage of the ice cage (D). The image has been edited from[11].

The first step is the desolvation of cavity, as illustrated in Figure B. Water molecules inside the cavity interact via hydrogen bonding with adjacent water molecules and with hydroxyl groups on the rim. Another contribution involves van der Waals interactions between the water and the CDs carbon atoms but this occur to a lesser extent. The water molecules present in the cavity are at a higher energy state and thus less favourable compared to the hydrogen bond network of the bulk water. This causes the water to be released to the bulk water which results in a higher degree of hydrogen bonding and thereby a decrease in enthalpy. The release of these water molecules to the bulk water is a crucial driving force for complex formation. With respect to the entropy, this process is unfavourable due to the water in the cavity has a lower degree of rotational freedom and hence higher entropy compared to the bulk water [7] [12].

In the following step, the freed cavity enables the hydrophobic molecule surrounded by an unfavorable aqueous medium to be included in the CD, as depicted in Figure C. This interaction results in the formation of favourable intermolecular bonds during the host-guest inclusion complex hence a lowering of the enthalpy. However, the formed complex contributes to a more confined structure leading to a lower degree of freedom which lowers the entropy [12].

Furthermore, the guest is also desolvated prior to complexation. The water molecules tend to increase the interaction between themselves whereas the guest molecules tend to

minimize their contact with water. This leads to aggregation of the hydrophobic molecules lowering the surface area of the guests. The water molecules residing in the cavity is also affected by this effect causing their release due to the unfavourable interaction with the hydrophobic cavity compared to the bulk water. This behaviour of the molecules is described as the hydrophobic effect [13].

Another term that is associated with the hydrophobic effect is the formation of an ice cage. This aspect is more specific for this effect and involves the presence of water bonding to itself around the guest, the host and the complex in a structure resembling ice hence the name. The complexation results in a lower surface area requiring fewer water molecules to form the ice cage relative to the amount of water around the separate host and guest. As a consequence of the complexation process, water molecules are being freed to the bulk water from the newly formed ice cage which yields fewer tightly bound water molecules resulting in a positive enthalpy. This is compensated by an increase in entropy due to a higher degree of orientational freedom making this part of the complex formation favourable [14] [15].

To summarize, whether the complexation is thermodynamically favourbale depends on the value of the Gibbs free energy. The enthalpy is negative for the release of water from the cavity and the interaction between the host and the guest making this process favourable and enthalpy driven. Although, as the ice cage shrinks during this interaction, the enthalpy increases due to a lower degree of hydrogen bonding.

During the complexation, the entropy is to some extent also favourably since the hydrophobic effects results in fewer hydrogens bond and a higher degree of freedom of the water molecules due to a smaller ice cage around the complex. However, this process is hindered due to the restricted movement of the guest in the cavity and the lower orientational freedom of ejected water molecules from the cavity resulting in a negative entropy.

Though native CDs possess the ability to form inclusion complexes, modification of the CDs to alter their properties for a wide range of applications is often desired which is known as amphiphilic cyclodextrins (ACDs) CDs are obtained by grafting alkyl chains onto the primary, secondary or both rims which is denoted as amphiphilic cyclodextrins (ACDs).

1.1.1 Amphiphlic cyclodextrins

Synthesis of ACDs are mainly obtained by grafting alkyl chains onto the primary, secondary or both hydroxyl groups. The aim of this modification is to enhance the affinity between the CD derivatives and the hydrophobic molecules by adding extra space for hydrophobic interactions which depends on the location, length and number of substituents. Another advantage of ACDs is their ability to self-assemble into nanoparticles in aquoues solutions without the presence of surfactants. Through this process, the CDs still retain their ability to form inclusion complexes which is especially utilized for pharmaceutical applications

such as drug delivery [16].

Configuration of ACDs can result in various structures. Some of these structures are depicted in Figure 1.3

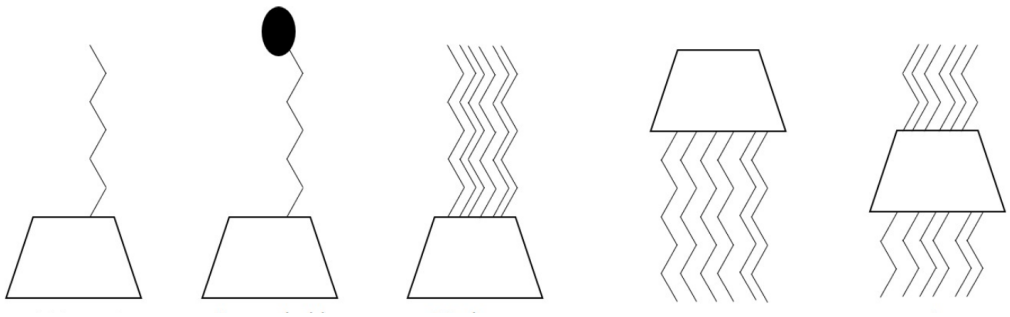

Figure 1.3. Illustration of five types of ACDs. From left to right: lollipop, cup-and-ball, medusa-like, skirt-like and bouquet-shaped. [17]

.

The two first ACDs are the lollipop and cup-and-ball structures which are monosubstituted on the primary hydroxyl groups. The first ACD is grafted with a single alkyl chain that is prone to intramolecular inclusion with the cavity, hence the term intramolecular self-assembly. The latter ACD has a bulky group attached to the end of the alkyl chain which prevents the self-inclusion. The third and fourth structures are fully substituted with respect to the primary hydroxyl groups for the medusa-like ACD and secondary hydroxyl groups for the skirt-like ACD, respectively. Lastly, the bouquet-shaped ACD is polysubstituted with respect to both rims [17] [18]. Synthesizing the described ACDs requires different pathways, each with specific conditions. Of these, modification of the primary hydroxyl groups is the least complex synthetis route. Besides ACDs use in pharmaceutical formulations, functionalization of surfaces with ACDs is of interest.

In general, two methods can be used to attach ACDs to solid surfaces, which are covalent and non-covalent functionalization. Covalent linkage offers a stable and more durable interaction due to the formation of covalent bonds. However, this technique requires advanced equipment, use of harsh organic solvents and the process is generally quite costly [19]. On the other hand, non-covalent functionalization of surfaces is much weaker, largely due to van der Waals interactions, but the process is simpler, faster and cheaper.

One study has shown the prospect of non-covalently modifying the surface of polymeric materials such as polypropylene (PP) and polyurethane with ACDs leading to self-assembled layers of ACDs on the surface [20]. ACDs were synthesized with a varying number of substituents at different locations and the material in question was coated with ACDs by dipping the material in a coat mixture with different concentrations of ethanol and water for a few seconds. The coated material rendered more hydrophilic and was proven to be relatively stable when in contact with water.

With this acquired feature of the materials, it is feasible to investigate their possible applications such as water treatment due to the intrinsic ability of CDs to form inclusion

complexes. For this purpose, another study by the same authors used the synthesized ACDs as mentioned in [**?**] to coat PP with the aim of removing volatile organic compounds such as benzene and toluene which showed high efficiency in the removal of these compounds [21].

As previously mentioned, the presence of PFAS in the environment is a major concern. Given the promising potential of surface functionalization with ACDs, investigating this approach for PFAS removal is of great interest.

The aim of this project is to remove PFOS using ACDs coated onto PP. The litterature has shown promising results with regards to remove PFOS using ACDs. Hence, the removal of PFOS will be tested

In advance to this, a range of experiments will be conducted such as DLS measurements, contact angle measurements, determination of coat amount and morphological assesment of the coat formation using SEM

This has led to the following problem statement:

Does amphiphilic cyclodextrins coated onto polypropylene remove PFOS to a considerable higher degree than non-coated PP? And if, does the degree of substitution affect the uptake capacity of the amphiphilic cyclodextrins?

Experimental contemplations 2

In the following section, the experiments to be conducted will be considered based on the knowledge of coating surfaces with ACDs and the complexation between coated materials and hydrophobic molecules.

2.1 Synthesis and characterisation of amphiphilic cyclodextrins

In order to obtain a sufficient coating on a hydrophobic surface, and thereby achieve a high uptake of PFOS, the synthesis route of the ACDs is considered. As previously reported, the coating of esterified ACDs with varying DS was effective in removing pollutants from water [21].

Therefore, randomly substituted ACDs with a fixed carbon chain and varying DS will be synthesised through an esterification between β-CD and octanoyl with pyridine acting as a solvent, base and nucleophilic catalyst. The overall reaction for this process is shown in Figure **??**

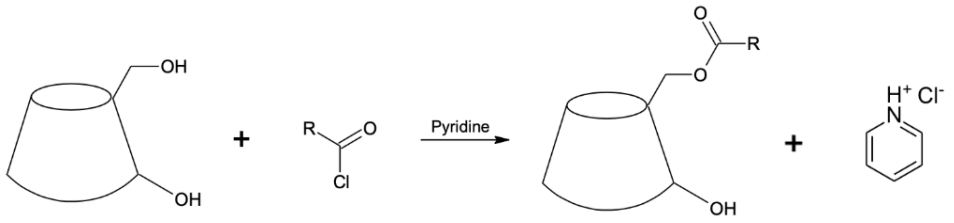

Figure 2.1. Reaction scheme for the esterification of ACDs. The CD and ACD are represented by the truncated cone. The acyl chloride corresponds to octanoyl chloride, hence R is a carbon chain of 8 carbon atoms
. Modified from [22]

Several reaction mechanisms are involved in the synthesis of ACDs. The different steps are displayed in Figure 2.2

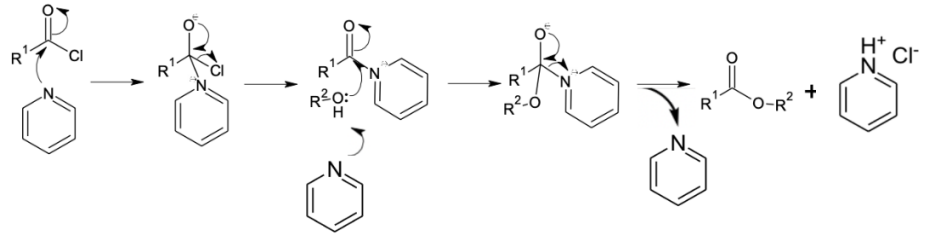

Figure 2.2. Reaction mechanisms for the esterification of ACDs. Modified from [22]

.

In the first step, pyridine acts as a nucleophile by attacking the electrophilic carbonyl carbon of octanoyl chloride, forming a tetrahedral intermediate. Subsequently, the chloride ion is expelled as a leaving group which restores the carbonyl double bond and results in a trigonal intermediate.

A hydroxyl group from the CD, most likely from the primary rim due to less steric hindrance, then reacts with the intermediate. This attack leads to the release of pyridine, while the hydrogen atom from the hydroxyl group is deprotonated by another pyridine molecule, forming pyridinium as a byproduct and enabling the formation of an ester bond characteristic of ACDs

Lastly, pyridinium neutralises the released Cl-atom by creating pyridinium chloride.

The reaction mixture is then poured into a diluted HCl solution which protonates residual pyridine molecules to form pyridinium chloride in solution. The ACDs are then precipitated and collected by filtration of the aqueous phase.

Finally, purification of the product is obtained by dissolving the solid in ethanol followed by addition of a NaCl solution to the organic phase. This causes the synthesized product to precipitate out of the mixture while remaining salts and other soluble byproducts are removed by filtration.

To validate whether the desired ACDs have been synthesized, ^{1}H nuclear magnetic resonance (NMR) and mass spectrometry (MS) will be used to characterize the obtained products.

2.2 Coating behaviour of amphiphilic cyclodextrins

Parameters affecting the coating amount and uptake capacity of the coat have been investigated by Lumholdt [23], where the composition of the coating mixture was shown to influence the coatability of ACDs. It was found that the ethanol concentration significantly impacts coat formation, depending on the specific ACD used. Characteristics of the ACDs such as the number of substituents, alkyl chain length, and degree of substitution (DS), also affect the coat amount.

To understand how the coating mixture influences the ability to coat, the formation of

nanoparticles at different ethanol/water ratios (E/W) was investigated. E/W ratios were observed to be suspensions until a certain concentration of ethanol was reached in which ACDs were in solution. This transition from suspension to solution is referred to as the transition point (TP) and the higher the DS of the ACD in question, the higher ethanol concentration is required to dissolve the ACDs.

In general, the size of the nanoparticles increased as the suspensions approached TP after which the ACDs were in solution. Initially, large unstable particles were believed to be the driving force for the coat formation. However, the most efficient coating in terms of uptake capacity was obtained by using a suspension containing smaller stable particles, as found by Lumholdt [23].

Based on this knowledge, the behaviour of ACDs in different E/W ratios will be investigated by measuring the transmittance of the coating mixtures to indicate when the ACDs transition from suspensions to solutions. Subsequently, DLS will be used to examine the particle sizes and the polydispersity index (PDI) of ACDs in suspension. In alignment with Lumholdt [23], an ACD concentration of 1 mg/mL in the coating mixture was initially prepared.

A hypothesis for the configuration of the coat has been proposed by Lumholdt [23], in which ACDs form mulitlayers on hydrophobic surfaces. It is suggested that a channel-like structure is formed that elongates the cavities with an orientation of alkyl chains away from the cavities stabilised by van der Waals forces and hydrophobic interactions between the alkyl chains and hydrogen bonds between the hydroxyl groups. Lumholdt, [23] also found that the hydrophobicity of the PP surface rendered more hydrophilic by coating with ACDs.

The less substituted the ACDs were, the more hydrophilic the surface became which could be due to the coat configuration. In this project, the ability of ACDs to reduce the hydrophobicity of a surface is determined by measuring the contact angle of water droplets on coated PP sheets.

Untreated isotactic PP were kindly provided by Fibertex A/S and is used as a support material due to its hydrophobic nature, inertness and high surface area. For the experiments, PP are cut into suitable pieces followed by a washing step with a mixture of hot ethanol and DMSO to remove any contaminants and manufacturing residues. The sheets are then dried, dipped into a prepared coating mixture and dried again Lastly, the sheets are washed with water to remove any residual ethanol and then dried. In the adsorption experiments, PP sheets will be weighed after coating.

Furthermore, the coating amount will be quantified by ^{1}H-NMR by using maleic acid in DMSO-d6 as an internal standard as this chemical have one distinctive signal that does not interfere with the ACD signals [24]. For this purpose, PP sheets will be weighed prior to coating.

The morphology of the ACD coat formation is also of interest and will be examined using

scanning electron microscopy (SEM)

2.3 Preliminary investigation of uptake capacity using bisphenol A

When working with PFOS, strict safety precautions are recommended due to its toxicity as described earlier, thus a different molecule was used at first to evaluate the ability of coated ACDs to form inclusion complexes. Therefore, bisphenol A (BPA) in solution is selected as a model compound to investigate possible adsorption via interaction with the ACD coat. BPA is a synthetic aromatic compound that is primarily used in the manufacturing of plastics and is regarded a pollutant because of its widespread presence in the environment [25]. The structure of BPA can be seen in Figure 12

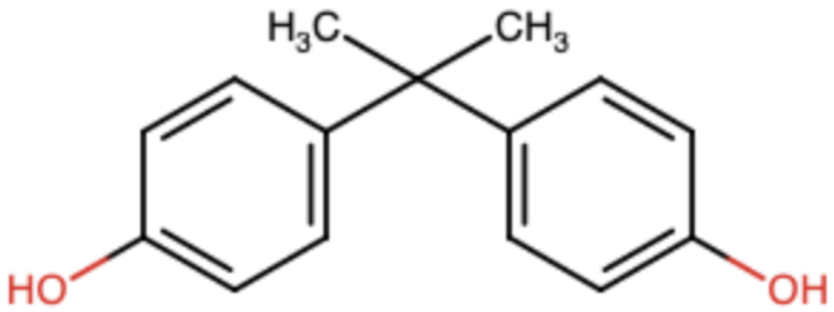

Figure 2.3. Molecular structure of BPA

.

A standard curve of BPA is to be prepared and a simple static adsorption kinetics experiment is performed to indicate if an equilibrium concentration is reached for BPA in solution. Due to BPA being an aromatic compound, the removal capacity was determined via HPLC with a UV-Vis detector [26].

2.4 Adsorption of PFOS using ACD-coated polypropylene

It is chosen to examine PFOS as an adsorbate due to its widespread occurrence in the environment. PFOS exhibits an amphiphilic character due to its hydrophobic perfluorinated carbon chain and hydrophilic sulfonic acid functional group. However, in aqueous medium the acid is deprotonated yielding a sulfonate ion due to the low pK_a at -3 [27]. The structure of PFOS can be seen in Figure 2.4

Figure 2.4. Molecular structure of PFOS in aqueous solution.

As stated by Lumholdt [23], the uptake capacity is believed to be a combination of the elongated ACD cavity and non-specific adsorption sites from the alkyl chains through hydrophobic interactions. The PFOS molecules are therefore thought to be adsorbed through these mechanisms. Furthermore, it is plausible that the sulfonate group can interact with the hydroxyl groups of the ACD through electrostatic interactions

In alignment with the adsorption experiment of BPA, a standard curve of PFOS is prepared and the coated PP sheets are exposed to the PFOS solution to determine removal efficiency. The amount of removed PFOS will be analysed via HPLC with a conductivity detector.

Materials and Methods 3

In this section, the experimental methods as well as the chemicals and instruments used in this project will be presented. The methods include the synthesis and characterization of the ACDs, investigation of the ACDs behaviour in different E/W ratios, coating procedure of the PP sheets, contact angle measurements of coated PP sheets, a performance study with BPA, determination of the coating amount, morphological analysis of the coat and a static adsorption experiment for the removal of PFOS using ACD-coated PP sheets.

3.1 Chemicals

The chemicals used for the synthesis of the ACDs and all subsequent experiments, are detailed in Table 3.1

Table 3.1. List of the chemicals used

Chemicals	CAS-number	Supplier
α-cyano-4-hydroxycinnamic acid (CCA)	28166-41-8	Sigma-Aldrich
β-cyclodextrin	7585-39-9	Wacker Chmie AG
Acetonitrile	75-05-8	Fluka
Bisphenol A (BPA)	80-05-7	Sigma-Aldrich
Boric acid	10043-35-3	Sigma-Aldrich
Dimethyl sulfoxide (DMSO) $\geq$ 99%	67-68-5	Sigma-Aldrich
Dimethyl sulfoxide-d6 (DMSO-d6) $\geq$ 99%	2206-27-1	Sigma-Aldrich
Ethanol (96%)	64-17-5	VWR Chemicals
Hydrochloric acid (37% w/w)	7647-01-0	Sigma-Aldrich
Maleic acid	110-16-7	Sigma-Aldrich
Nitrocellulose (NC)	9004-70-0	Bio-Rad
Octanoyl chloride	111-64-8	Sigma-Aldrich
Perfluorooctanesulfonic acid (PFOS)	1763-23-1	Sigma-Aldrich
Pyridine $\geq$ 99%	110-86-1	VWR Chemicals
Sodium chloride	7647-14-5	VWR Chemicals
Sodium hydroxide	1310-73-2	VWR Chemicals
Sulfuric acid	7664-93-9	VWR Chemicals
Trifluoroacetic acid (TFA)	76-05-1	Fluka

3.2 Synthesis of amphiphilic β-cyclodextrins

In this project, six randomly substituted ACD derivatives with a chain length of 8 carbon atoms and desired DS of 3, 4, 5, 6, 7, and 8 were synthesized.

At first, β-cyclodextrin was dried in a vacuum bell at 110 C overnight and molecular sieves were dried in a muffle furnace at 300 C overnight. The molecular sieves were then added to pyridine to dehydrate the liquid overnight

10 g of β-cyclodextrin was added to 200 mL pyridine and dissolved in a round bottom flask under stirring at 400 rpm. A fixed volume of octanoyl chloride was then poured into the solution dropwise via a syringe with a needle. The mixture was left to react for 24 hours under stirring.

Afterwards, the solution was added to 2M HCl with a volume of 2L in a beaker under stirring and subsequently transferred to a ceramic filter connected to a filtration flask to precipitate the product using a vacuum pump. The product was dried under vacuum at 50 C overnight.

The obtained product was then dissolved in 96 % ethanol at 60 C under stirring. The ethanol solution was then poured gradually into a fixed volume of a 1M NaCl solution to purify the product. The product was dried under vacuum at 70 C overnight

This procedure was repeated six times by varying the molar ratio of octanoyl chloride and β-CD to obtain randomly substituted ACDs with target DS of 3, 4, 5, 6, 7, and 8, respectively. The volume of octanoyl chloride, ethanol, the NaCl solution and the theoretical mass of ACDs are presented in Table 3.3

Table 3.2. Overview of the desired DS, volume of octanoyl chloride, 96% ethanol, 1 M NaCl solution and theoretical mass of ACDs.

DS	C8COCl [mL]	96% EtOH [mL]	1 M NaCl solution [mL]	Theoretical mass of ACDs [g/mol]
3	4,5	133	1330	13,3
4	6	144	1440	14,4
5	7,5	156	1560	15,6
6	9	167	1670	16,7
7	10.5	178	1780	17,8
8	12	189	1890	18,9

3.3 Nuclear Magnetic Resonance

To characterise the obtained products, ^{1}H-NMR was performed on all synthesised ACDs. 20 mg of each ACD were dissolved in 550 L DMSO-d6 and ^{1}H-NMR spectra of the ACD derivatives were recorded on a Bruker DRX600 spectrometer with a 5 mm CPP-TXI probe at 600 MHz (Bruker Daltonik, Germany). Bruker Topspin 3.6.3 was used to process the ^{1}H-NMR data.

3.4 Mass Spectromety

Matrix-assisted laser desorption/ionization time of flight mass spectrometry (MALDI-TOF MS) was performed to characterise the ACDs using a Reflex III mass spectrometer (Bruker Daltonics, Bremen, Germany). For sample preparation, the double layer method was used consisting of a nitro-cellulose (NC) and α-cyano-4-hydroxycinnamic (CCA) matrix. A thin layer of freshly prepared 1:4 (v/v) mixture of NC and saturated CCA in acetone was deposited on a MALDI target plate and allowed to dry. 3 mg of each ACD was then dissolved in 10 mL 96% ethanol and deposited directly onto the target plate by adding a 1 μL droplet of a 1:1 solution of ACD and saturated CCA in aqueous solution of 2:1 (v/v) 0.1% trifluoroacetic acid and 80% acetonitrile.

3.5 Investigating the behaviour of ACDs in different concentrations of ethanol

A stock solution of 5 mg/mL was prepared for all ACDs by gently adding 50 mg to a volumetric flask containing 10 mL of 96% ethanol and dissolving it under heating. E/W ratios of the ACDs ranging from 10/90 to 90/10 with an interval of 10 percentage points were then made in the following order: 1.5 μL of the stock solution was poured into a HPLC vial and the appropriate amount of ethanol and water was subsequently added to yield a final concentration of 0.5 mg/mL. The amount of ethanol and water used for the E/W ratios can be seen in Table 3.3

Table 3.3. Volumes of ACD stock solution, 96% ethanol and demineralised water used for investigation of the coating behvaiour

ACD stock solution [μL]	96% ethanol [μL]	Demineralised water [μL]
1.5	7.5	1345
1.5	165	1185
1.5	325	1030
1.5	470	885
1.5	630	720
1.5	790	560
1.5	945	405
1.5	1105	250
1.5	1260	90

Each ACD in different E/W ratios was transferred to a disposable Sarstedt polysterol/polysterene cuvette (10 x 4 x 45 mm) for transmittance measurements using a Varian 50 Bio UV-Visible spectrophotometer at a wavelength of 600 nm. Demineralised water was used as a reference.

DLS was used to measure the particle size and polydispersity index (PDI) of all ACDs across E/W ratios until each ACD reached the TP. Measurements were performed using a Malvern Zetasizer Nano ZS, with a calibration time of 120 seconds. The temperature was set to 22C, and measurements were performed at a backscatter angle of 173. For each

ACD, one measurement was taken consisting of 10 runs with a duration of 10 seconds per run. The cell used was a quartz cuvette.

3.6 Coating of polypropylene sheets with amphiphilic cyclodextrins

PP with three different areal densities at 5, 10 and 20 g/m^2 were cut into suitable sizes depending on the experiment. The PP sheets were washed in a mixture of 96% ethanol and DMSO (80:20, v/v) to remove impurities, then dried overnight on crystallization dishes.

A stock solution of ACDs at 5 mg/mL was prepared as described earlier. A fixed volume of the stock solution was transferred to a beaker followed by addition of 96% ethanol and demineralized water in volumes specific to each ACD to obtain a coating mixture with a final ACD concentration of 0.5 mg/mL. The E/W ratios of the coating mixtures correspond to the final suspension (before TP) for all ACDs. The specific E/W ratios before TP for each ACD are listed in Table **??**

The PP sheets were dipped into the coating mixture for approximately 10 seconds and left to dry overnight on crystallization dishes. Lastly, the coated sheets were washed with demineralised water and dried overnight on crystallization dishes. A reference sheet of non-coated PP was washed in the same ethanol and DMSO mixture, dried overnight on crystallization dishes, then washed with demineralised water and dried overnight again on crystallization dishes.

For adsorption experiments, PP sheets were weighed after coating. Furthermore, the PP sheets used in the process for determination of the coating amount via ^{1}H-NMR, were weighed before coating. This approach was used to coat PP sheets in all experiments and is referred to as the standard procedure.

Table 3.4. Overview of E/W ratios used in the coating mixtures before TP and the TP values for each ACD

ACD	E/W ratio before TP	TP
ACD1	60/40	60/70
ACD2	60/40	60/70
ACD3	60/40	60/70
ACD4	70/30	70/80
ACD5	70/30	70/80

3.7 Contact angle measurements

PP with areal densities of 5, 10, and 20g/m^2 were cut into 1.5 cm x 1.5 cm sheets and coated with each ACD using 2mL of stock solution, following the standard procedure. A non-coated sheet was used as a reference and the experiment was done in triplicate. The hydrophobicity of the samples was examined by measuring the contact angle using a Biolin Scientific Attension Theta Lite optical tensiometer. A demineralised water droplet of 4μL

was gently placed on each sample and an image was recorded immediately after contact. The image recording settings were 30.0 s at 1% (2 FPS) and the water temperature was set to 20 °C.

3.8 Scanning Electron Microscopy

PP with an areal density of 20 g/m^2 was cut into three 1 cm x 1 cm sheets and coated separately with ACD1 and ACD4 using 2 mL of stock solution, following the standard procedure. A non-coated sheet was used as a reference. SEM was performed by coating the samples with sputtering gold from an Edwards sputter coater S150B and examined on a Zeiss Evo 60 SEM.

3.9 Quantification of the amount of coating

PP with areal densities of 5, 10, and 20 g/m^2 were cut into 3 cm x 3 cm sheets and coated separately with ACD1 and ACD4 using 4 mL of stock solution, following the standard procedure. The experiment was done in duplicate. The samples were transferred to HPLC vials, and 700 μL of DMSO-d6 containing 0.01 mg/mL maleic acid was added. The coating was dissolved using a heat gun. The amount of coating on each sample was quantified by ^{1}H-NMR, using maleic acid in DMSO- d6 as an internal standard, on a Bruker DRX600 spectrometer with a 5 mm CPP-TXI probe at 600 MHz (Bruker Daltonik, Germany). Bruker Topspin 3.6.3 was used to process the ^{1}H-NMR data

3.10 Perfomance study with bisphenol A

The three areal densities of PP were cut into 12 x 15 cm sheets and coated with all ACDs using 4 mL of stock solution, following the standard procedure. A BPA solution with a volume of 250 mL at approximately 1.2 mg/L was prepared by diluting a stock solution of approximately 37.5 mg/L BPA. In addition, a standard curve of BPA was prepared, which can be found in Appendix X.

At first, an adsorption kinetics experiment was performed for the coated PP sheets with an areal density of 20 g/m^2 The coated PP sheets were placed in 50 mL centrifuge tubes and 30 mL of BPA solution was added to tubes. Samples were taken after 2 and 30 minutes, 1 hour, and 2 hours by transferring approximately 1.5 mL of BPA solution into HPLC vials for analysis. The initial concentration of BPA and a reference of non-coated PP were also analysed. This approach was done in triplicate for the first three time slots.

PP sheets with areal densities of 5 and 10g/m^2 were coated with ACD1 and ACD6 using the standard procedure. The adsorption experiments for these densities were conducted similarly, but samples were only taken after 1 hour. A non-coated PP sheet was used as reference and each experiment was performed in triplicate.

Quantification of BPA was performed via a HPLC system configuration which included a Dionex P680 HPLC Pump, Dionex UVD170U, Diode Array Detector and Dionex ASI-100 Autosampler. The column was a Kinetex 5 microm EVO C18 100Å (150 x 4.6 mm). The eluent consisted of 40% acetonitrile and 60% water, the flow rate was 1 mL/min, the runtime 7 minutes, the injection volume 100 μL and the detection wavelength 230 nm.

3.11 Removal of PFOS using polypropylene sheets coated with amphiphilic cyclodextrins

PP with an areal density of 20 g/m^2 were cut into 12 x 15 cm sheets and coated with all ACDs using 4 mL of stock solution, following the standard procedure.

An already prepared PFOS solution with an initial concentration at approximately 0.002 mM was used for the experiment and a standard curve was already prepared. The standard curve can be found in Appendix X. A static adsorption experiment was conducted by placing each coated PP sheet in a 50 mL centrifuge tube and 30 mL of PFOS solution was poured into the tube. After 1 hour, a sample of approximately 1.5 mL PFOS solution was transferred to a HPLC vial for analysis. A non-coated PP sheet was used as reference, and the initial concentration of PFOS was also analysed. All samples were done in triplicate.

For quantification of PFOS, the HPLC system configuration included a Dionex ICS-6000 DP pump, Dionex ACRS 500 suppressor, Dionex AS-AP Autosampler and a ThermoScientific Conductivity detector. An Acclaim PA2 C18 analytical column (2.1 x 150 mm) was used. The mobile phase was an eluent consisting of 20 mM boric acid, 32% acetonitrile and pH adjusted to 8 with 100 mM NaOH. A flow rate at 0.2 mL/min, injection volume of 100 μL, column temperature at 30 °C, regenerant solution of 10 mM H2SO4 and regenerant flow at 1.3 mL/min were used.

Results and discussion 4

In this section, the results from the experiments will be presented and discussed. Firstly, the synthesised ACDs were characterised, followed by investigation of the ACDs behavior in different E/W ratios. Next, the change in hydrophobicity of the coated ACDs were examined. Furthermore, a perfomance study with BPA was evaluated to determine potential uptake capaciy of coated PP sheets. The amount of coating and the morphology of the coat was also investigated. Lastly, the main experiment of this project was conducted by testing the ability of coated PP surfaces to adsorb PFOS.

An overview of all the data can be found in Appendices

4.1 Synthesis of amphiphilic cyclodextrins

Through characterization of the synthesized ACDs, the desired DS was not achieved for all samples. Nevertheless, the ACDs were used, as variations in DS could still influence their coating behavior across different E/W ratios. When preparing coating mixtures, the expected transition from a cloudy suspension to a transparent solution with increasing ethanol concentration was not observed. Instead, all E/W ratios yielded what appeared to be solutions containing salts.

To verify the presence of salts, five droplets of silver nitrate solution were added to a centrifuge tube containing 5 mg of ACD and 2 mL of demineralised water. The solution turned from clear to opaque, confirming the presence of salts. As a result, an additional purification step was performed, yielding two purified ACDs, which were used in the subsequent experiments.

A new batch of ACDs with target DS of 4, 5, 7, and 8 was synthesised. Of these, three were used in the remaining experiments. The ACD with a desired DS of 7 was discarded, as the product remained partially yellow despite further purification.

The ^{1}H-NMR and MS spectra of the discarded ACDs, along with an image of the salt detection experiment and the E/W ratios of salt-containing ACDs, are provied in Appendix 14

Each ACD were weighed to determine the mass and calculate the yield, which is presented in Table 4.1

Table 4.1. Yield, actual mass, theoretical mass, and DS of the synthesized ACDs

DS	Theoretical mass [g]	Actual mass [g]	Yield [%]
3.1	13.45	5.85	43.50
3.6	14.00	7.60	54.29
4.9	15.45	7.59	49.13
5.9	16.56	9.57	57.80
6.6	17.34	9.84	56.75

4.1.1 Characterisation through ^{1}H-NMR

To validate whether the desired ACD derivatives have been synthesised, the obtained products were analysed via ^{1}H-NMR. The ^{1}H-NMR spectrum of ACD5 can be seen on Figure 4.1

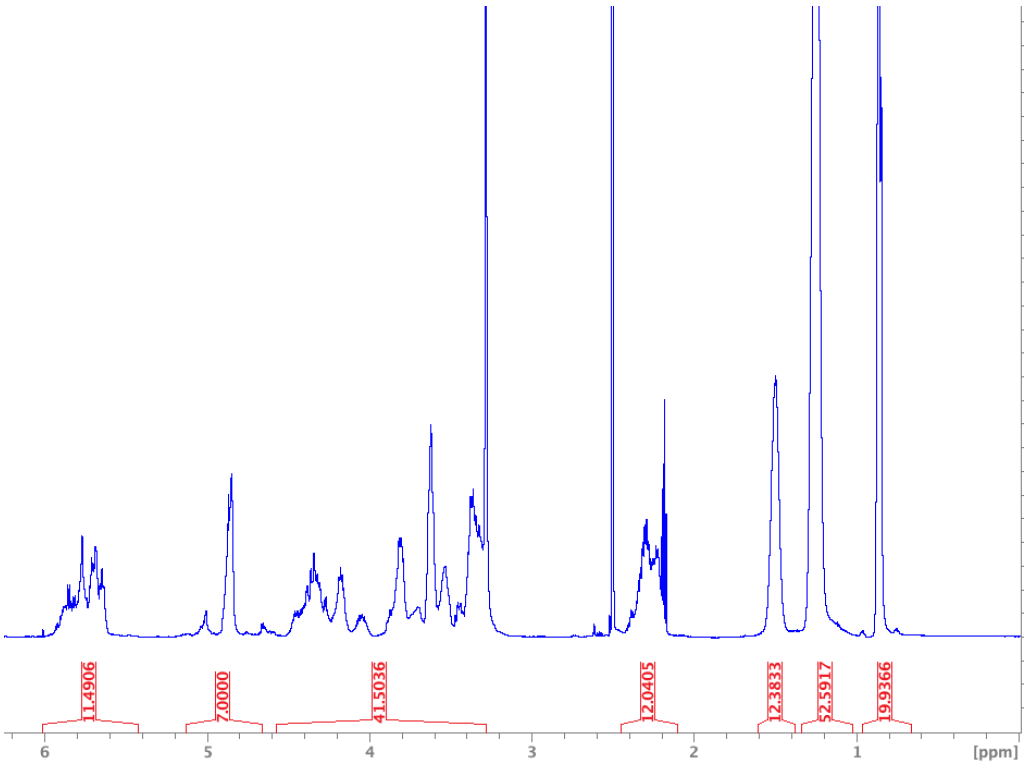

Figure 4.1. ^{1}H-NMR spectrum of ACD5

As seen from the spectum in Figure, two major signals with chemical shifts (δ) of 2.5 ppm and 3.3 ppm are present. These signals correspond to the DMSO-d6 solvent and the water present in DMSO-d6, respectively.

The integrals in the spectrum are calibrated with respect to the integral of the anomeric proton at δ = 4.8-5.0 ppm which is assigned the value of 7 due to β-cyclodextrin consisting of 7 glucose units. The DS is found by dividing the integral of the peak at δ = 0.9 ppm with three. This corresponds to a DS of 6.6 for ACD5. The peak used to calculate the DS is assigned to the distinctive methyl group, originating from the octanoyl group.

The peak at δ = 5.8-6.0 ppm arises from the secondary hydroxyl groups and the substitution of these groups, can be calculated by taking the integral of this peak into account. The value of the integral is 11.4906, and due to β-CD possessing 14 hydrogen atoms, 17.92 % of the hydroxyl groups on the wider rim are substituted. Upfield from the spectrum, three peaks are observed around δ = 1.0-1.3 ppm, δ = 1.4-1.6 ppm and δ = 2.1-2.4 ppm. These peaks are assigned to the methylene groups within the octanoyl group

Furthermore, the integral of 41.5036, ranging from δ = 3.3-4.6 ppm corresponds to the remaining hydrogen atoms present in β-CD. The same procedure is used to calculate the DS of the other ACD derivatives. The characteristics of the respective ACDs can be seen in Table 4.2 and the H^1NMR spectra of each ACD are found in Appendix 7

Although the synthesis of the ACDs did not yield all of the desired DS, it is still considered successful, as the DS range is likely to differ in uptake capacity.

Table 4.2. Overview of the synthesised ACD derivatives. Sub. of sec. OH: substitution of secondary hydroxyl groups.

Average DS (^{1}H-NMR)	Sub. of sec. OH (%)	Average DS (MS)	Average molecular weight (g/mol)
3.1	7.12	2.50	1526.07
3.6	5.22	2.45	1589.14
4.9	14.60	2.49	1753.14
5.9	8.35	2.98	1879.29
6.6	17.92	3.18	1967.59

4.1.2 Characterization through Mass spectrometry

To further elucidate the structure of the synthesised products, MALDI-TOF MS is used to characterise the ACDs. For MS, the DS is calculated using the following equation:

$$DS = \frac{\sum_i (I_i \cdot DS_i)}{\sum_i (I_i)} \tag{4.1}$$

where I_i is the intensity of the i'th peak, and i denotes the degree of substitution corresponding to the i'th peak [20]. The MS spectrum for ACD5 is displayed in Figure 4.2

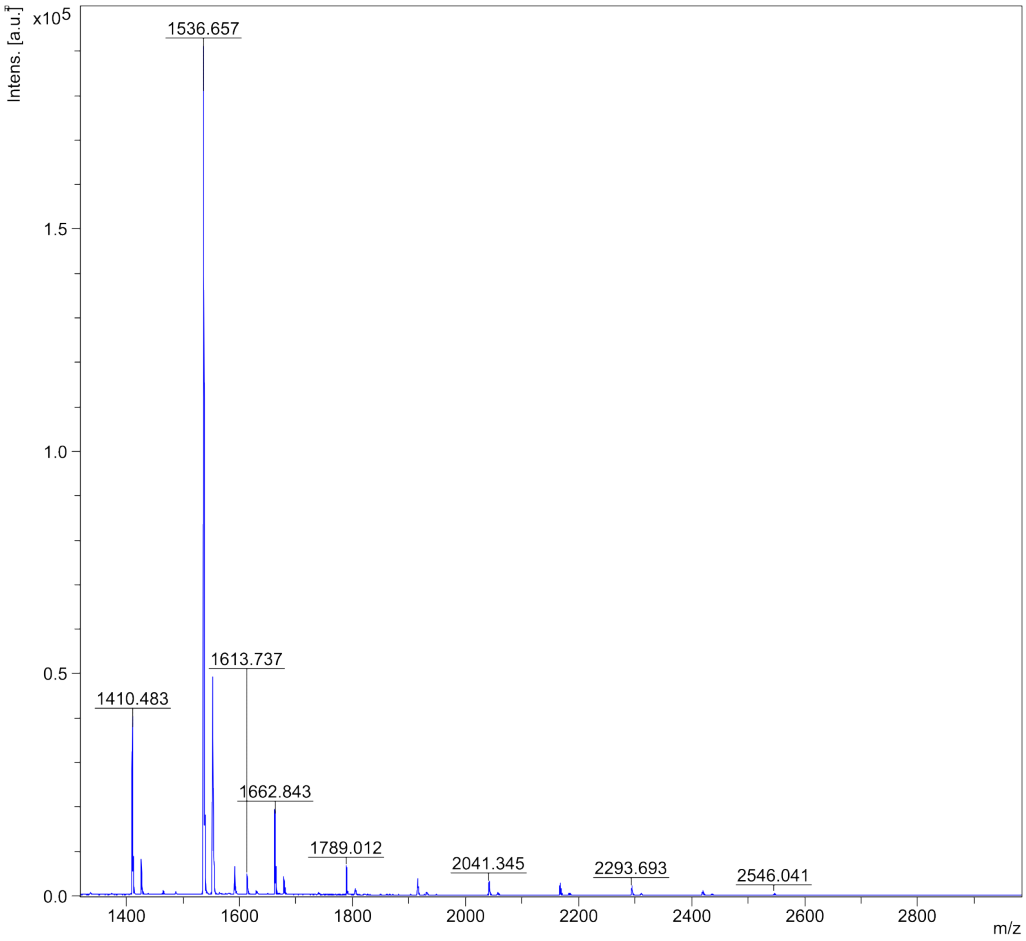

Figure 4.2. Mass spectrum of ACD5

As seen in the spectrum, a repeating unit is observed between the peaks with a mass difference of approximately 126m/z. This corresponds to the octanoyl group grafted onto -CD. When interpreting the spectrum, it is essential to account for the formation of adducts. For example, the base peak appears at 1536.657 m/z. This indicates that three octanoyl groups are grafted onto the -CD along with the formation of a sodium adduct. The same approach is applied to the remaining peaks by considering the repeating unit. By using Equation 4.1, the DS of ACD5 is calculated to be 3.18.

As seen from Figure X, the DS of NMR are higher than the DS from MS. Despite the difference in DS, this tendency is expected as MS is prone to ionize and hence detect ACDs with lower DS. For this reason, the DS obtained through NMR analysis is considered as the most reliable while MS serves as fingerprint for the number of substituents present in the different ACDs. The MS analysis therefore serves

As seen in Figure X, the DS obtained from NMR are consistently higher than the DS from MS. However, this difference is expected as MS tends to ionize and detect ACD species with lower DS [**?**]. Therefore, the DS obtained from NMR are considered more reliable. On the other hand, MS serves as a fingerprint for estimating the presence and distribution of substituents within the ACDs.

4.2 Impact of amphiphilic cyclodextrins in different concentrations of ethanol

The composition of the coating mixture has shown to play a huge role in the formation of coat on hydrophobic surfaces, thus influencing the adsorption capacity of the coated surface.

Initially, E/W ratios of the five ACDs were investigated at 1 mg/mL in the coating mixture with the results reported by Lumholdt [23] However, the quality of the results was too poor for DLS measurements. A concentration of 0.75 mg/L was then proposed but the outcome was the same. Finally, a concentration at 0.5 mg/L was made and feasible results were obtained through DLS.

Firstly, transmittance measurements were conducted to indicate when TP was reached, as it can not be confirmed with certainty what appears to be a clear and transparent solution, actually is a solution. These measurements are shown in Table 4.3

Table 4.3. Transmittance (%) of 0.5 mg/mL ACDs at different E/W ratios

E/W Ratio	ACD1	ACD2	ACD3	ACD4	ACD5
10/90	56.989	30.136	20.318	38.144	42.002
20/80	61.717	38.650	59.113	49.694	61.253
30/70	62.067	26.703	34.103	44.648	38.020
40/60	58.498	24.050	37.012	45.344	41.947
50/50	60.239	33.813	31.736	50.582	42.047
60/40	70.987	41.379	45.528	54.320	67.906
70/30	88.334	85.148	87.627	70.266	73.081
80/20	89.929	90.438	92.515	96.968	94.362
90/10	97.837	95.045	94.433	99.988	99.550

Through the results obtained from the transmittance, it was assumed that E/W ratios exceeding 80% transmittance contained ACDs in solution. This is substantiated by the clear and transparent appearance of all ACDs with transmittance level exceeding this value. The E/W ratios of ACD5 is shown in Figure 4.3

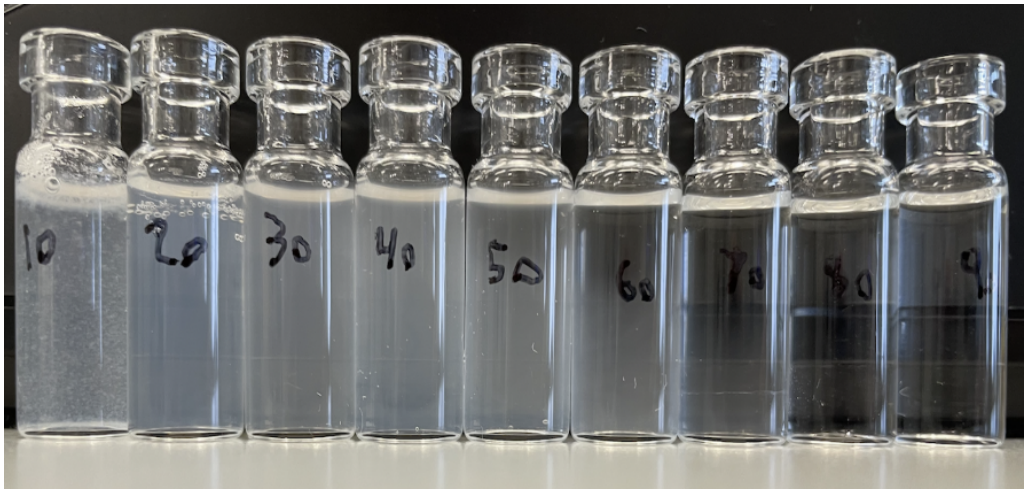

Figure 4.3. E/W ratios and coating suspensions/solutions of ACD5. The numbers represent the volume fraction of ethanol.

By studying the appearance of the coating mixture of ACD5, it appears that the suspensions transition to solutions at 70% ethanol. Comparing this observation with the transmittance of this particular E/W ratio, it could be argued that the mixture actually is a suspension. This emphasises the importance of combining transmittance measurements with DLS in examining the coating behaviour of ACDs in different E/W ratios. Therefore, the nanoparticle size and PDI of ACD5 in a 70/30 ratio of ethanol and water will be measured by DLS.

Each ACD was analysed across the E/W range using DLS to determine particle size and PDI. The results of the ACD derivatives are shown in Figure 4.4

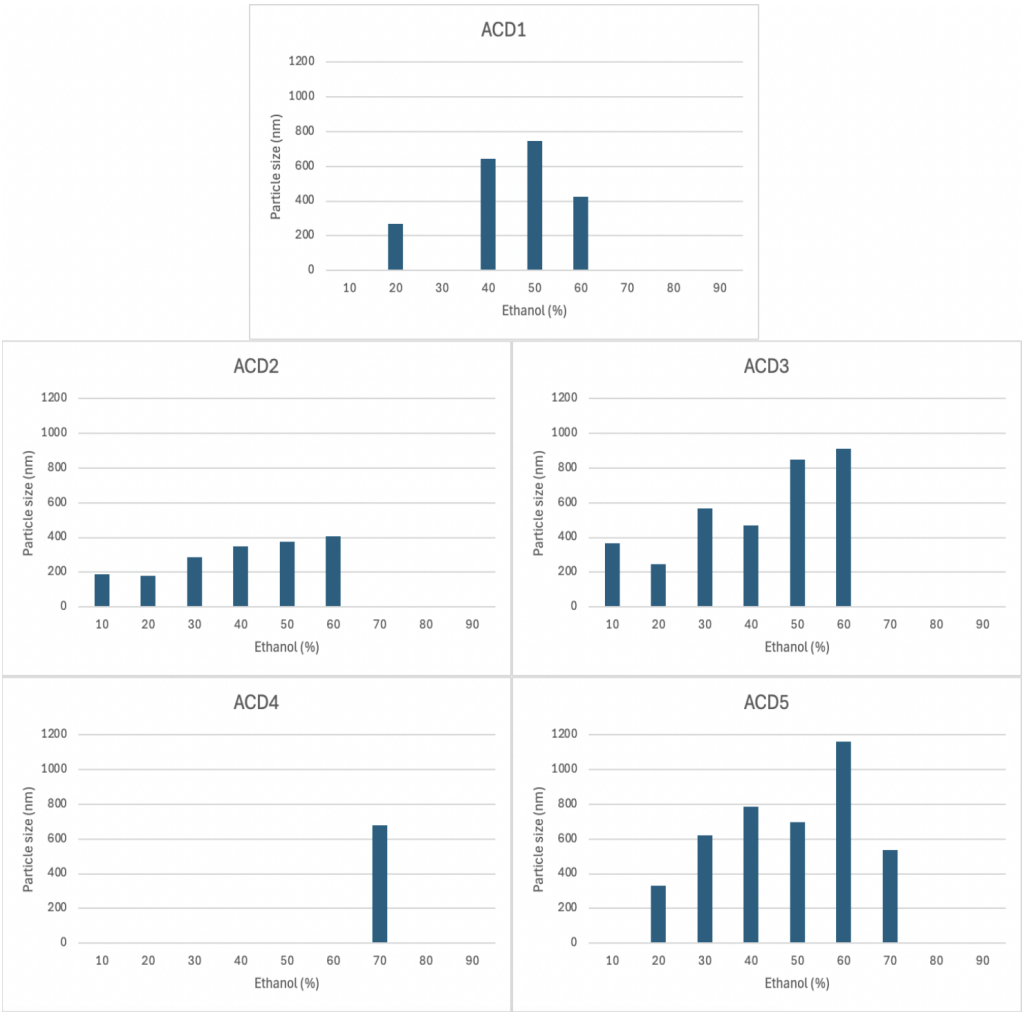

Figure 4.4. Particle sizes of 0.5 mg/mL of all ACDs in different concentrations of ethanol

In general, ACD1, ACD2, ACD3 and ACD5 increase in particle size with increasing amount of ethanol. Another tendency is that, a higher DS of the respective ACDs results in particle formation at higher ethanol concentrations. These tendencies were also observed by [23]. However, the particle sizes decrease before TP with respect to ACD1 and ACD5. This decrease in size at the respective E/W ratios could be attributed to the ACDs being partly solvated, as indicated by the coating mixtures of these ACDs. (See Appendix 8).

For the three ACDs with the lowest DS (ACD1, ACD2 and ACD3), the transition from suspension to solution is the same at 60/70 ethanol. The TP for ACD4 and ACD5 is likewise the same with a ratio at 70/80 ethanol. This finding is expected as it is consistent with observations of Lumholdt [**?**]Only one sufficient result is achieved for ACD4, which seems a bit peculiar when taking the E/W ratios into consideration (See Appendix 8). Here, the coating mixtures appeared as suspensions until 80% ethanol was present. Large and polydisperse particles or even aggregates, which could not be detected by DLS, are the most likely the reason for the lack of qualitative data with regard to ACD4. The visual appearance of ACD4 could indicate the formation of aggregates below 70% ethanol.

As ACD4 only has one measurable suspension and all ACDs formed nanoparticles just before the transition to solution, E/W ratios just before TP will be used in the following experiments. ACDs in solution tend to coat materials to a lesser extent than suspended ACDs, as stated by Lumholdt [23]. This might indicate a lower uptake capacity, hence coating with dissolved ACDs will not be tested.

Furthermore, the PDI of the ACDs in different ethanol concentrations was measured. This parameter can provide useful insight about the ability of ACDs to form a uniform distribution of coat on hydrophobic surfaces. The measured PDI of the particles are presented in Table 4.4

Table 4.4. PDI of the formed particles (nm) for all 0.5 mg/mL ACDs at different ethanol concentrations. The samples marked with grey squares are considered to be monodisperse.

Ethanol (%)	**10**	**20**	**30**	**40**	**50**	**60**	**70**	**80**	**90**
ACD1		0.22		0.378	0.162	0.028			
ACD2	0.137	0.069	0.079	0.171	0.085	0.1			
ACD3	0.292	0.079	0.285	0.087	0.064	0.044			
ACD4							0.128		
ACD5		0.12	0.359	0.249	0.031	0.122	0.087		

As seen from the PDI measurements, the particles are mainly monodisperse [**?**] for all ACDs, apart from ACD1. By increasing the ethanol amount, ACDs with polydisperse particles at lower E/W becomes monodisperse. Besides that, all ACDs before TP are monodisperse which could suggest an even coat formation, thus another argument for selecting each ACD before TP.

4.3 Contact angle measurements

By coating the PP sheets with the different ACDs, it was believed that hydrophobicity of the PP surfaces would decrease. This observation was confirmed by the results, as the coated surfaces rendered more hydrophilic, visualised in Figure 4.5. Furthermore, it was clear that the lower the DS of the ACDs, the more hydrophilic the surface becomes, illustrated in Table 4.5

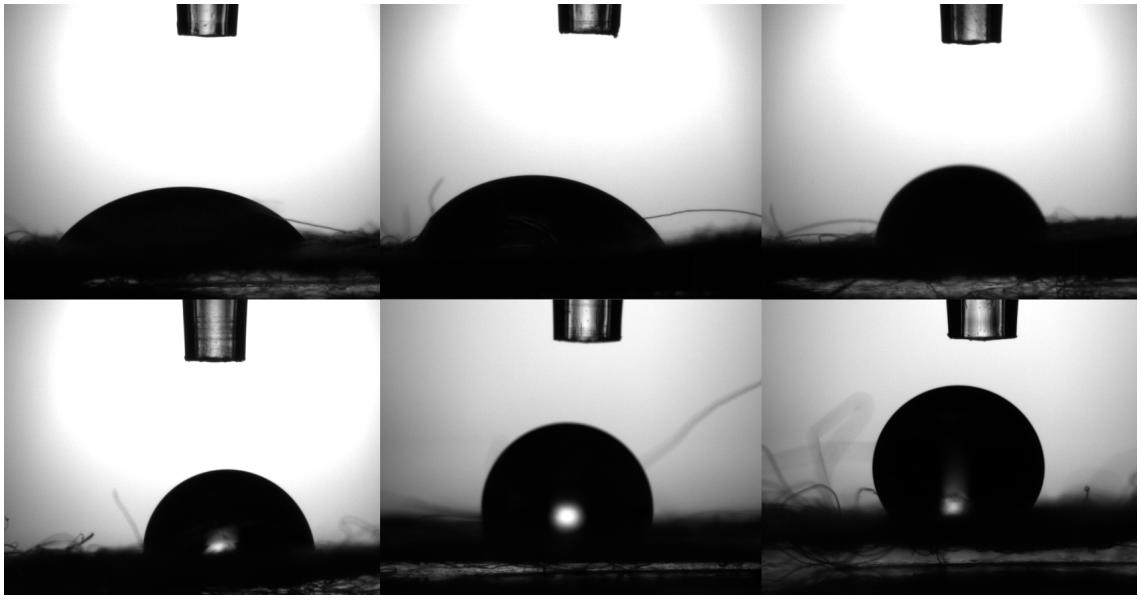

Figure 4.5. Contact angle measurements of coated PP with an areal density of 20 g/m^2.
From upper left to right: ACD3.1, ACD3.6 and ACD 4.9.
From lower left to right: ACD 5.9, ACD 6,6 and a non-coated reference.
PP sheets were coated before TP.

Table 4.5. Contact angles of coated PP sheets with each ACD at 20 g/m^2. Samples were done in triplicate.

Sample	ACD1	ACD2	ACD3	ACD4	ACD5	Reference
Contact angle (θ)	$\approx 45°$	$\approx 50°$	$\approx 75°$	$\approx 90°$	$\approx 105°$	$\approx 120°$

By coating PP sheets with areal densities of 5 and 10 g/m^2, the same tendency was observed. This is in alignment with the findings of Lumholdt [23], which could be explained by the coat formation with an orientation of less substituted ACDs towards the bulk water and more substiuted ACDs orientated towards the hydrophilic surface. The contact angles of all ACD coatings at each areal density are shown in Figure 4.6

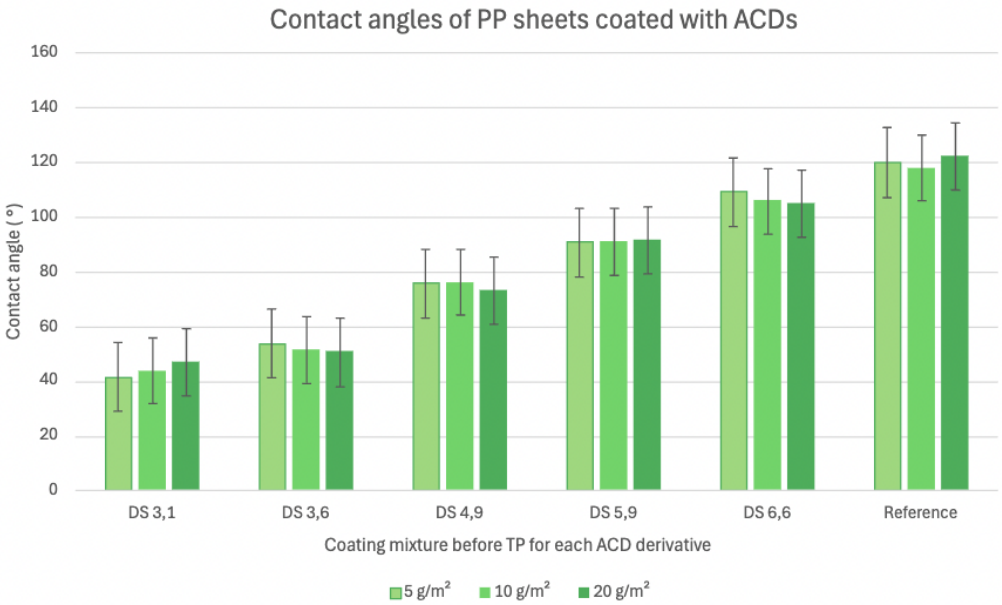

Figure 4.6. Contact angle measurements of PP sheets coated with each ACD before TP. All three areal densities were coated. The reference is non-coated PP. All samples were done in triplicate and error bars indicate standard deviation (SD)

No considerable change in contact angle was observed across the different areal densities of coated PP. However, the contact angles measured for ACD1 (DS 3.1) and ACD2 (DS 3.6) differ slightly from each other. This is not unexpected as the distribution of substituents for the ACDs can be quite even. Consideration of the MS spectra of these two ACDs (see Appendix 7) may offer an explanation. However, as mentioned earlier, MALDI-TOF MS might ionise lower substituted derivatives to a larger extent compared to more substituted derivatives, so this tendency have to be taken into account. Overall, this demonstrates the ACDs ability to coat PP sheets regardless of the areal density.

4.3.1 Perfomance study with Bisphenol A

In order to examine if the coated PP sheets were capable of complexation with a hydrophobic molecule, and thus remove unwanted substances BPA was chosen as candidate for this purpose

At first, it was decided to conduct a simple adsorption kinetics experiment to evaluate if an equilibrium concentration of BPA, hence adsorption limit of the ACDs were reached. All ACDs were coated onto PP sheets of 20 g/m^2. The adsorption experiment can be seen in Figure 4.7

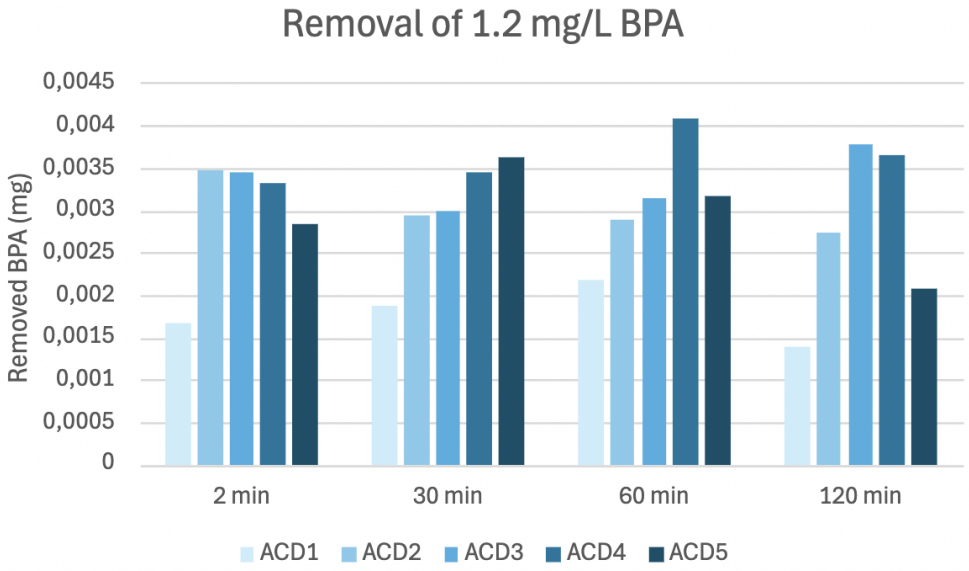

Figure 4.7. Adsorption kinetics experiment for removal of BPA at 1.2 mg/L.

As it appears, the amount of removed BPA is lower for ACD3 and ACD4 after 2 hours compared to the removal to 30 and 2 minutes, respectively. This suggests that a longer interaction time is needed to establish equilibrium between the inclusion complexation and BPA in solution using the two ACDs. With regards to the other ACDs, it can not bed rejected that equilibrium is reached after 2 hours, as the highest uptake capacity of BPA is observed at this time slot. For ACD2, it could be argued that equilibrium is reached due to the slight difference in removed amount of BPA between 1 hour and 2 hours. Given that BPA was primarily a proof of concept molecule, the adsorption kinetics experiment was not repeated, despite three of the ACDs potentially reaching equilibrium.

Instead, measuring the change in BPA concentration after 1 hour using all three ACDs were done in triplicate. The average removal of BPA after 1 hour can be seen in Figure 4.11

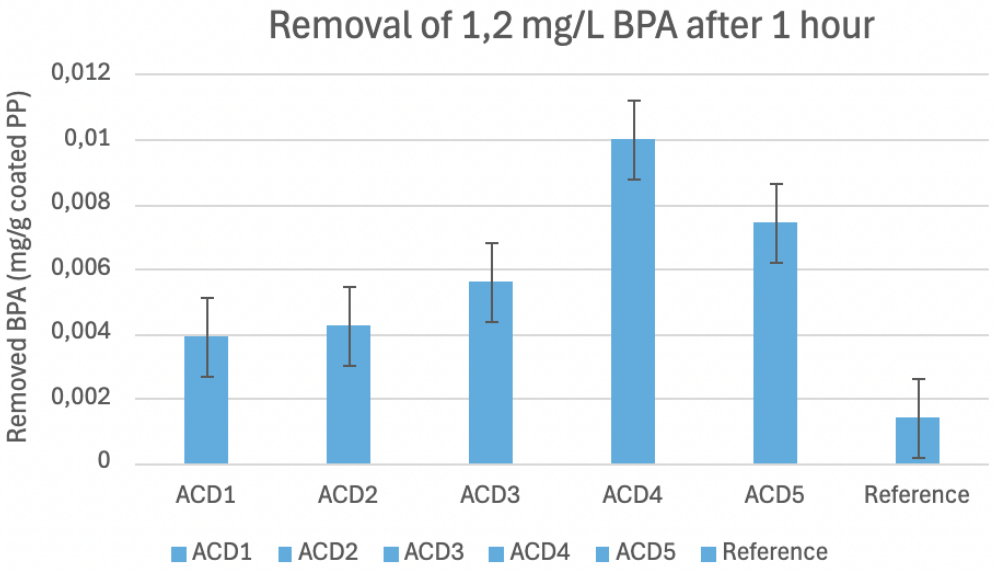

Figure 4.8. Average removal of BPA at 1.2 mg/L after 1 hour. Error bars indicate SD

ACD4 clearly has the highest uptake capacity, removing approximately 7 times as much BPA as the non-coated reference. A pattern is observed from ACD1 to ACD4 where the adsorption of PFOS increases with the DS. However at ACD5, the amount of removed BPA is reduced, which could be caused by steric hindrance impeding access to the cavity.

The experiment was repeated for PP sheets at 5 and 10 g/m^2 coated with ACD1 and ACD5. It was of interest to see if there was any significant difference in the removal of BPA depending on the areal density of PP. The comparison of uptake capacity between different PP sheets are shown in Figure

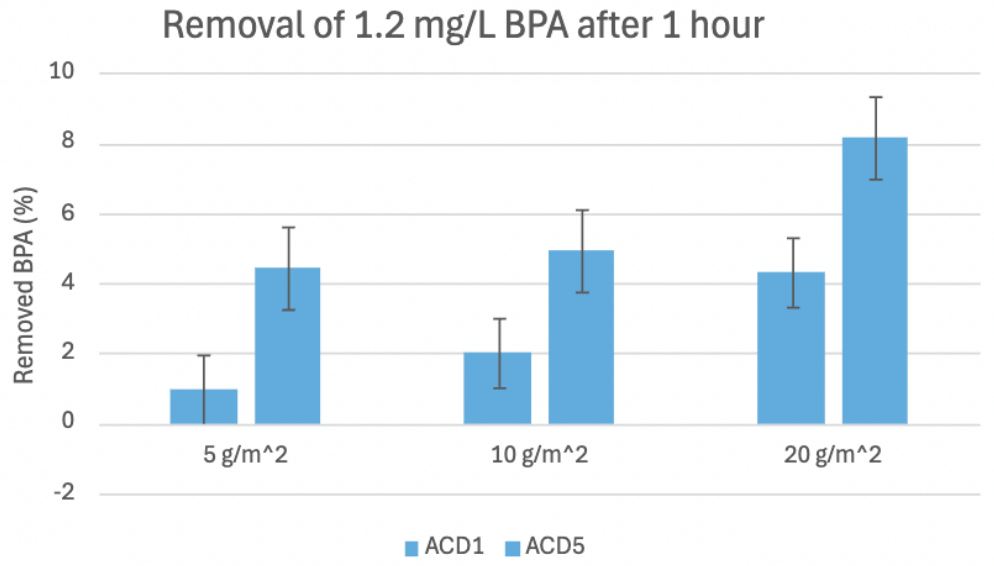

Figure 4.9. Percentage removal of BPA at 1.2 mg/L after 1 hour. ACD1 is the left column. Error bars indicate SD

As expected, coated PP at 20 g/m^2 adsorbs more BPA than the other areal densities. The difference in removal for ACD5 between 5 and 10 g/m^2 is quite low, which could indicate that coating PP at either 5 or 10 g/m^2 could lead to a similiar coating amount. Lastly, the high SD for ACD1 could be attributed to the low DS (3.1), resulting in a higher affinity to water compared to ACD5.

4.3.2 Quantification of the coating amount

It is believed that the highest areal density at 20 g/m^2 leads to a higher coating amount due to a higher degree of PP present at the surface. In other words, more interaction sites are exposed to the ACD coating which is likely to cause a greater amount of coat on this particular areal density. Furthermore, a higher quantity of coating on the PP surface could potentially facilitate a greater adsorption of PFAS.

Based on the results of the BPA experiment, it was decided to choose ACD1 and ACD4 as these ACDs had the highest and lowest uptake capacity of BPA. Additionally, quantification of coating on PP with areal densities of 5 and 10 g/m^2 were examined. It was of interest to see, if the degree of coating could explain the difference in uptake capacity and if the amount of coating differs considerably depending on the areal density of PP. Therefore, it was decided to determine the coating amount through ^{1}H-NMR.

Maleic acid was used an internal standard for this purpose, due to its distinct signal at δ = 6 ppm. DMSO-d6 with a maleic acid concentration of 0.01 mg/mL was added to the coated PP sheets to dissolve the ACD coating. A ^{1}H-NMR spectrum of the ACD4 coating from PP with an areal density of 20 g/m^2 can be seen in Figure 4.10. All ^{1}H-NMR spectra for the quantification of the coating amount can be found in Appendix 9.

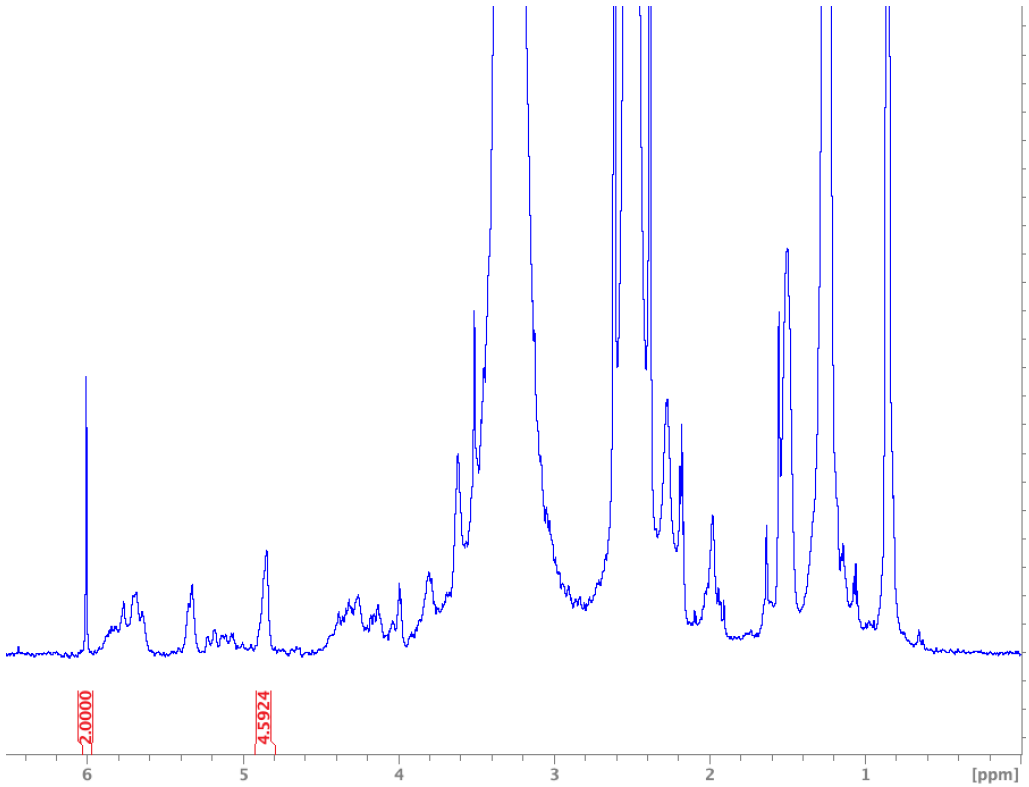

Figure 4.10. ^{1}H-NMR spectrum of the ACD4 coating from PP with an areal density of 20 g/m^2. $\delta = 6$ ppm corresponds to the maleic acid peak with an integral of 2. The integral of 4.5924 stems from the anomeric proton peak at $\delta = 4.8$ ppm.

The integrals are calibrated with respect to two equivalent hydrogen atoms followed by integrating the anomeric proton at $\delta = 4.8$ ppm to determine the coating amount. As seen in Figure X, the integral of the anomeric proton is approximately 4.6, which corresponds to a coating amount of 0.039 μmol ACD. The weight of the PP sheet prior to coating is 0.0191 g, and by dividing the coating amount with the weight of the PP sheet, the coating amount relative to the weight of PP can be calculated. This is done to provide insight to how well the ACDs coat the respective areal densitites of PP. For this particular sample, the amount of ACD4 is 2.07 μmol / g PP. The amount of ACD coating on the PP sheets of all three areal densities is listed in Table 4.6

Table 4.6. Overview of the coating onto PP sheets at the three areal densities coated with ACD1 and ACD4. SD is the standard deviation of each ACD coated at each areal density of PP.

	PP at 5 g/m^2	**PP at 10 g/m^2**	**PP at 20 g/m^2**
	[μmol ACD/g PP]		
ACD1	3.21	3.06	3.05
ACD4	4.65	3.33	2.05
SD of ACD1	± 0.49	± 0.42	± 0.14
SD of ACD4	± 0.68	± 1.08	± 0.026

From the values presented in Table **??**, the amount of relative coat decreases when the

areal densities increase. This is logical, as the PP sheets are at fixed dimensions of 3 cm x 3 cm. Thus, a coated PP sheet at 5 g/m^2 will possess the greatest amount of coat relative to its weight. As expected, a greater relative amount of coat is observed for ACD4, which is probably due to its more hydrophobic nature. However, the coating amount of ACD1 onto PP sheets of 20 g/m^2 derivates from this trend. No logically explanation was found for this observation.

Furthermore, the coating amount of ACD relative to the area of PP was also investigated. By calculating this value, an estimation of the distribution of coat on the PP sheets can be made. This relationshiop is shown in Table 4.7

Table 4.7. Overview of the distribution of coat onto PP sheets at the three areal densities coated with ACD1 and ACD4. SD is the standard deviation of each ACD coated at each areal density of PP.

	PP at 5 g/m^2	**PP at 10 g/m^2**	**PP at 20 g/m^2**
	[μmol ACD/cm^2 PP]		
ACD1	0.0019	0.0034	0.006
ACD4	0.0029	0.0034	0.0042
SD of ACD1	± 0.00020	± 0.00045	± 0.00038
SD of ACD4	± 0.00035	± 0.00095	± 0.00015

A clear trend is observed, as the coating covers a larger area when the areal density of PP increases. This finding could serve as a possible explanation as to why ACD1 removed more BPA when the areal densities of PP increases. The more dispersed the coating is, the more adsorption sites are likely present, hence a greater uptake capacity.

4.3.3 Examination of coating via scanning electron microscopy

It was decided to gain knowledge about the distribution of the coating of ACD1 and ACD4 on PP with an areal density of 20 g/m^2 since these derivates showed the highest and lowest uptake capacity of BPA.

These ACDs along with a reference of non-coated PP was investigated through SEM. The pictures from ACD1, ACD4 and the reference can be seen in Figure.

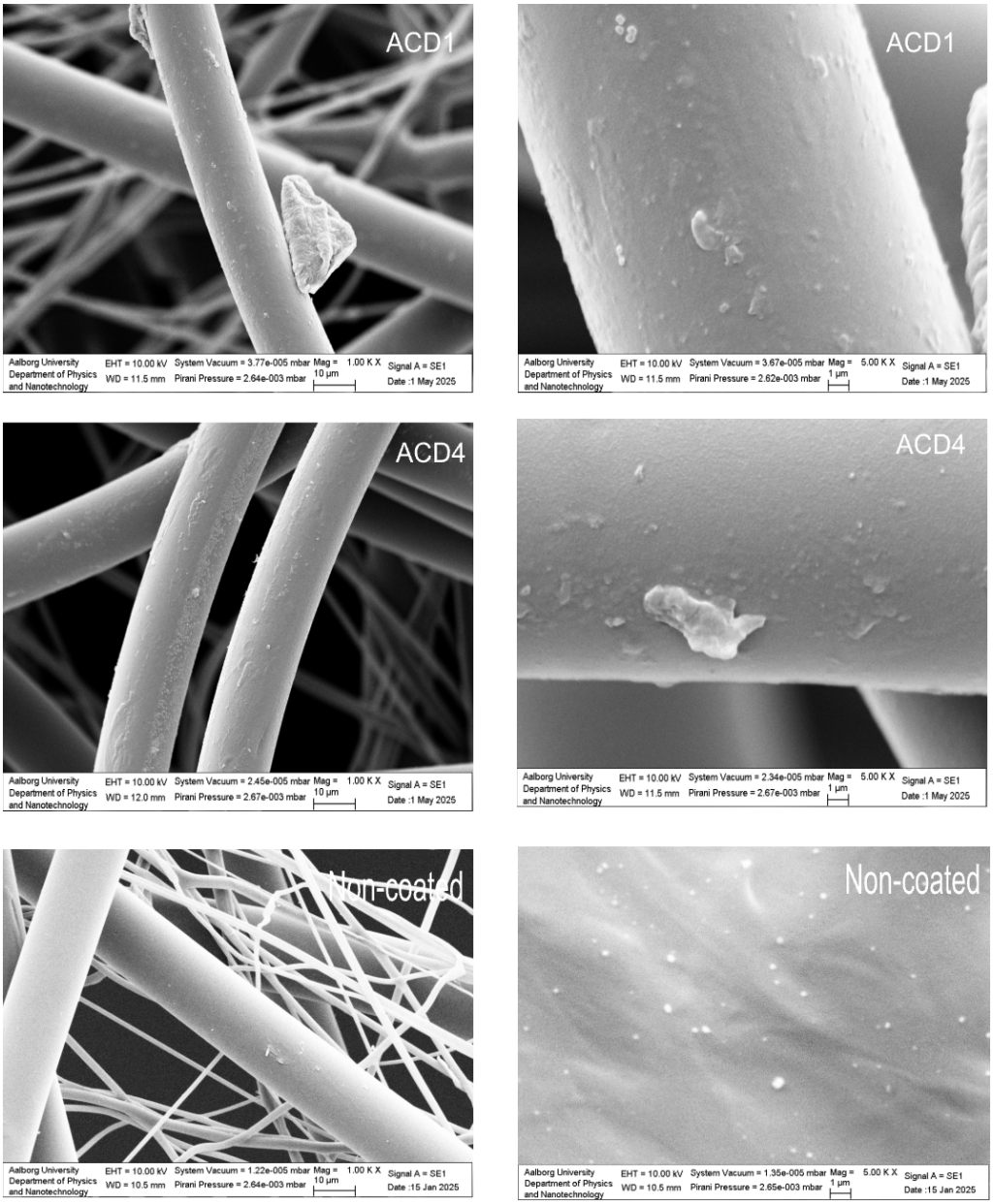

Figure 4.11. SEM pictures of 20 g/m^2 PP sheets coated with ACD 1 and ACD 4. A non-coated reference is also shown

Examing the pictures, an uniform distribution of particles are not shown, although a thin layer of coat could possible be present along the fiber of ACD4. On the other hand, what appear to be a large particle or a small aggregate for ACD4, is more pronounced than a distribution (See Appendix 10).

With regards to ACD1, the formation of coat tends to form large aggregates rather than small particles as. However, zooming in on ACD1, small particles seems to assemble. This is noticably seen on the top of the PP fiber This relatively heterogeneous coat formation of both ACDs could be due to nanoparticles being unstable just before TP, thus forming aggregates. By looking at the PDI and particle sizes of the two ACDs, a more even coating

could theoretically be formed.

Overall, the distribution of coat seems quite patchy with small areas consisting of coat. Looking at the picture of the reference, an even distribution of particles are observed, which is likely due to some sort of contamination

4.3.4 Removal of PFOS using amphiphilic cyclodextrins coated onto polypropylene sheets

It was decided to coat PP sheets with an areal density of 20 g/m^2 since the performance study showed a higher uptake capacity of BPA when coating with this PP. Furthermore, the coat appears more dispersed when coating with this areal density. All six ACD derivatives were coated onto PP sheets. At first, the amount of adsorbed PFOS was determined relative to the mass of coated PP sheets, as illustrated in Figure 4.12

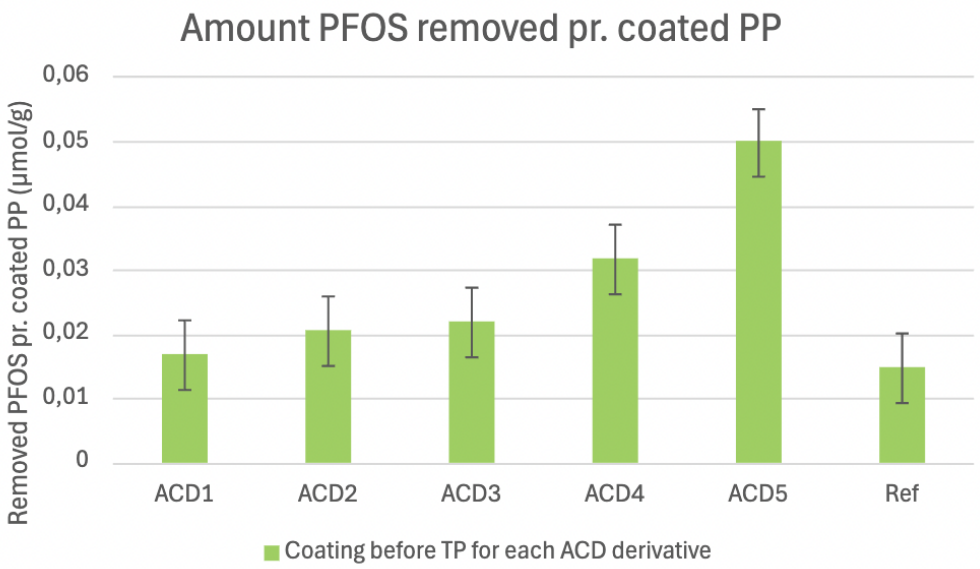

Figure 4.12. The relative amount of removed PFOS through complexation with coated PP sheets. Error bars indicate SD

The higher the DS, the higher the removal of PFOS, as seen in Figure 4.12. ACD5 (DS of 6.6) . This tendency makes sense, since PFOS are quite hydrophobic, and as a consequence, a higher affinity to the most substituted ACD. However, the uptake from the reference do not differ much from the removal from the lower ACDs. A possible explanation could be the decreased hydrophobicity of ACDs resulting in a weaker interaction with PFOS or potentially loss of coat due to some affinity to the bulk water. However, the latter scenario seems unlikely based on the findings by Lumholdt [23] where all ACD derivatives turned out to be water stable. It could also be due to the of amount of coating or the orientation of the coat potenitally making the cavitites inaccessible to some extent. Another finding by Lumholdt [23]. The removal of PFOS in % was also calculated as seen in Figure 4.13.

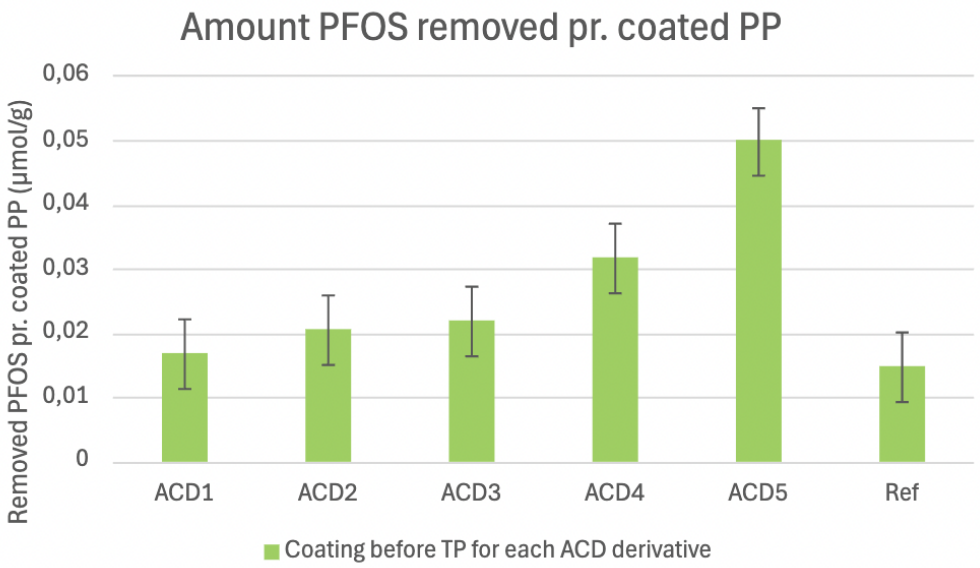

Figure 4.13. The relative amount of removed PFOS through complexation with coated PP sheets. Error bars indicate SD

Among the tested ACDs, ACD5 exhibited the highest removal of PFOS by adsorbing nearly 35% percent, significantly outperfoming the other ACDs.

So to conclude, the PFOS experiment did show increased removal of PFOS by coating the ACDs compared with the reference for all ACDs. However the reference did perform nearly as good as three ACDs with the lowest DS. ACD Therefore, further optimization of the preparation of the coating mixture and the synthseis of ACDs might be done to acheive a more efficient removal of PFOS.

.

Conclusion 5

In this project, ACDs with DS of 3.1, 3.6, 4.9, 5,9 and 6.6 were synthesised and used to coat polypropylene (PP) sheets for the purpose of removing PFOS.

The ethanol/water ratio making up the coating mixtures significantly influenced ACD behavior, with particle formation and the transition point to solution shifting to higher ethanol concentrations as DS increased. Dynamic light scattering indicated that more substituted ACDs tended to form particles in higher ethanol concentrations, and the optimal coating conditions were found just before the TP.

Contact angle measurements showed that coating PP sheets with ACDs rendered the surface more hydrophilic, with lower ACDs of lower DS

BPA adsorption experiments confirmed that the ACD-coated surfaces were capable of inclusion complexation. Removal efficiency generally increased with higher DS, although a drop was observed at the highest DS, possibly due to steric hindrance. PFOS removal experiments similarly demonstrated the uptake ability of ACD-coated PP,.

Quantification of coating amount was done via ^{1}H-NMR which showed higher amount of coat, with higher density of PP. SEM analyses indicated that the coating were rather forming aggregates than a unifrom distribution.

Overall, the project demonstrated that ACDs can be effectively used to functionalize polypropylene surfaces for the adsorption of PFOS and other micropollutants, such as BPA The degree of substitution plays a critical role in both coating behavior and uptake capacity, emphasising the importance of optimising ACD structure for environmental applications.

Further work 6

Additionally, the stability of the ACD coat could be investigated when in contact with water or a water-based loading solution to obtain knowledge about possible detachment of ACD's from the PP sheets into the liquid. This could be of great importance since potential loss of coat in an aqueous solution could be crucial for the adsorption and hence removal of PFOS.

Regeneration of the PP sheets could also be of interest. This process could be done by using an organic solvent like methanol or acetonitrile to dissolve the the ACD-PFOS inclusion complex after an equilibrium concentration of PFOS has been reached. PFOS is then extracted as a concentrate and disposed. Following these steps, the used PP sheets are rinsed with water to remove residue, dried and recoated with new ACD's. The procedure can then possibly be repeated for multiple cycles to ensure sustainability and limited usage of materials.

Bibliography

[1] Kasper Skovbølling Hedegaard, Thorbjørn Terndrup Nielsen, and Mads Koustrup Jørgensen. Removal of pfos using cyclodextrin-coated polypropylene membranes. Presented at the 20th Nordic Filtration Symposium, Aalborg University, 2024, 2024.

[2] Fuqiang Liu, Joseph J. Pignatello, Runze Sun, Xiaohong Guan, and Feng Xiao. A comprehensive review of novel adsorbents for per- and polyfluoroalkyl substances in water. *ACS ESamp;T Water*, 4(4):1191–1205, March 2024.

[3] Francesco Calore, Elena Badetti, Alessandro Bonetto, Anna Pozzobon, and Antonio Marcomini. Non-conventional sorption materials for the removal of legacy and emerging pfas from water: A review. *Emerging Contaminants*, 10(3):100303, September 2024.

[4] Zahra Abbasian Chaleshtari and Reza Foudazi. A review on per- and polyfluoroalkyl substances (pfas) remediation: Separation mechanisms and molecular interactions. *ACS ESamp;T Water*, 2(12):2258–2272, November 2022.

[5] Zunaira Habib, Minkyung Song, Sadaf Ikram, and Zahra Zahra. Overview of per- and polyfluoroalkyl substances (pfas), their applications, sources, and potential impacts on human health. *Pollutants*, 4(1):136–152, March 2024.

[6] Qiming Liu, Yi Zhou, Jian Lu, and Yanbo Zhou. Novel cyclodextrin-based adsorbents for removing pollutants from wastewater: A critical review. *Chemosphere*, 241:125043, February 2020.

[7] E.M.Martin Del Valle. Cyclodextrins and their uses: a review. *Process Biochemistry*, 39(9):1033–1046, May 2004.

[8] Strategies to modify the drug release from pharmaceutical systems. Woodhead Publishing, 2015.

[9] Adelina-Gabriela Niculescu. Cyclodextrins – development and applications of these versatile oligosaccharides. *Biomaterials and Tissue Engineering Bulletin*, 7, 2020.

[10] Avilasha A. Sandilya, Upendra Natarajan, and M. Hamsa Priya. Molecular view into the cyclodextrin cavity: Structure and hydration. *ACS Omega*, 5(40), 2020.

[11] Fabricio Maestá Bezerra, Manuel José Lis, Helen Beraldo Firmino, Joyce Gabriella Dias da Silva, Rita de Cassia Siqueira Curto Valle, José Alexandre Borges Valle, Fabio Alexandre Pereira Scacchetti, and André Luiz Tessaro. The role of -cyclodextrin in the textile industry—review. *Molecules*, 25, 2020.

[12] Zsombor Miskolczy, Mónika Megyesi, and László Biczók. Entropy-driven inclusion of natural protoberberine alkaloids in sulfobutylether--cyclodextrin. *Molecules*, 27, 2022.

[13] Jonathan W. Steed, David R. Turner, and Karl J. Wallace. Core concepts of supramolecular chemistry. chapter 1.9. Wiley, 2007.

[14] Qiang Sun. The hydrophobic effects: Our current understanding. *Molecules*, 27(20):7009, oct 2022.

[15] Hydrophobic Interactions, jan 30 2023. [Online; accessed 2024-05-10].

[16] Erem Bilensoy and A Atilla Hincal. Recent advances and future directions in amphiphilic cyclodextrin nanoparticles. *Expert Opinion on Drug Delivery*, 6(11):1161–1173, August 2009.

[17] Gamze Varan, Cem Varan, Nazlı Erdoğar, A. Atilla Hıncal, and Erem Bilensoy. Amphiphilic cyclodextrin nanoparticles. *International Journal of Pharmaceutics*, 531(2):457–469, October 2017.

[18] Michel Roux, Bruno Perly, and Florence Djedaïni-Pilard. Self-assemblies of amphiphilic cyclodextrins. *European Biophysics Journal*, 36(8):861–867, July 2007.

[19] Philippe Le Thuaut, Bernard Martel, Gregorio Crini, Ulrich Maschke, Xavier Coqueret, and Michel Morcellet. Grafting of cyclodextrins onto polypropylene nonwoven fabrics for the manufacture of reactive filters. i. synthesis parameters. *Journal of Applied Polymer Science*, 77(10):2118–2125, 2000.

[20] Ludmilla Lumholdt, Nielsen Thorbjørn Terndrup, and Larsen Kim Lambertsen. Surface modification using self-assembled layers of amphiphilic cyclodextrins. *Journal of Applied Polymer Science*, 131(22), June 2014.

[21] Ludmilla Lumholdt, Sophie Fourmentin, Thorbjørn T Nielsen, and Kim L Larsen. Removal of volatile organic compounds using amphiphilic cyclodextrin-coated polypropylene. *Beilstein Journal of Organic Chemistry*, 10:2743–2750, November 2014.

[22] Jonathan Clayden, Nick Greeves, and Stuart Warren. *Nucleophilic substitution at the carbonyl group*, pages 279–282. Oxford University Press, March 2012.

[23] Ludmilla Lumholdt. *Non-covalent surface functionalisation with amphiphilic cyclodextrins*. PhD thesis, Aalborg University, 2014.

[24] Sigma Aldrich. Maleic acid.

[25] Abhishek Venkatratnam and Rebecca C. Fry. *The role of nutrition and epigenetics in environmental toxicology*, page 303–334. Elsevier, 2020.

[26] Yan Wu, Xue-Qi Zhang, Xiao-Jing Guo, Ling-Hui Kong, Rong-Fang Shen, Jiang-Tao Hu, Xi Yan, Yan Chen, and Wan-Zhong Lang. Construction of stable beta-cyclodextrin grafted polypropylene nonwoven fabrics for the adsorption of bisphenol a. *Radiation Physics and Chemistry*, 198:110223, September 2022.

[27] James A. Ashenhurst. *The Organic Chemistry Reagent Guide*. MasterOrganicChemistry, 2013.

^{1}H-NMR and MS Spectra of used ACDs

7

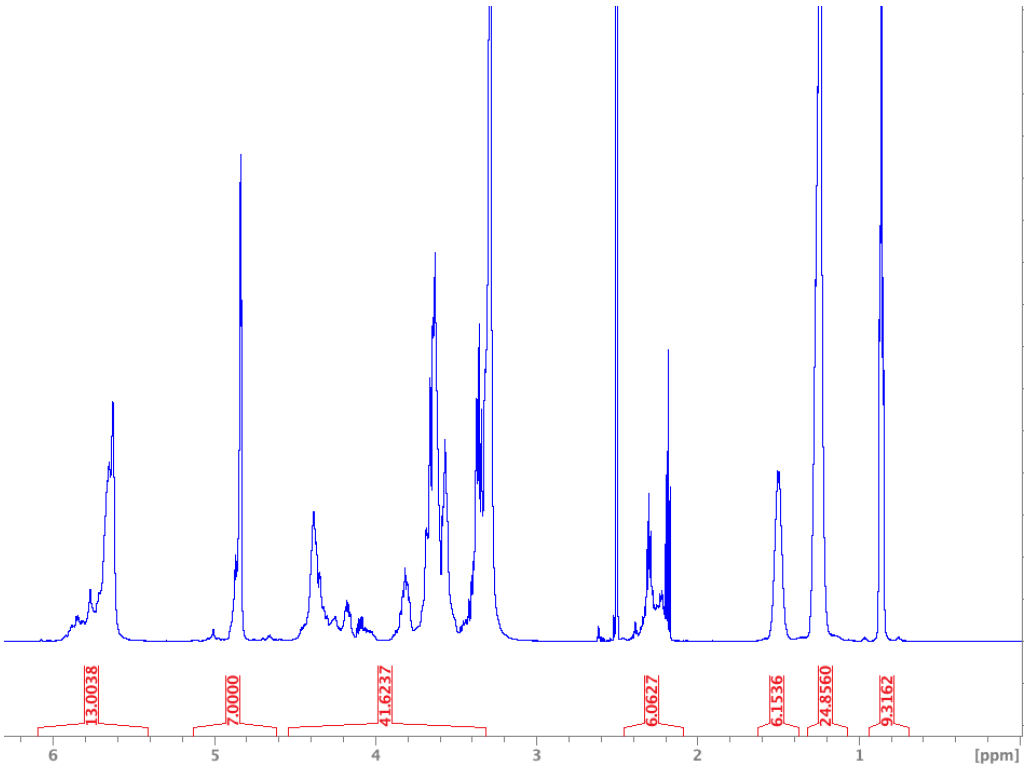

Figure 7.1. ^{1}H-NMR spectrum of ACD1 with a DS of 3.1

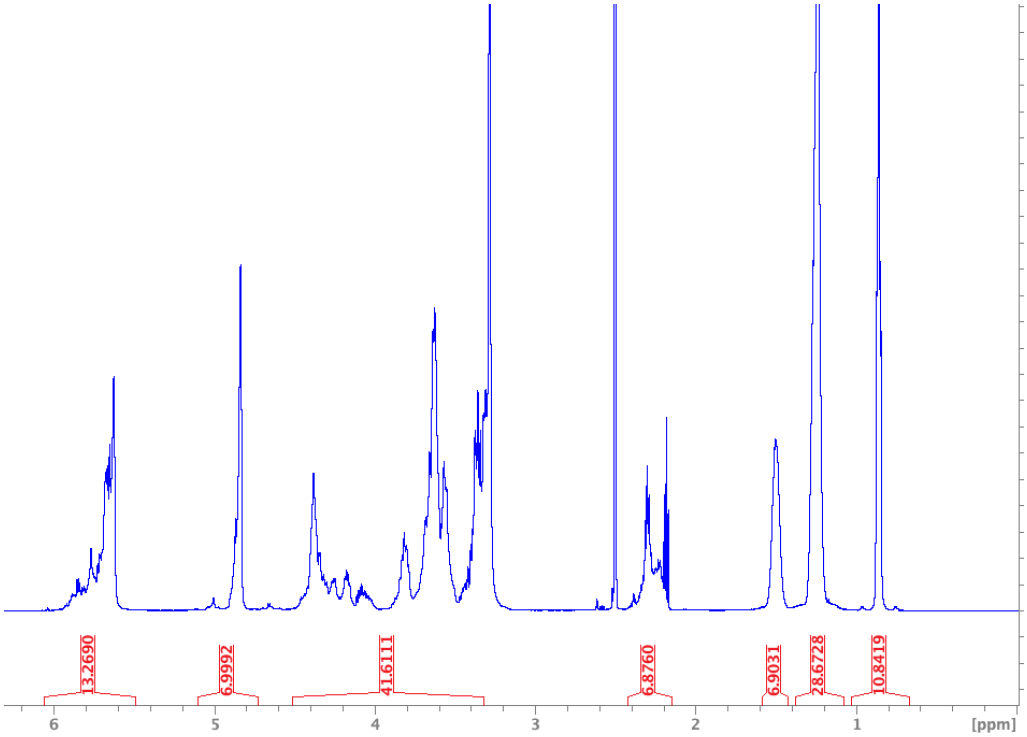

Figure 7.2. ^{1}H-NMR spectrum of ACD2 with a DS of 3.6

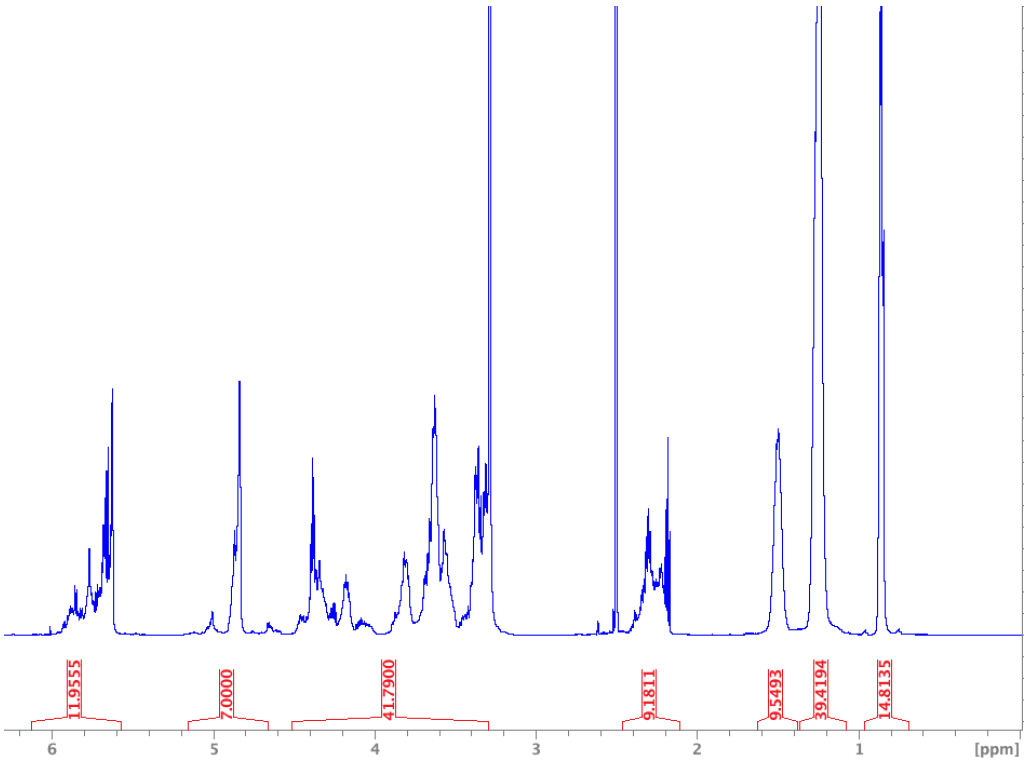

Figure 7.3. ^{1}H-NMR spectrum of ACD3 with a DS of 4.9

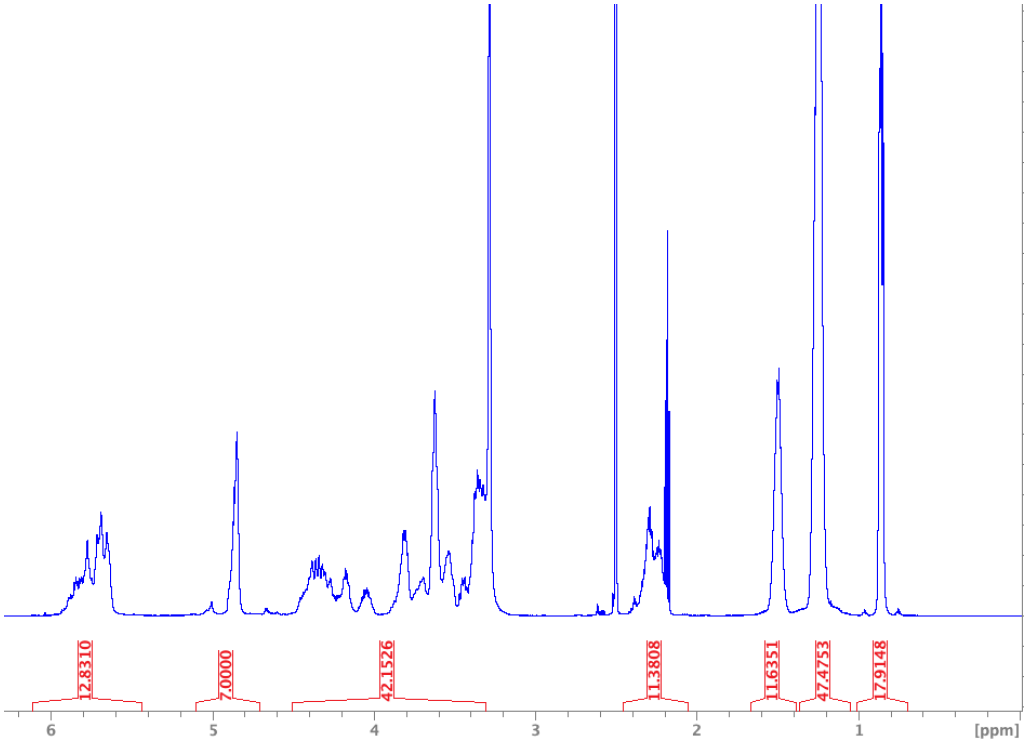

Figure 7.4. [1]H-NMR spectrum of ACD4 with a DS of 5.9

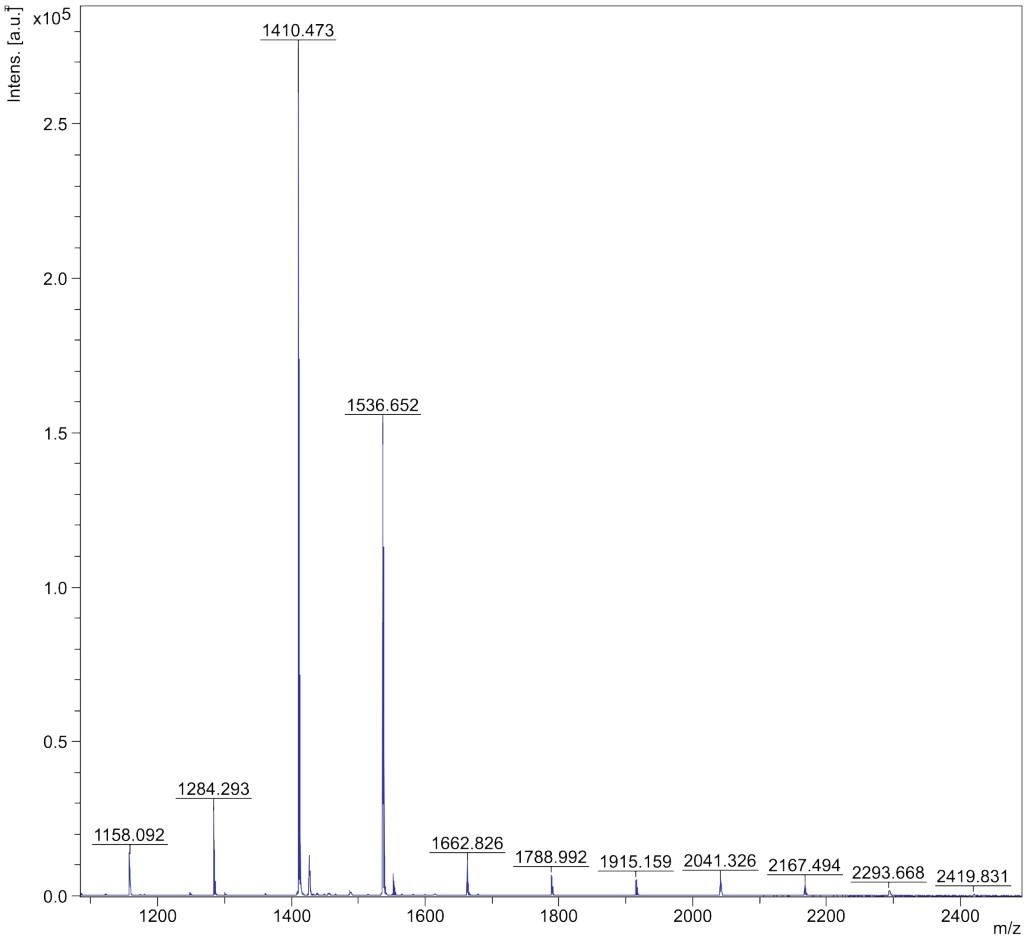

Figure 7.5. MS spectrum of ACD1 with a DS of 2.50

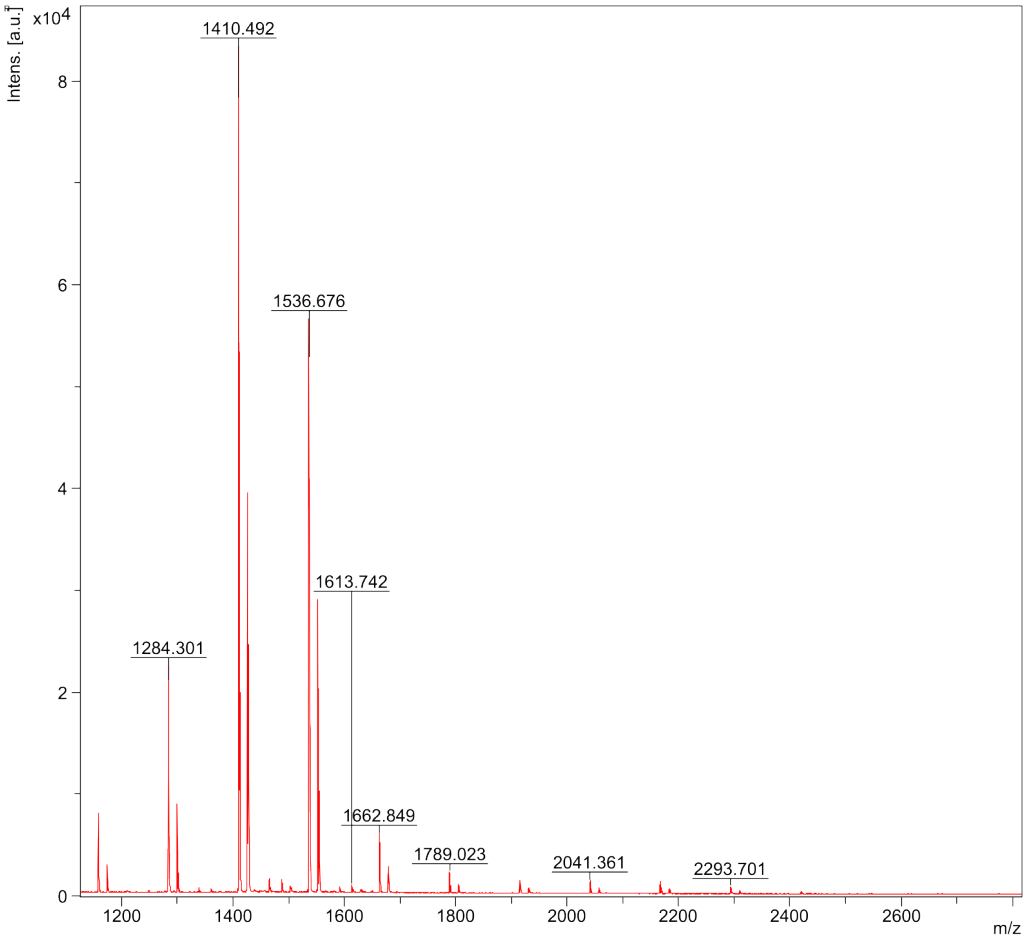

Figure 7.6. MS spectrum of ACD2 wiith a DS of 2.45

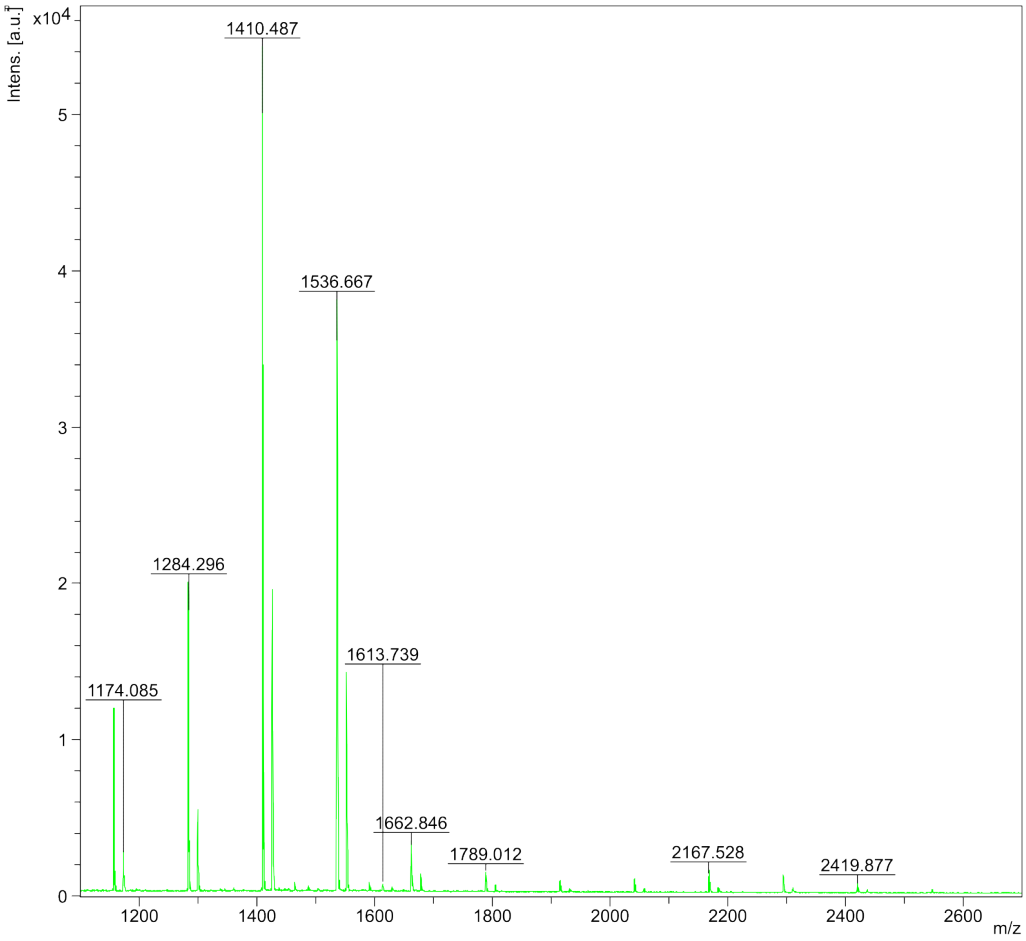

Figure 7.7. MS spectrum of ACD3 with a DS of 2.49

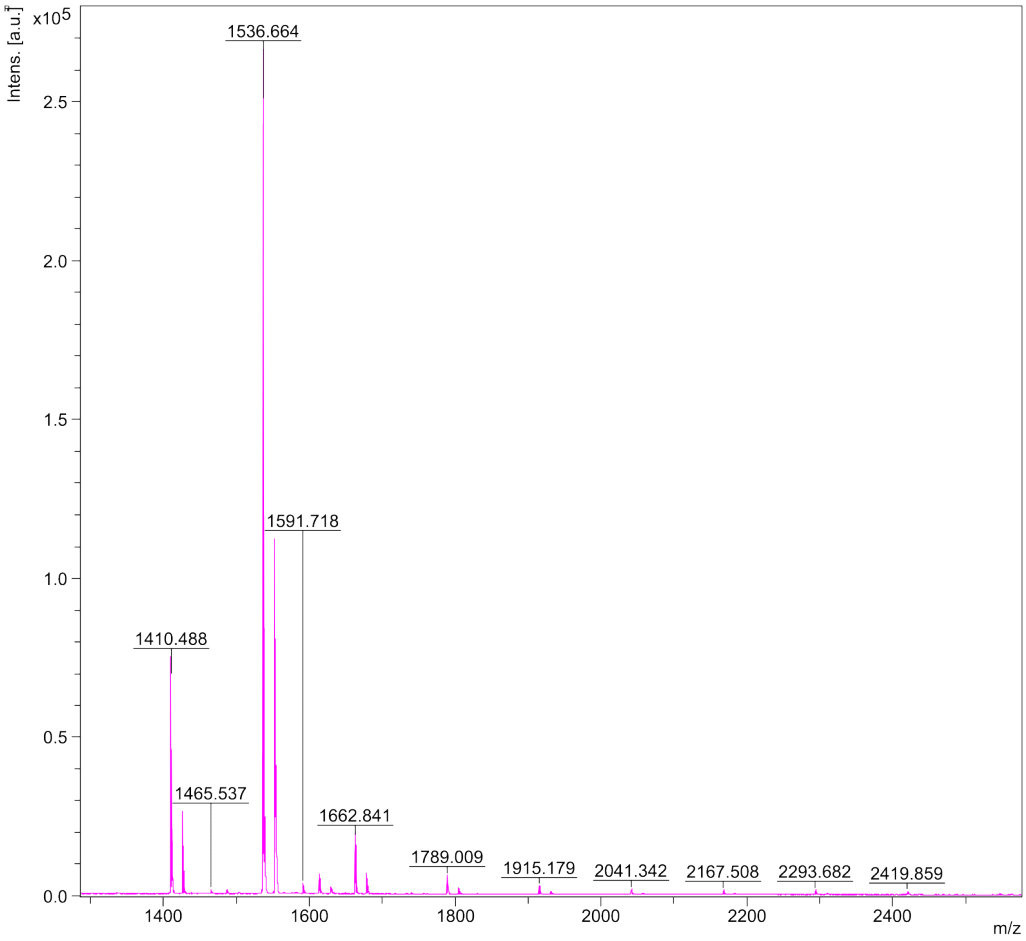

Figure 7.8. MS spectrum of ACD4 with a DS of 2.98

E/W ratios for the used ACDs 8

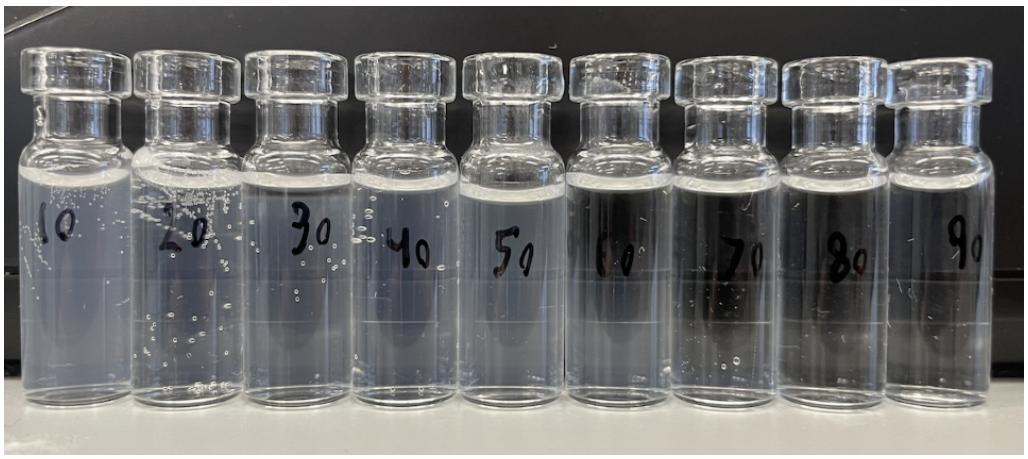

Figure 8.1. E/W ratios of ACD1

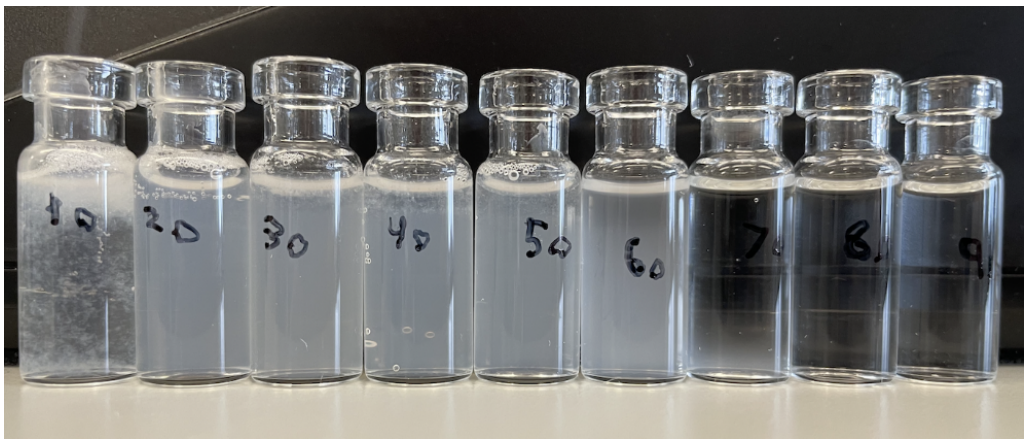

Figure 8.2. E/W ratios of ACD2

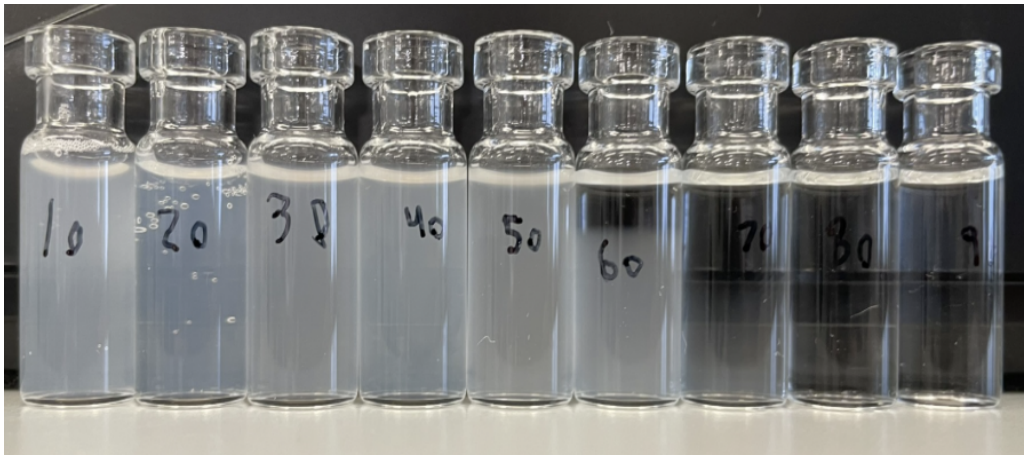

Figure 8.3. E/W ratios of ACD3

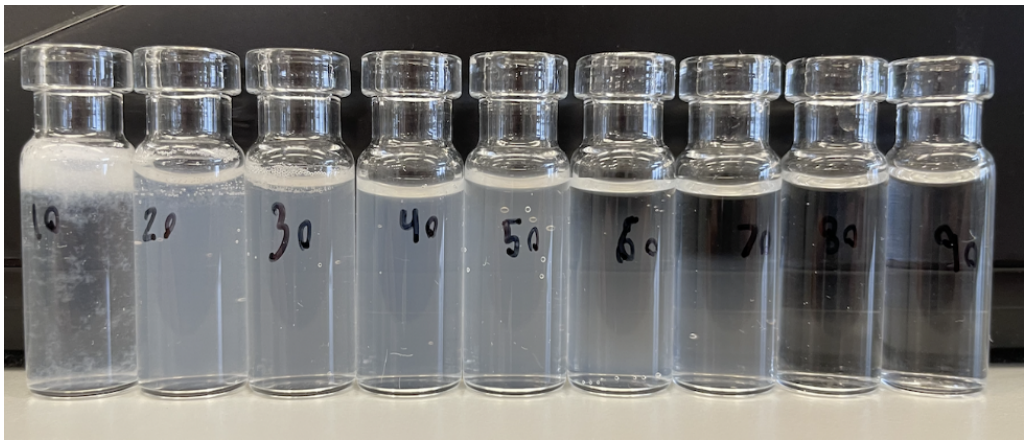

Figure 8.4. E/W ratios of ACD4

qNMR 9

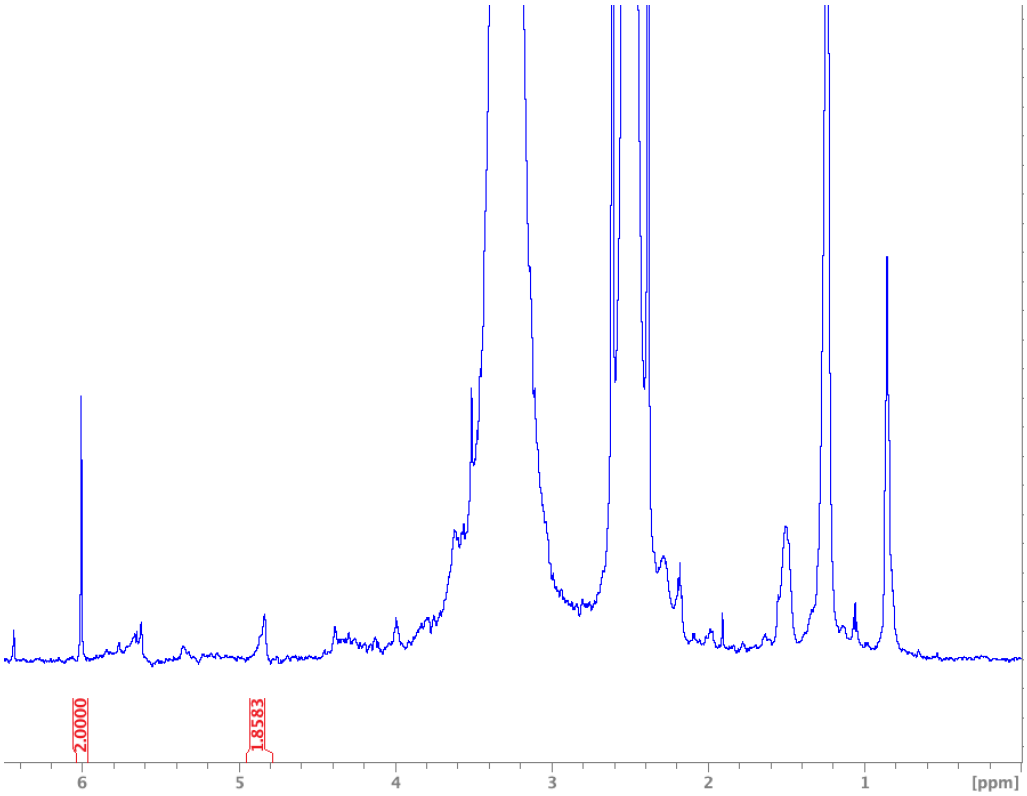

Figure 9.1. qNMR spectrum for ACD1. (PP of 5 g/m^2

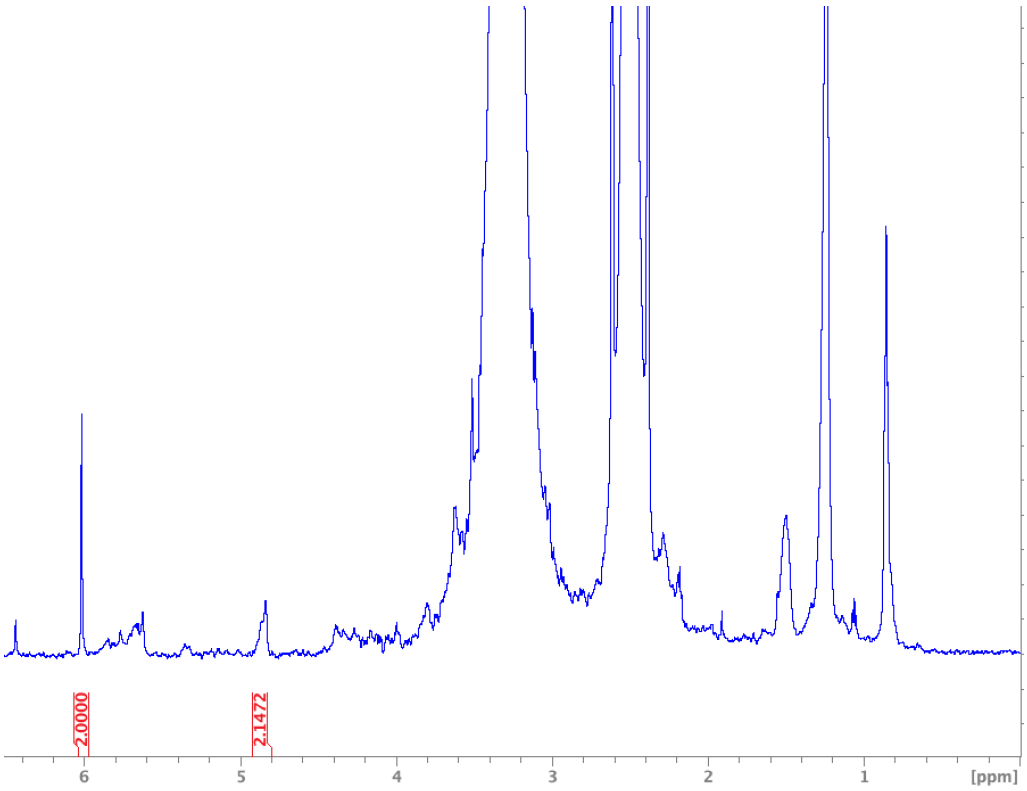

Figure 9.2. qNMR spectrum for ACD1. (PP of 5 g/m^2

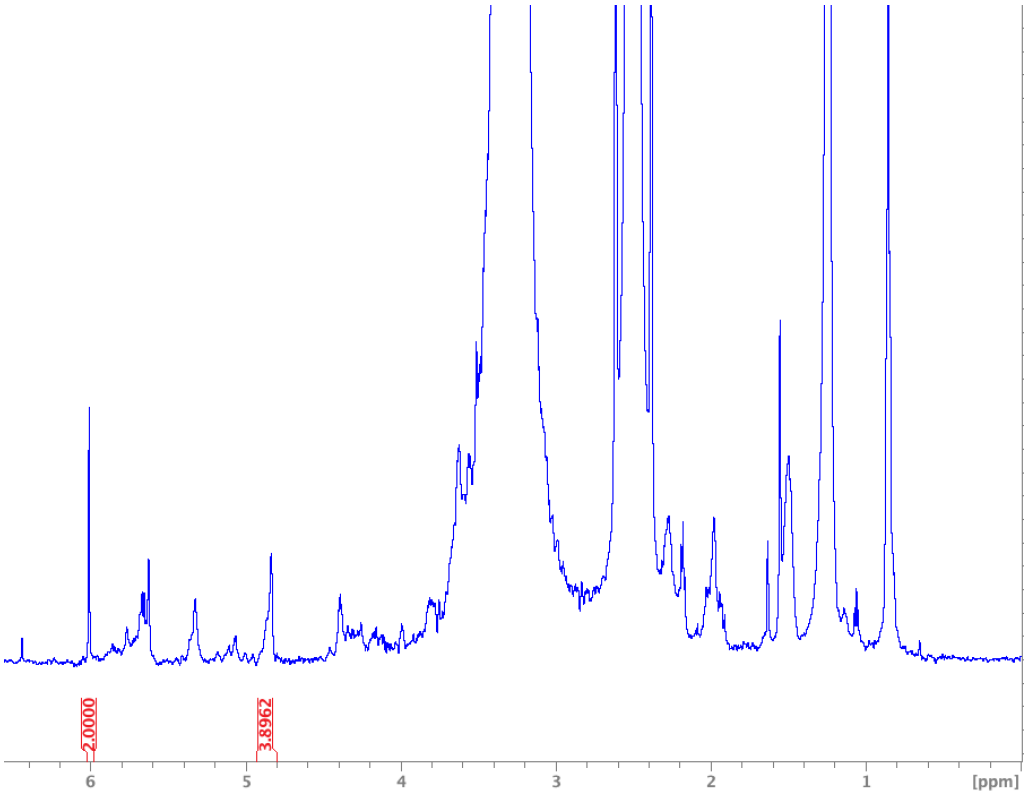

Figure 9.3. qNMR spectrum for ACD1. (PP of 10 g/m^2

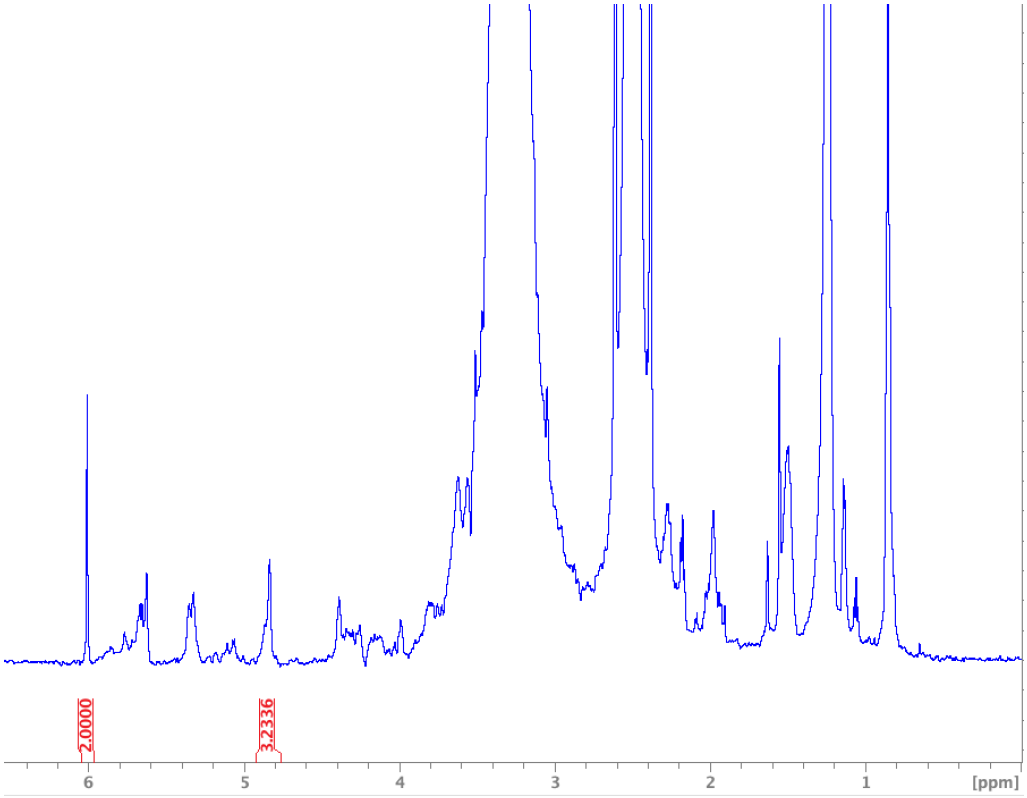

Figure 9.4. qNMR spectrum for ACD1. (PP of 10 g/m^2

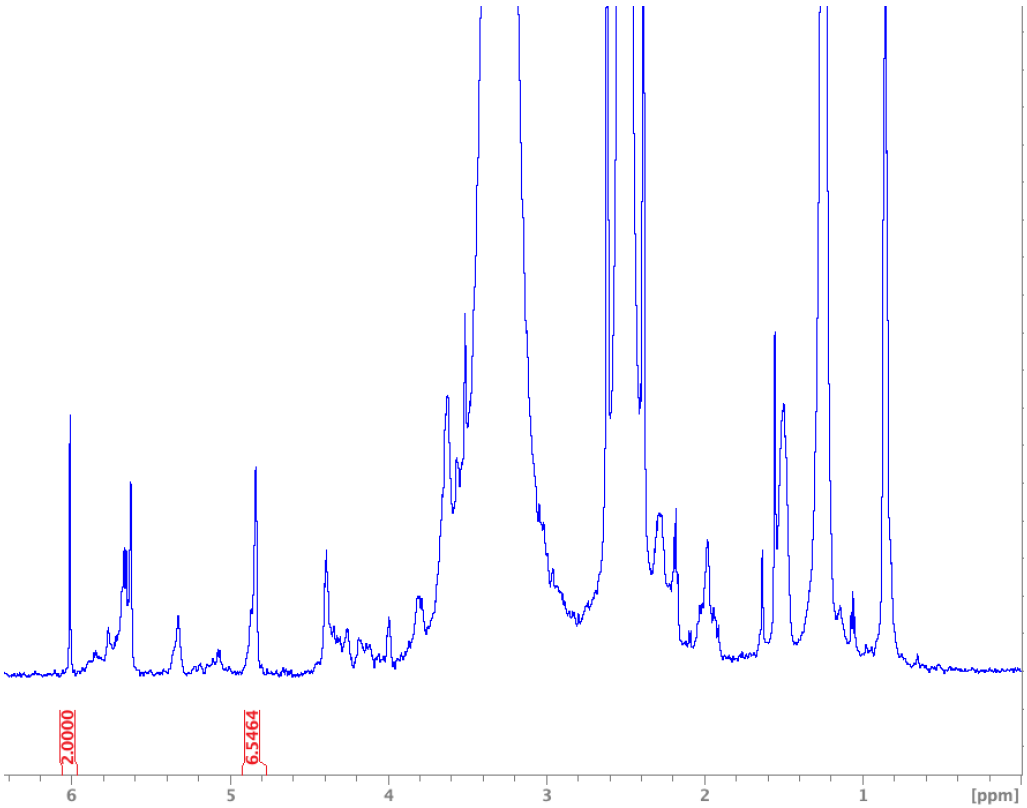

Figure 9.5. qNMR spectrum for ACD1. (PP of 20 g/m^2

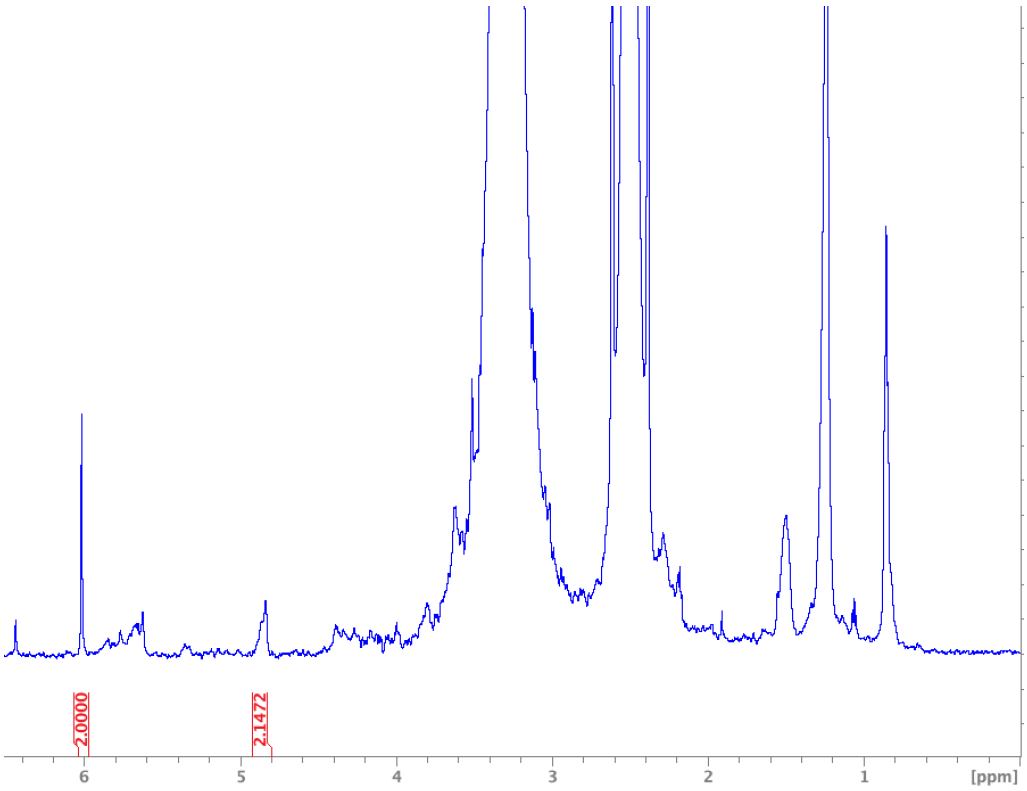

Figure 9.6. qNMR spectrum for ACD1. (PP of 20 g/m^2

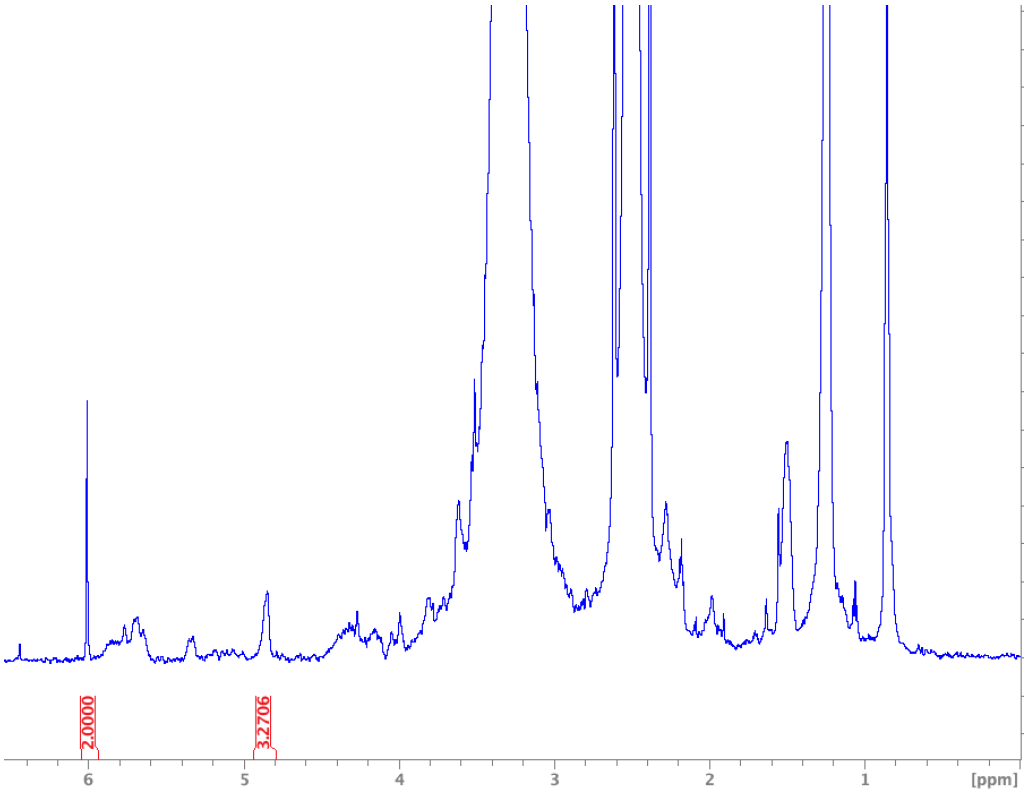

Figure 9.7. qNMR spectrum for ACD4. (PP of 5 g/m^2

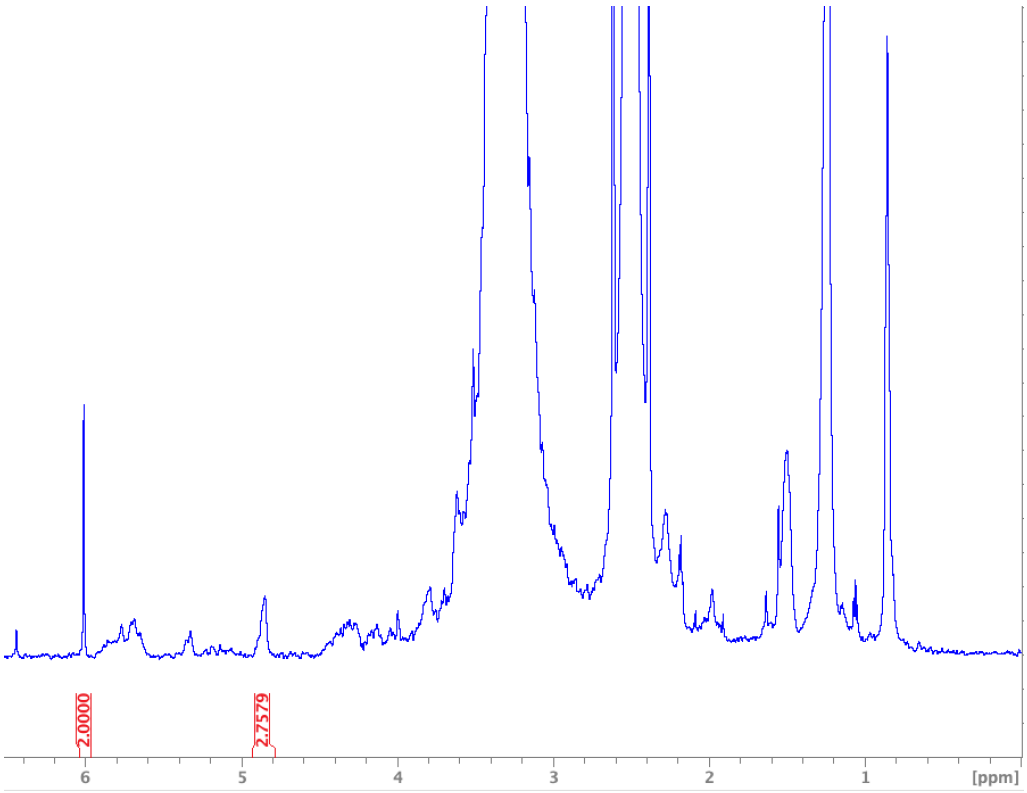

Figure 9.8. qNMR spectrum for ACD4. (PP of 5 g/m^2

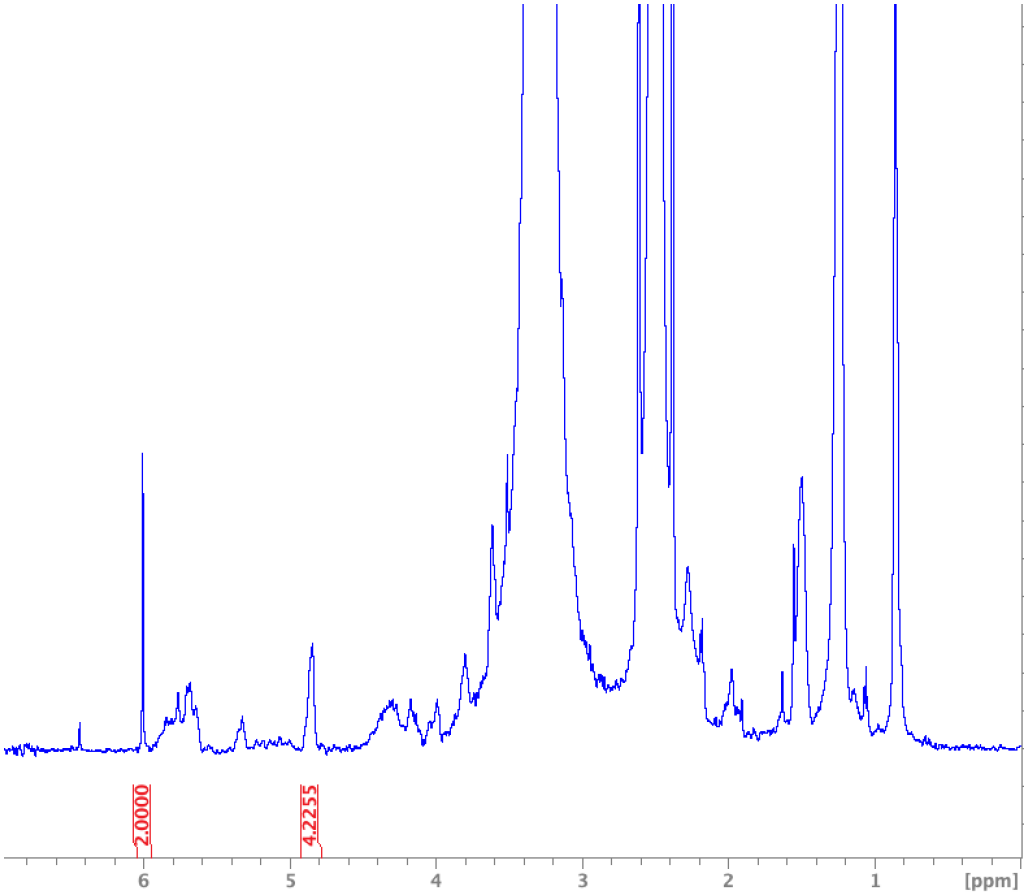

Figure 9.9. qNMR spectrum for ACD4. (PP of 10 g/m^2

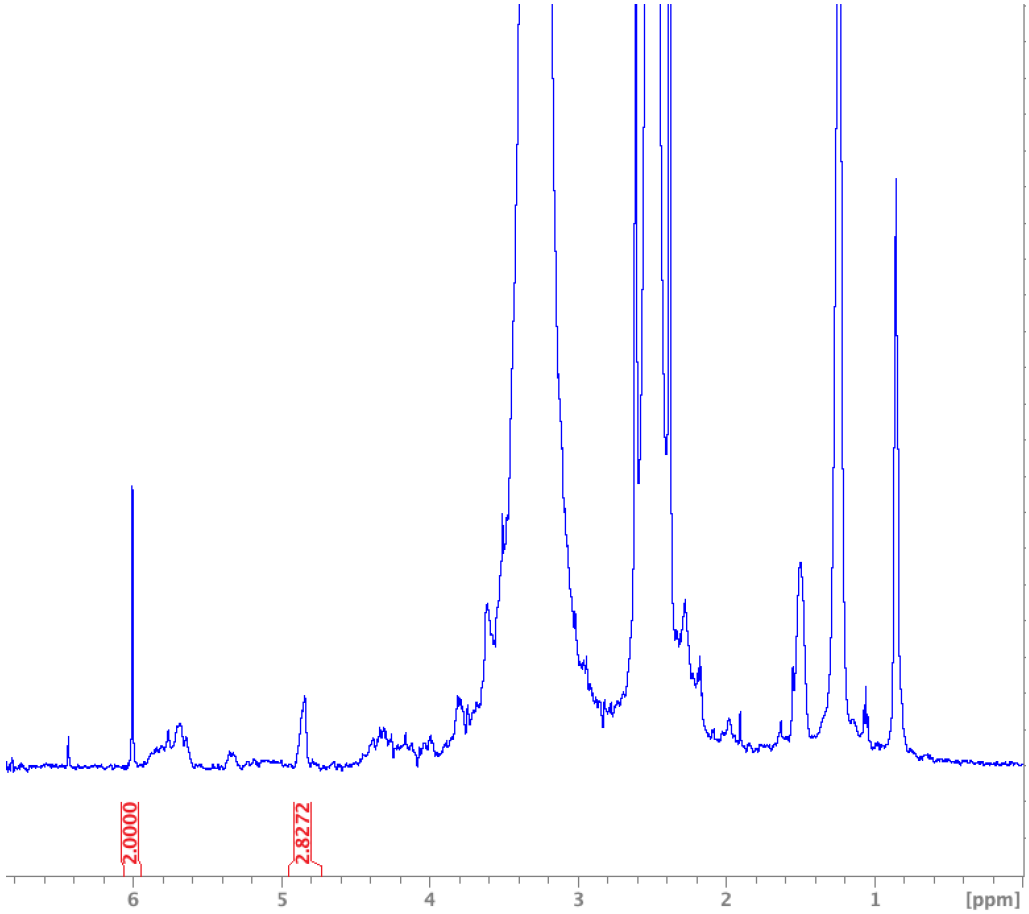

Figure 9.10. qNMR spectrum for ACD4. (PP of 10 g/m^2

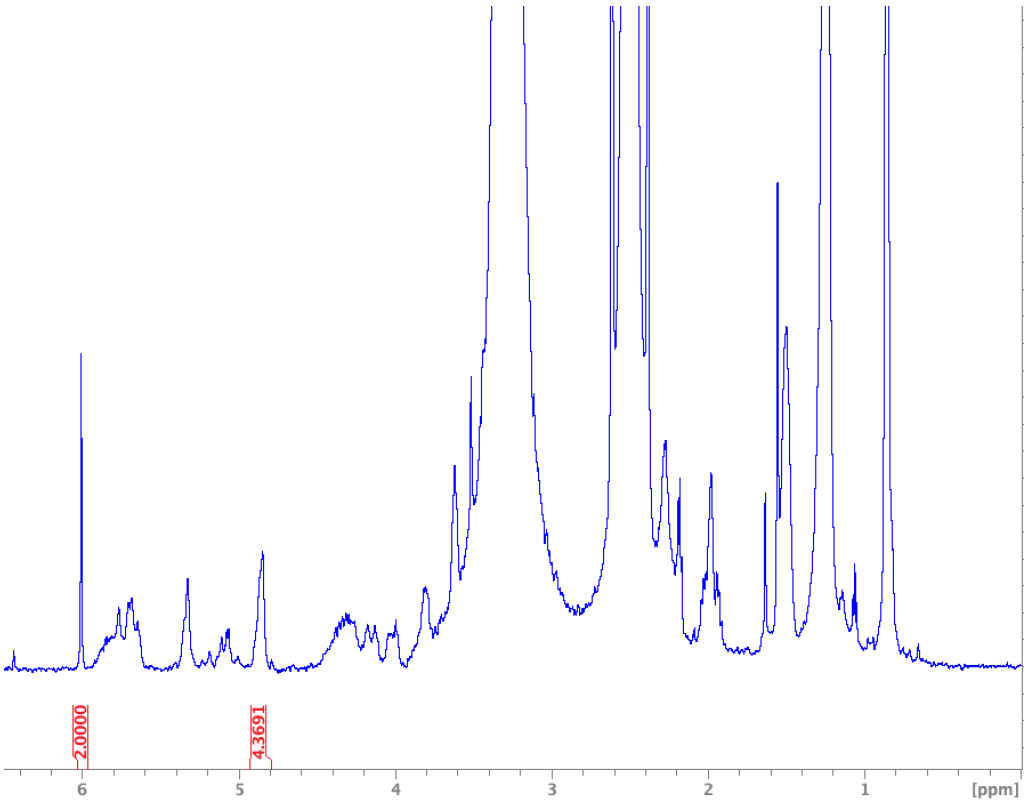

Figure 9.11. qNMR spectrum for ACD4. (PP of 20 g/m^2

SEM 10

10.1 Coat formation of ACD1

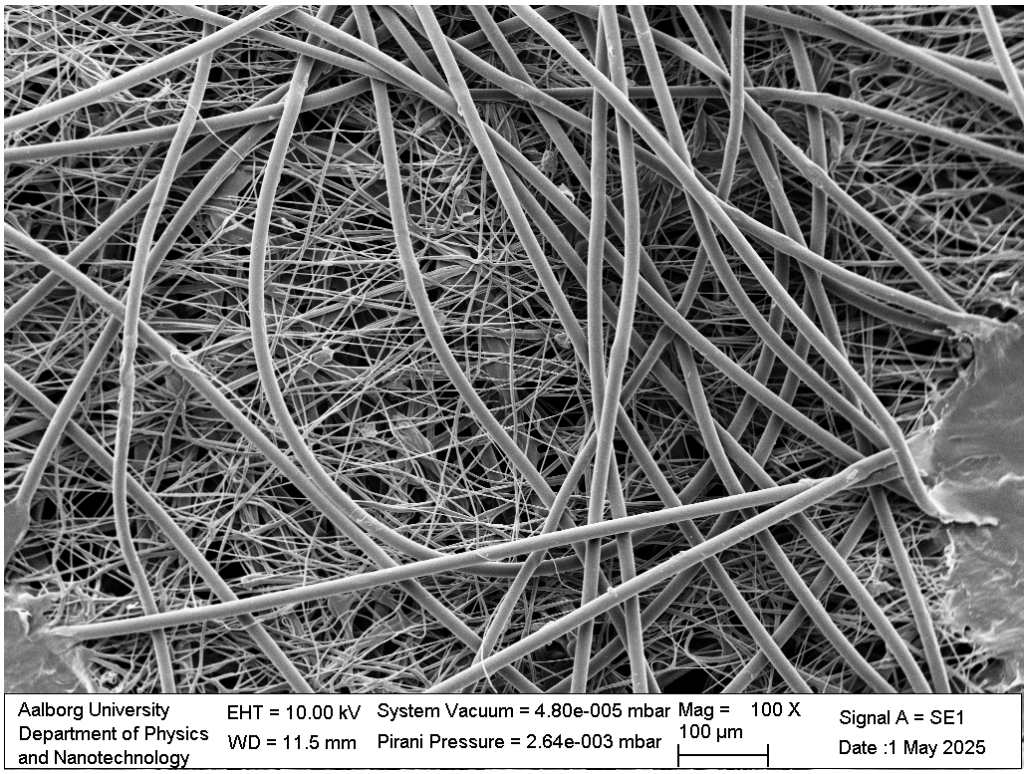

Figure 10.1. SEM of ACD1 coating

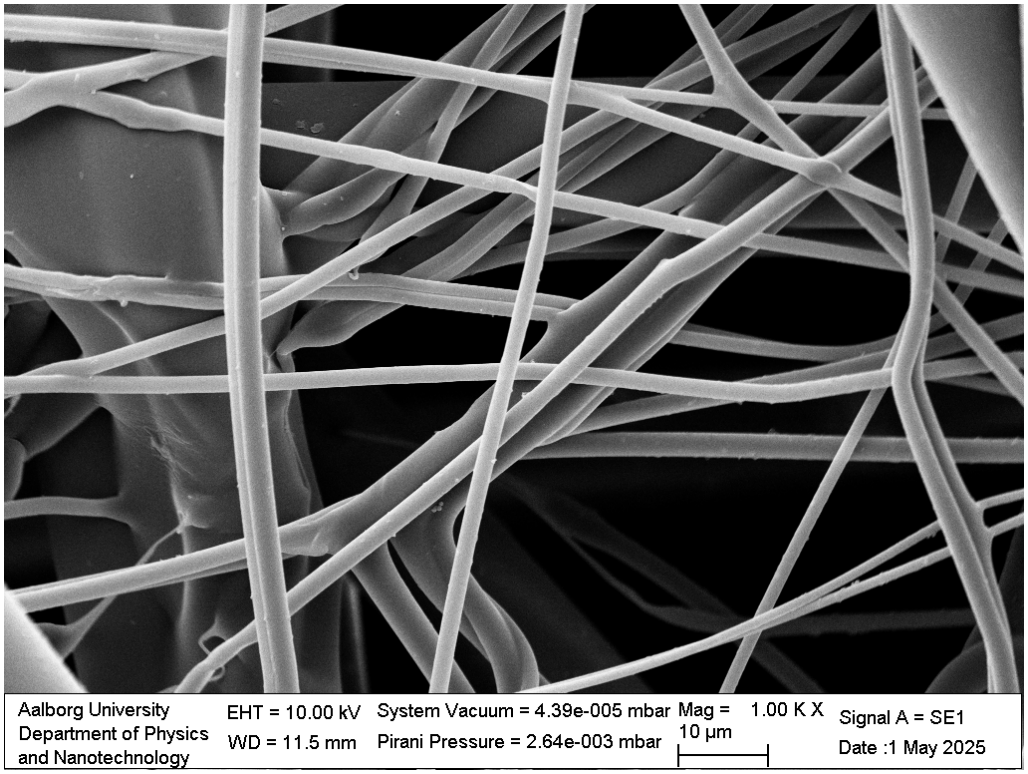

Figure 10.2. SEM of ACD1 coating

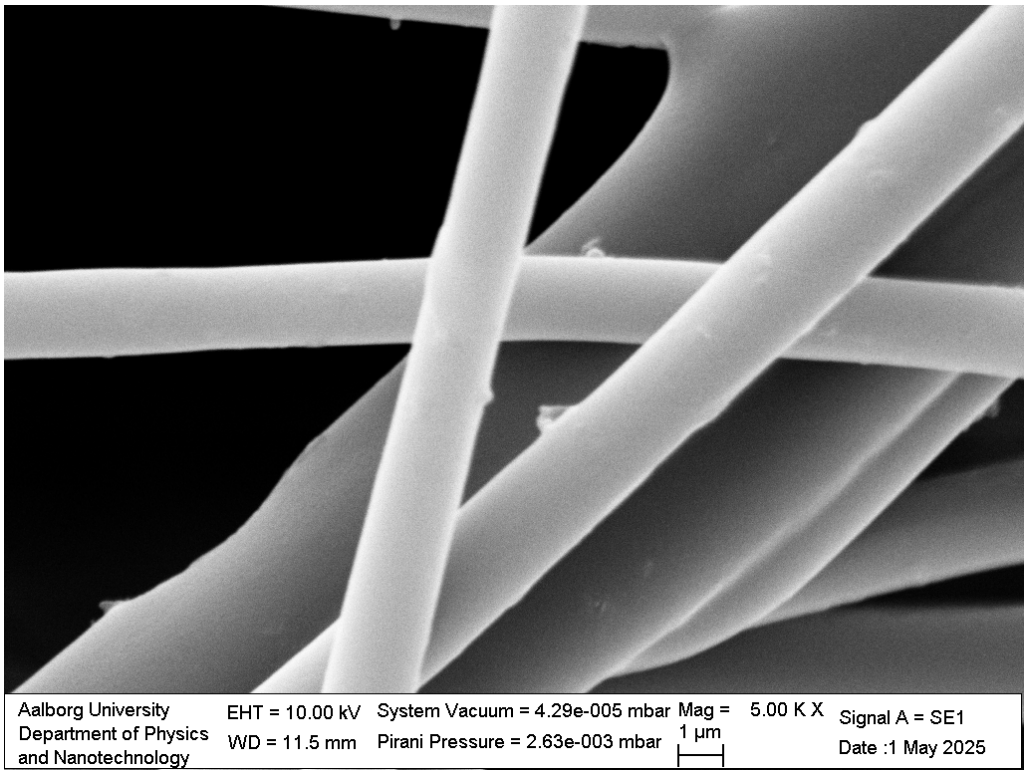

Figure 10.3. SEM of ACD1 coating

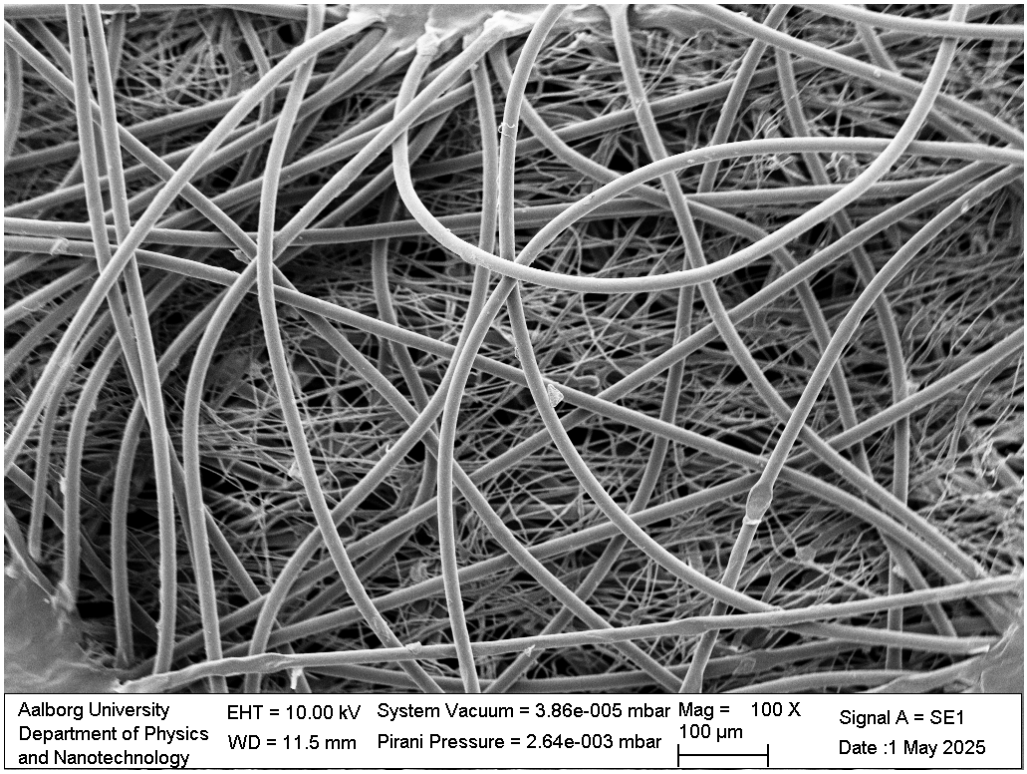

Figure 10.4. SEM of ACD1 coating

10.2 Coat formation of ACD4

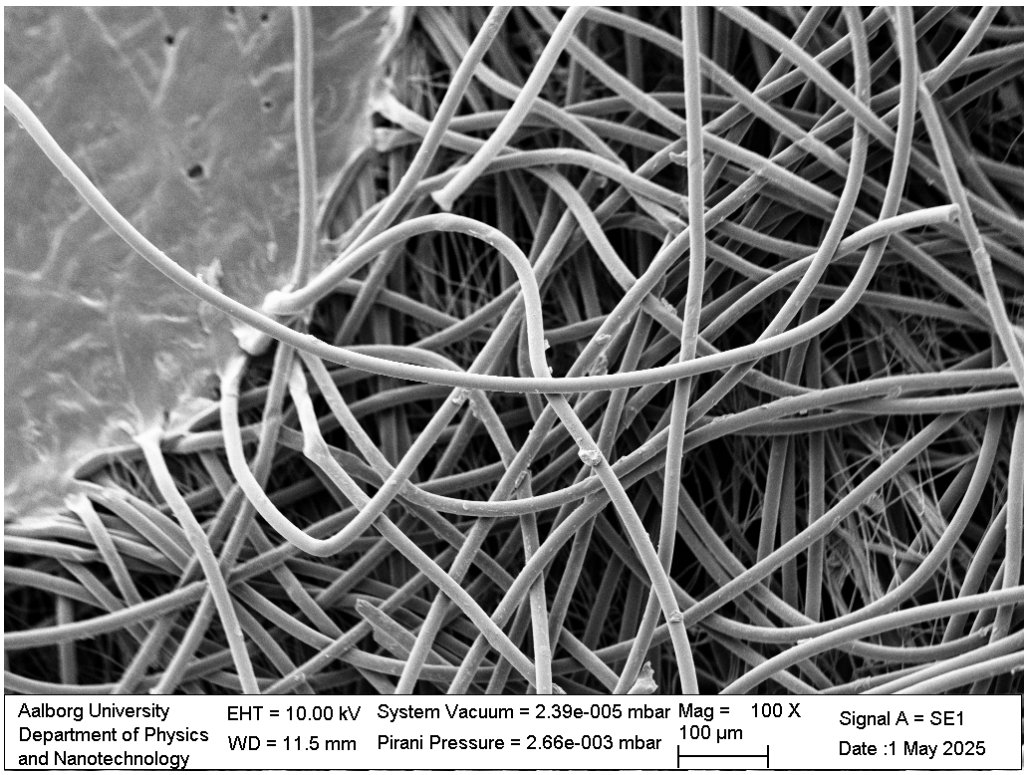

Figure 10.5. SEM of ACD4 coating

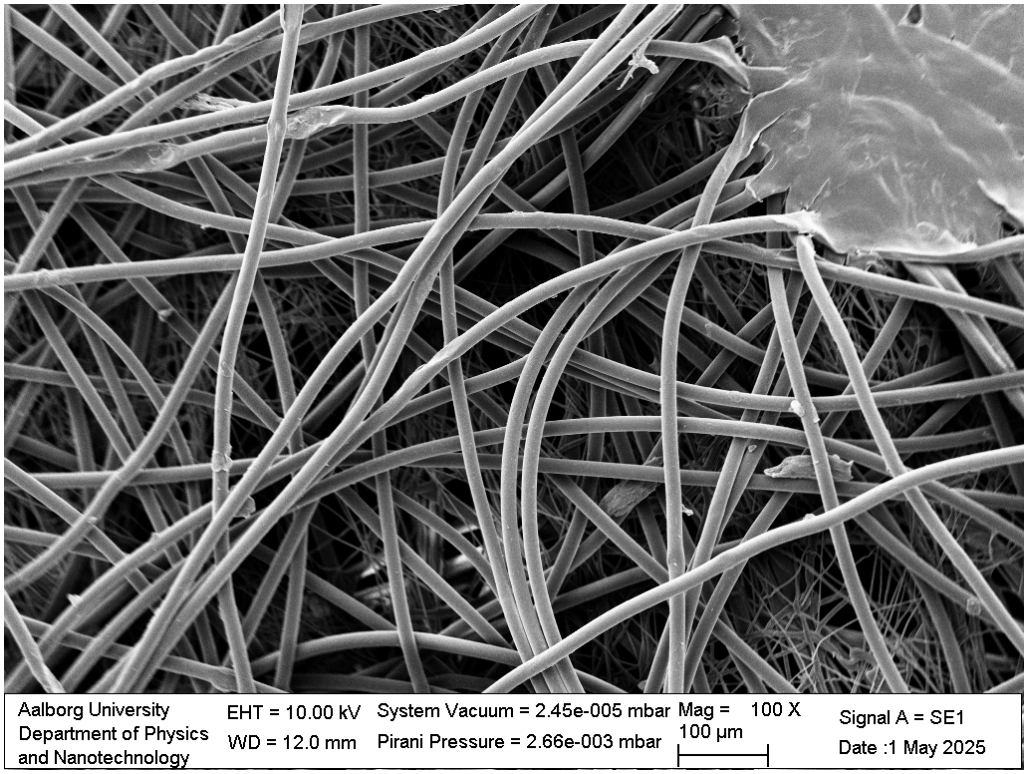

Figure 10.6. SEM of ACD4 coating

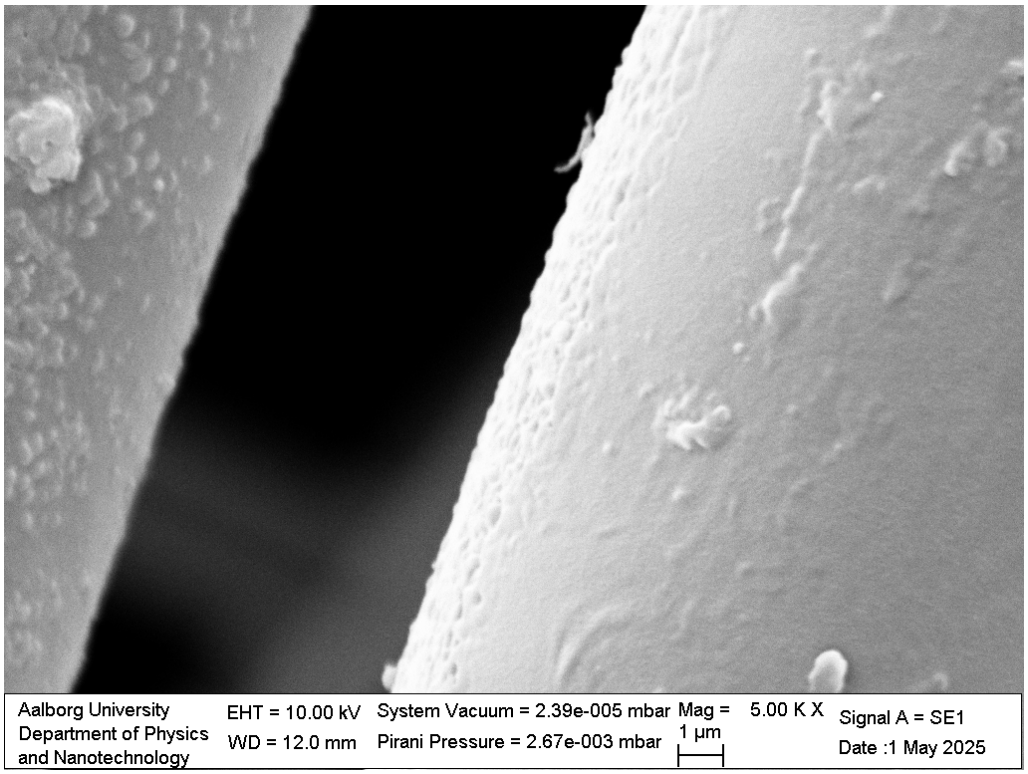

Figure 10.7. SEM of ACD4 coating

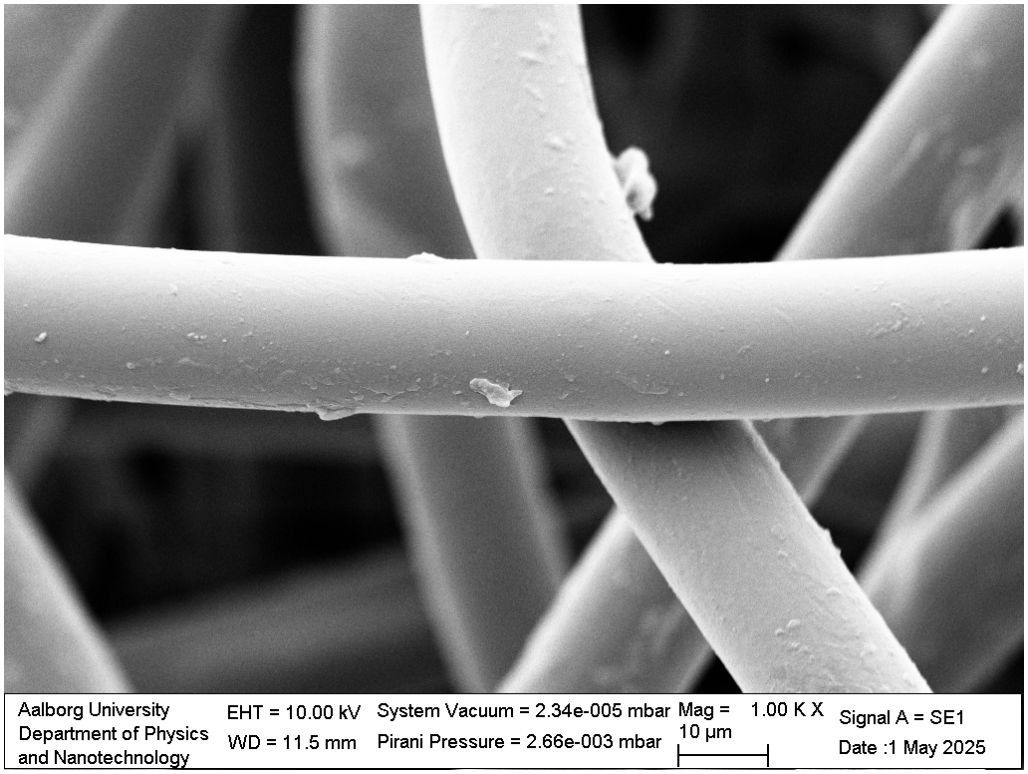

Figure 10.8. SEM of ACD4 coating

10.3 Reference

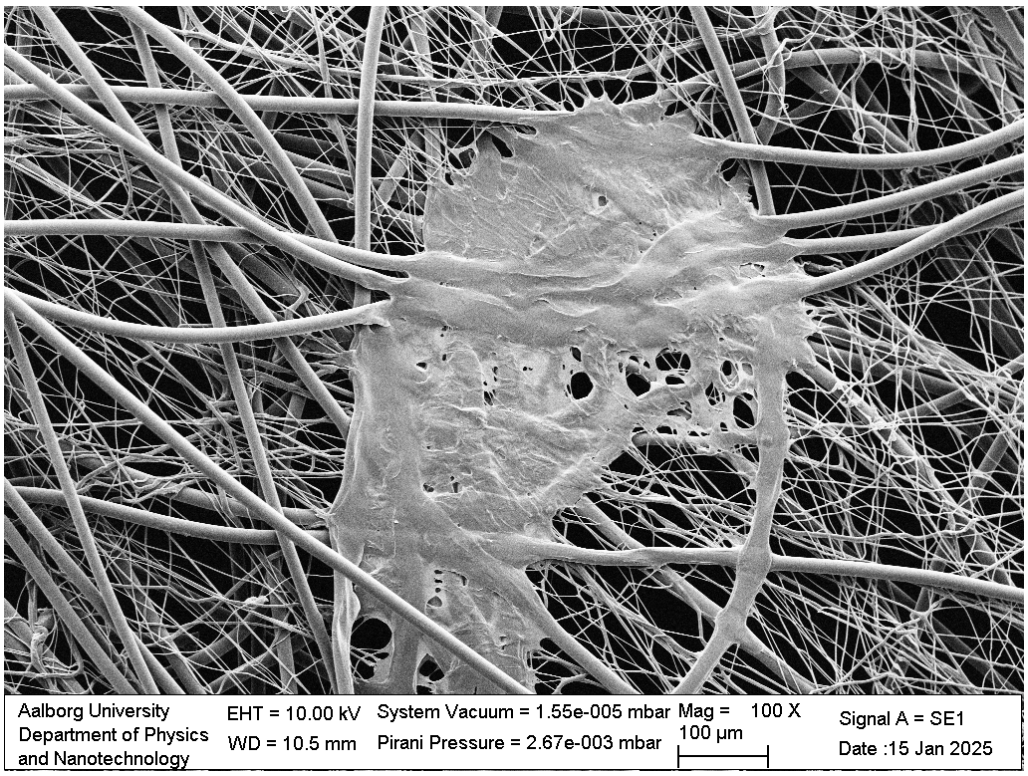

Figure 10.9. Non-coated PP reference

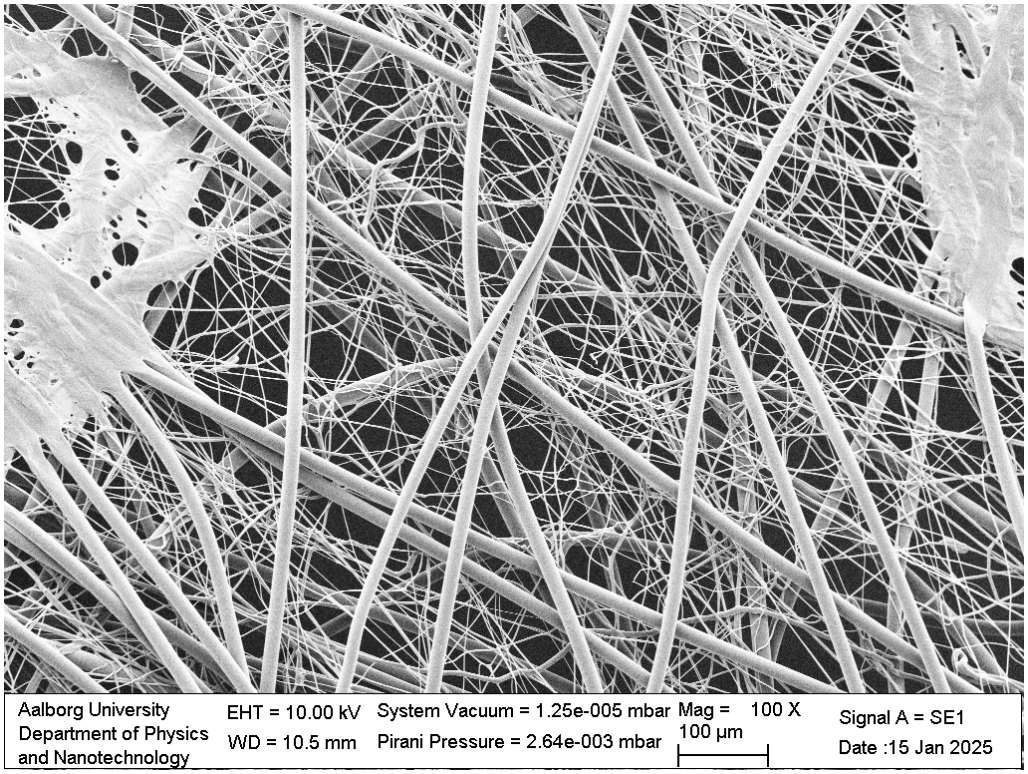

Figure 10.10. Non-coated PP reference

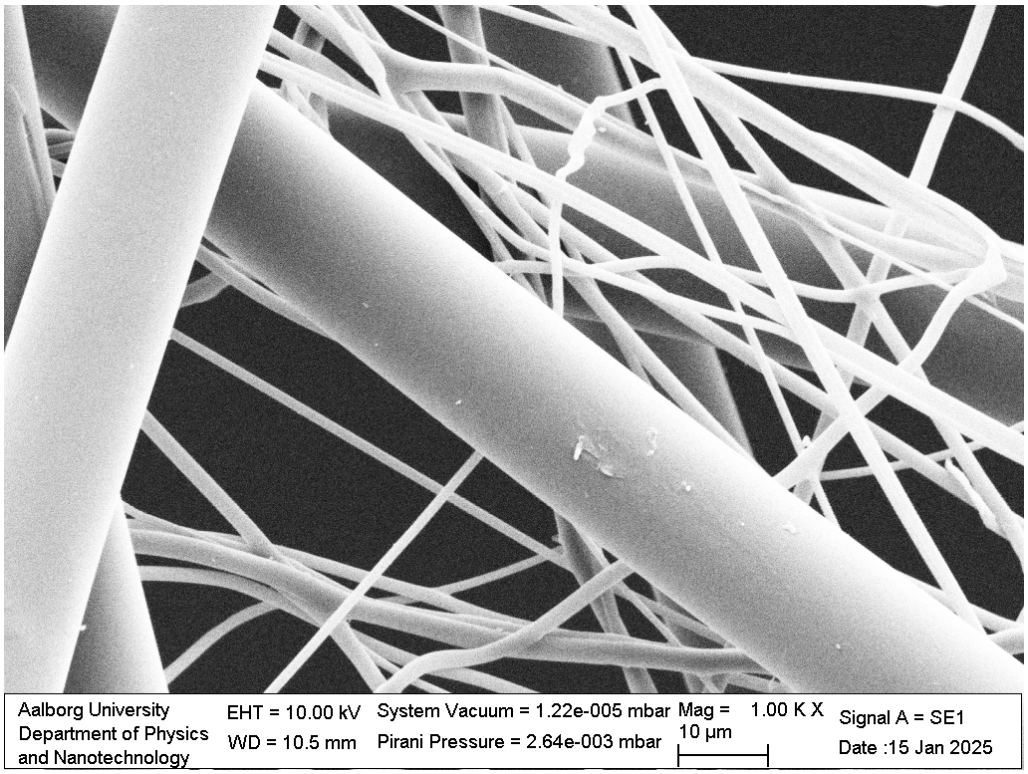

Figure 10.11. Non-coated PP reference

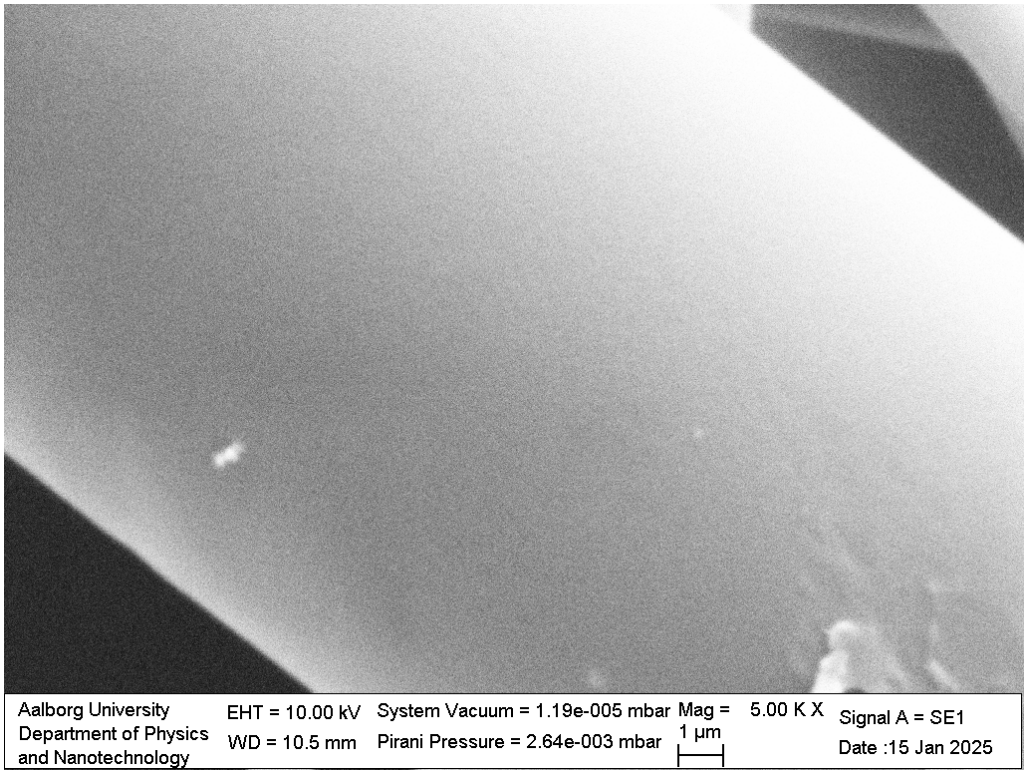

Figure 10.12. Non-coated PP reference

Adsorption experiment with PFOS 11

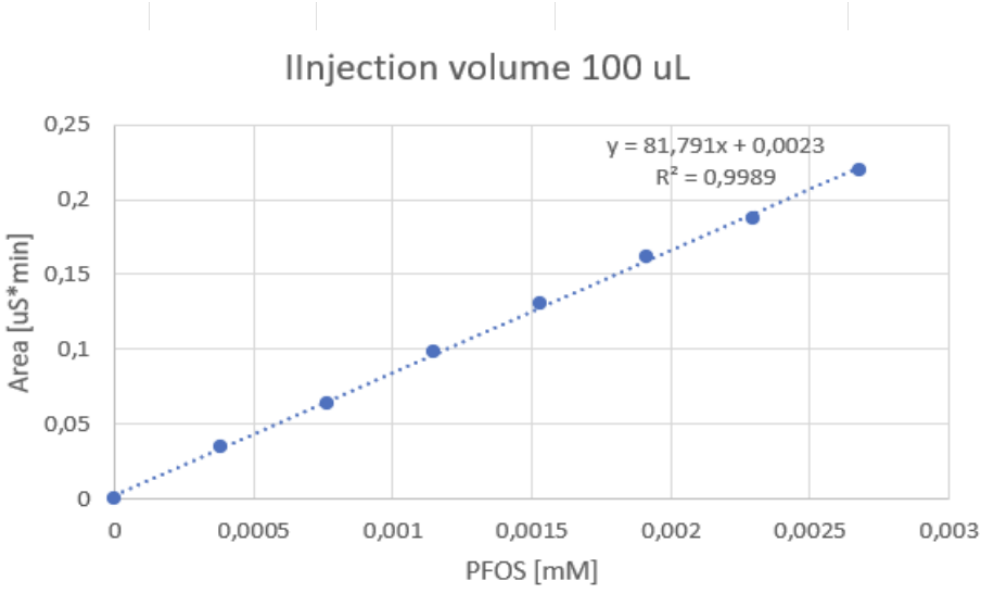

Figure 11.1. Standard curve of PFOS

Performance study with BPA 12

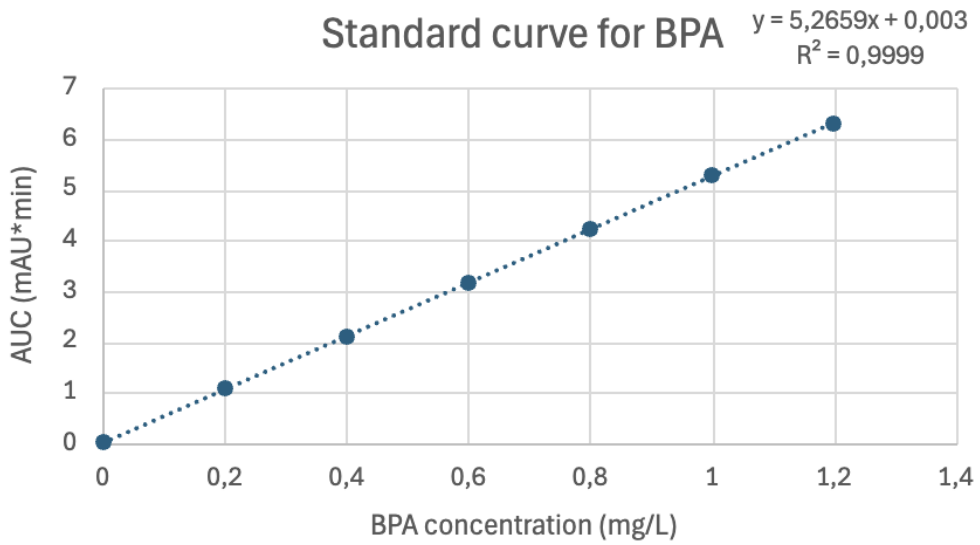

Figure 12.1. Standard curve of BPA

Contact angle measurements 13

13.1 PP coated at 5 g/m^2

Figure 13.1. ACD 1 with a contact angle of 39.51 °

Figure 13.2. ACD 1 with a contact angle of 46.88 °

Figure 13.3. ACD 1 with a contact angle of 38.27 °

Figure 13.4. ACD 2 with a contact angle of 55.25 °

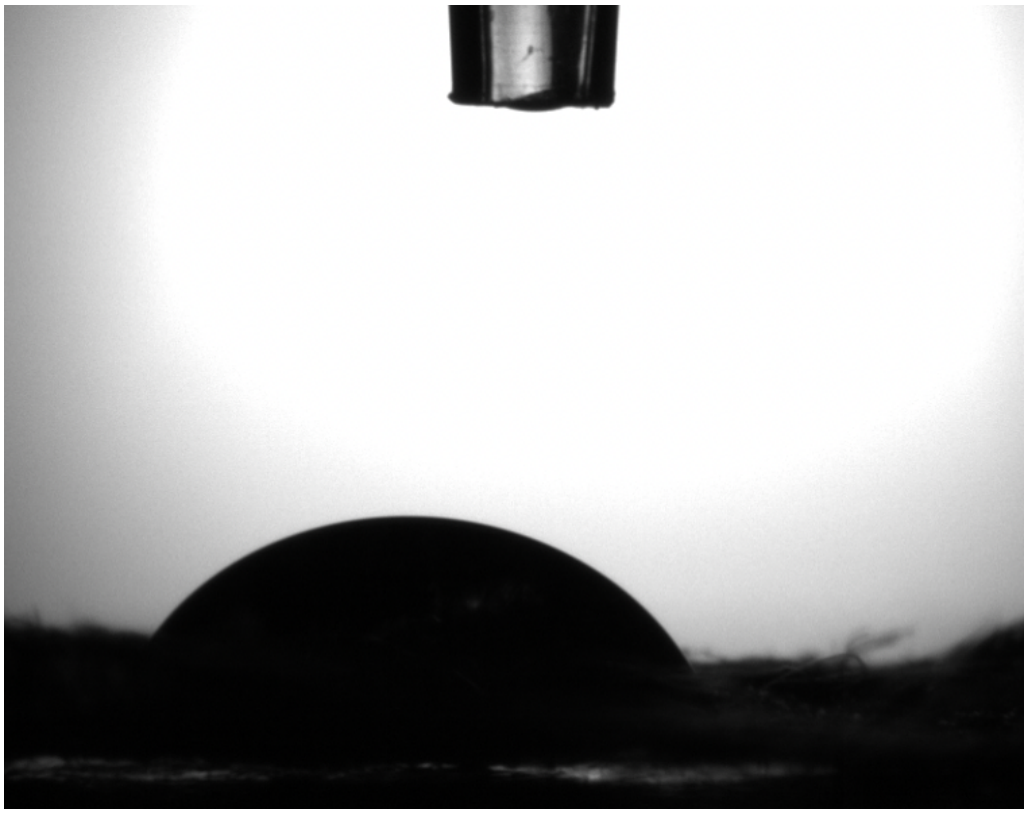

Figure 13.5. ACD 2 with a contact angle of 54.81 °

Figure 13.6. ACD 2 with a contact angle of 51.46 °

Figure 13.7. ACD 3 with a contact angle of 74.11 °

Figure 13.8. ACD 3 with a contact angle of 78.34 °

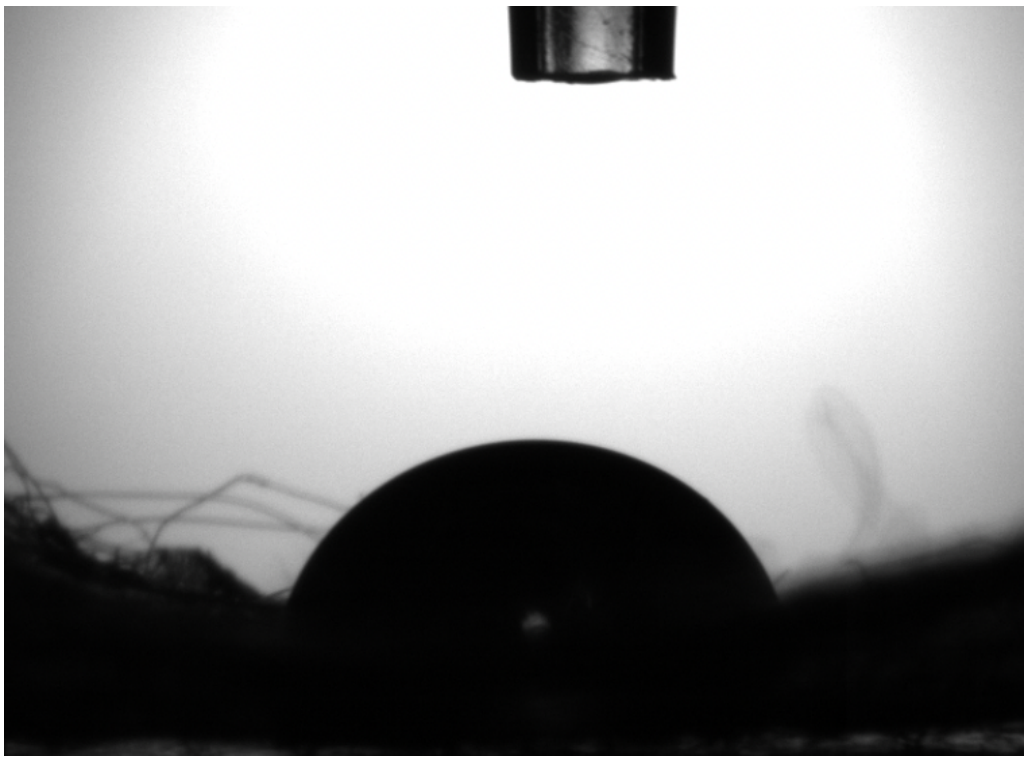

Figure 13.9. ACD 3 with a contact angle of 75.54 °

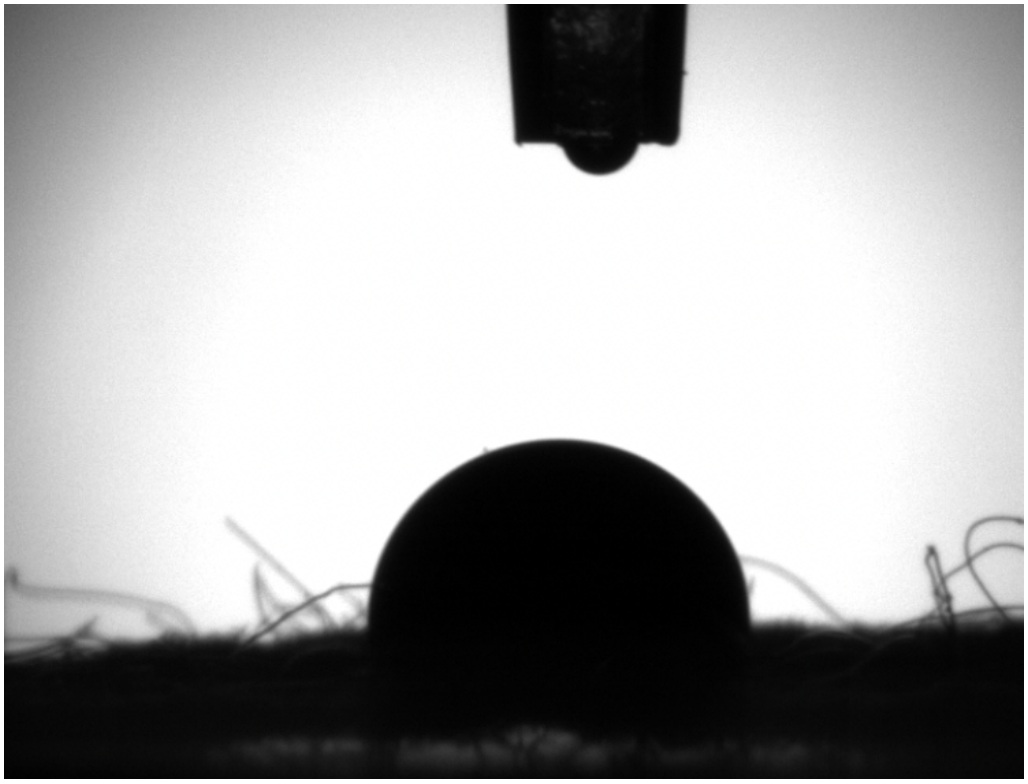

Figure 13.10. ACD 4 with a contact angle of 90.14 °

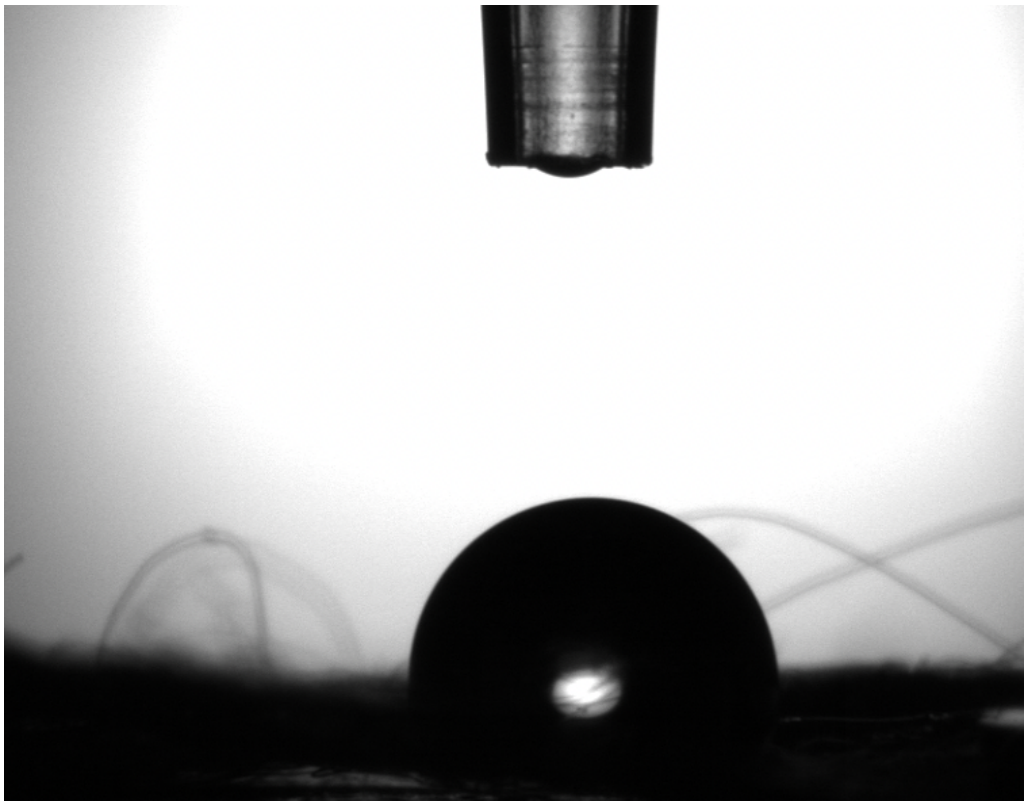

Figure 13.11. ACD 4 with a contact angle of 93.16 °

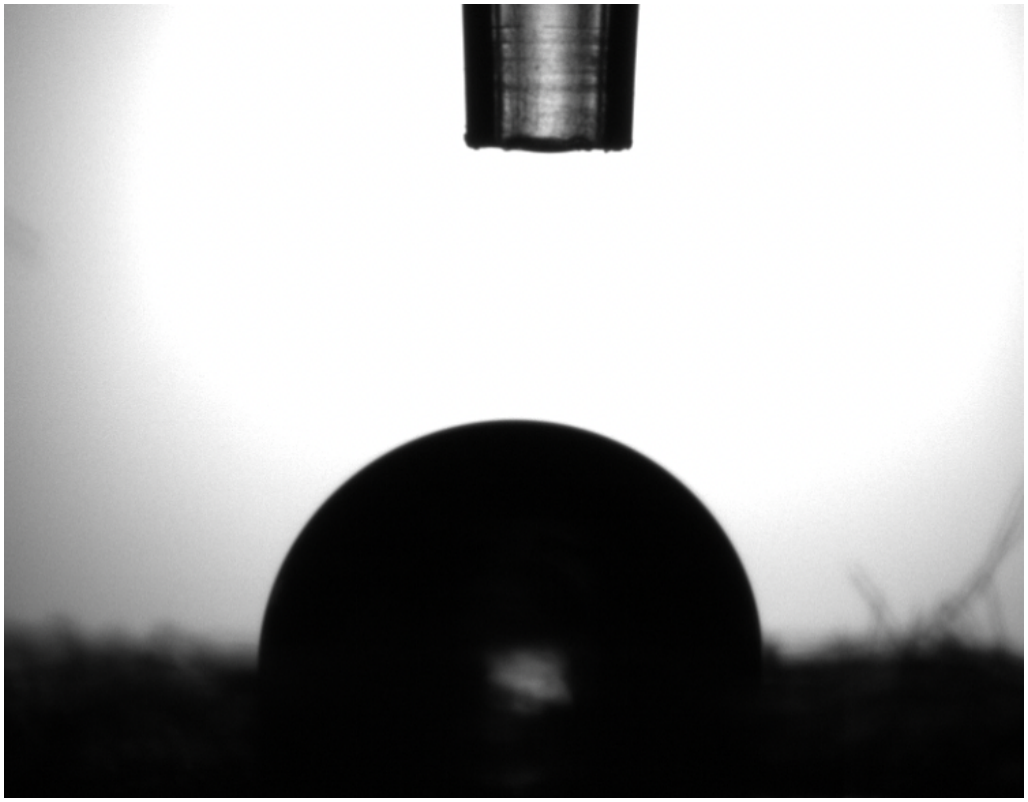

Figure 13.12. ACD 4 with a contact angle of 89.664 °

Figure 13.13. ACD 5 with a contact angle of 106.76 °

Figure 13.14. ACD 5 with a contact angle of 112.13 °

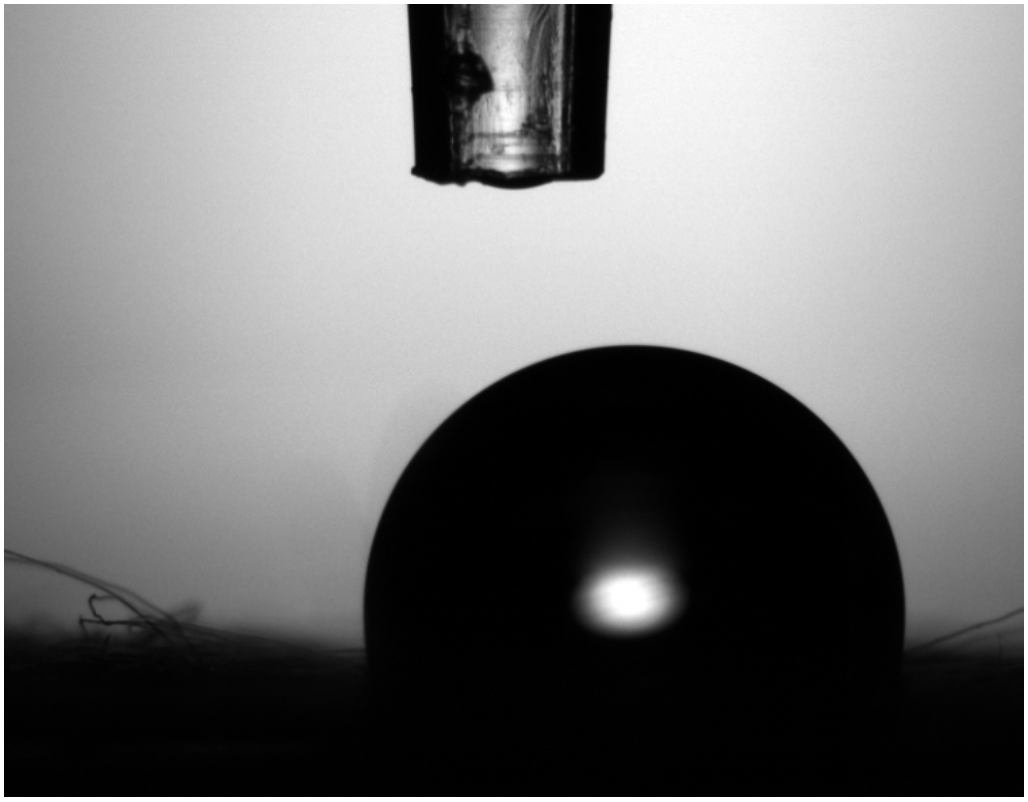

Figure 13.15. ACD 5 with a contact angle of 108.95 °

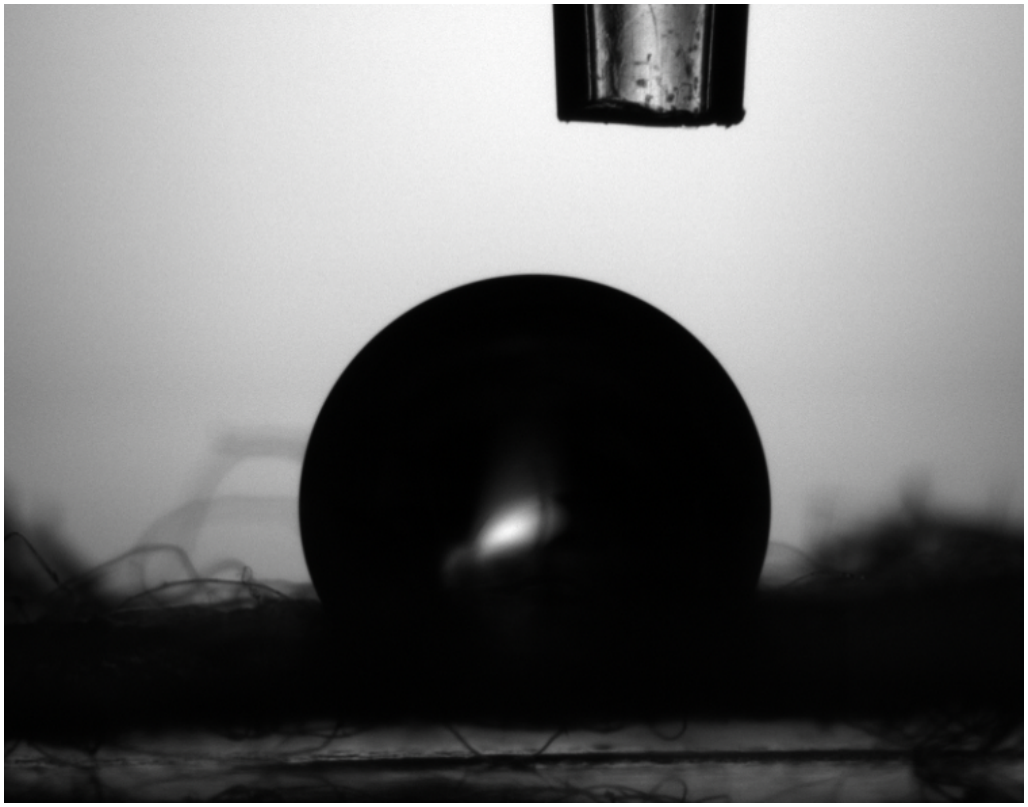

Figure 13.16. Reference with a contact angle of 117.24 °

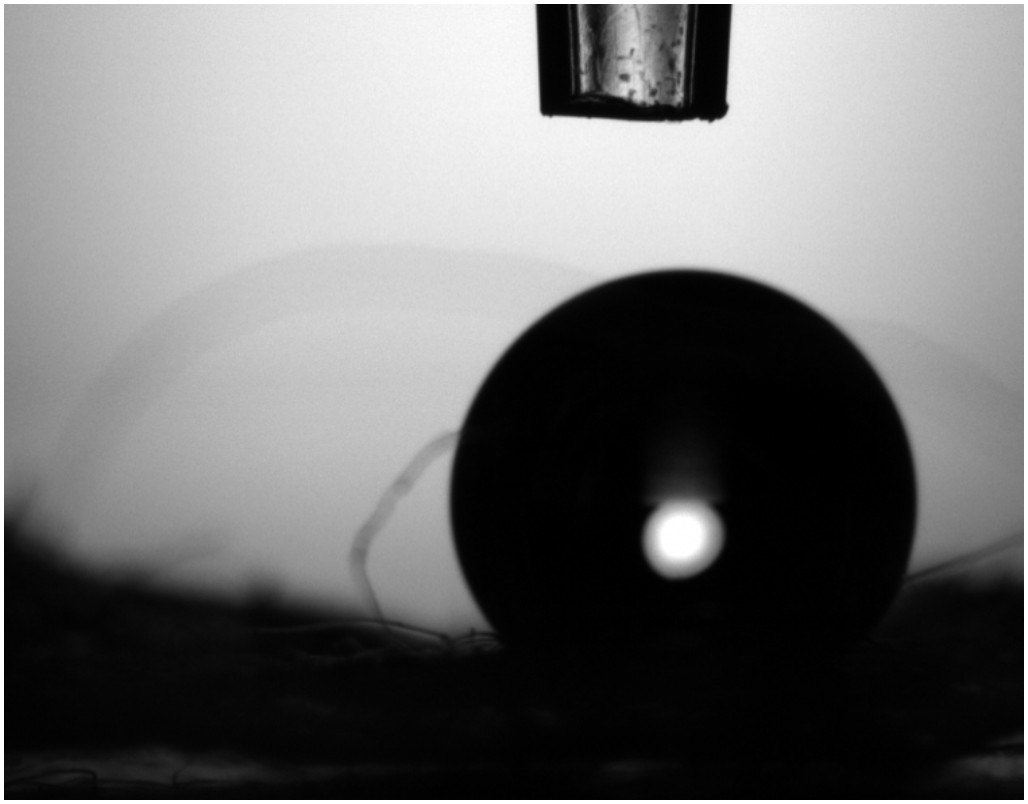

Figure 13.17. Reference with a contact angle of 119.16 °

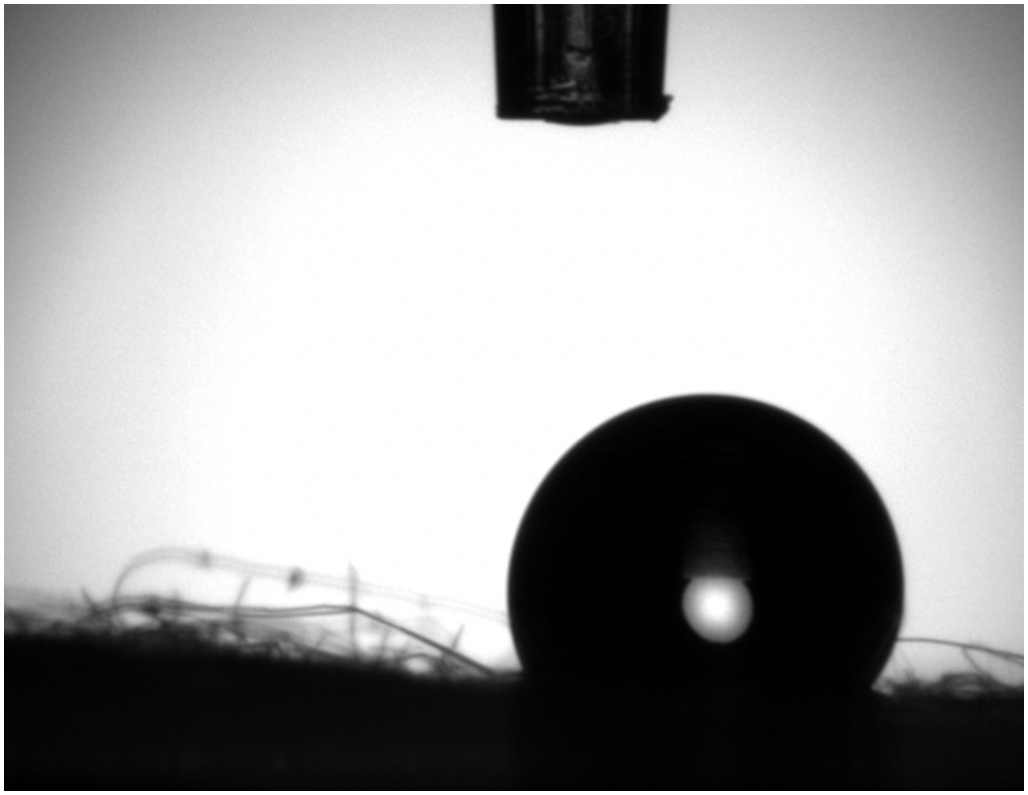

Figure 13.18. Reference with a contact angle of 123.95 °

13.2 PP coated at 10 g/m^2

Figure 13.19. ACD 1 with a contact angle of 37.51 °

Figure 13.20. ACD 1 with a contact angle of 44.27 °

Figure 13.21. ACD 1 with a contact angle of 49.75 °

Figure 13.22. ACD 2 with a contact angle of 52.33 °

Figure 13.23. ACD 2 with a contact angle of 51.9 °

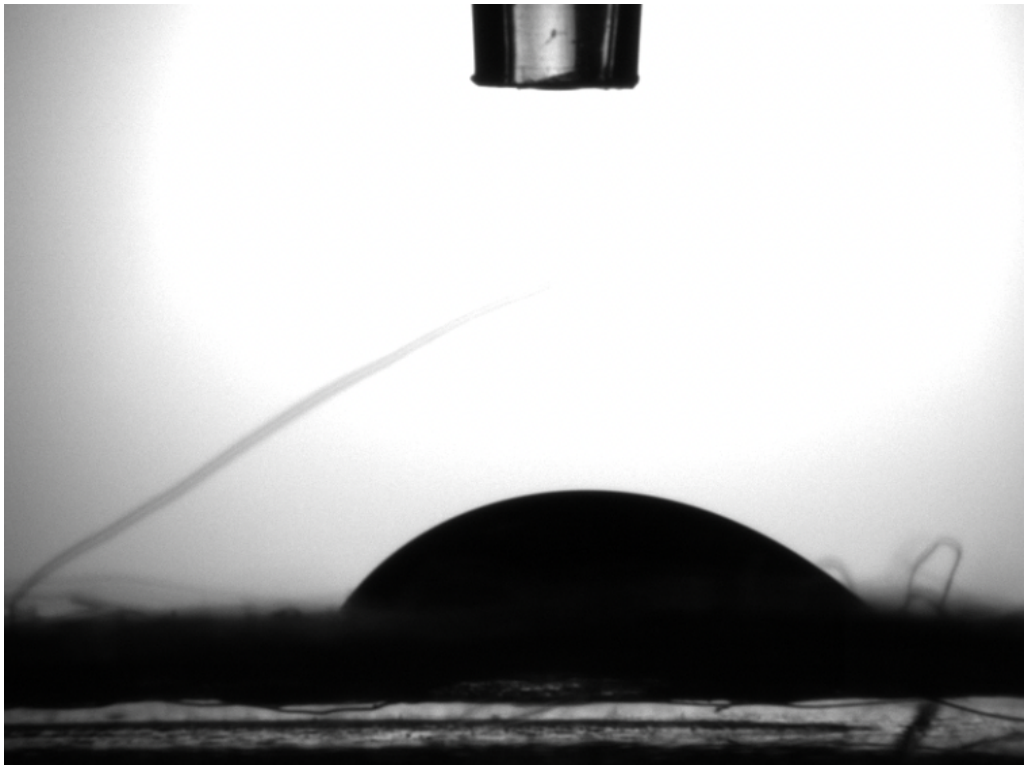

Figure 13.24. ACD 2 with a contact angle of 50.3 °

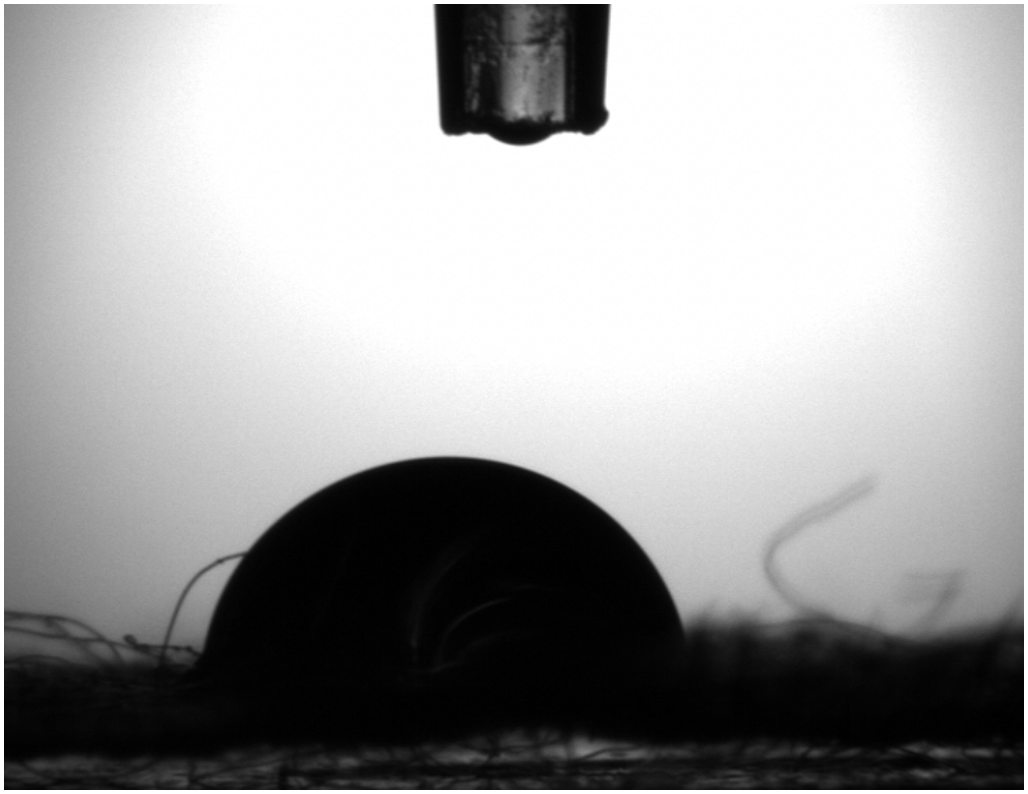

Figure 13.25. ACD 3 with a contact angle of 78.36 °

Figure 13.26. ACD 3 with a contact angle of 74.04 °

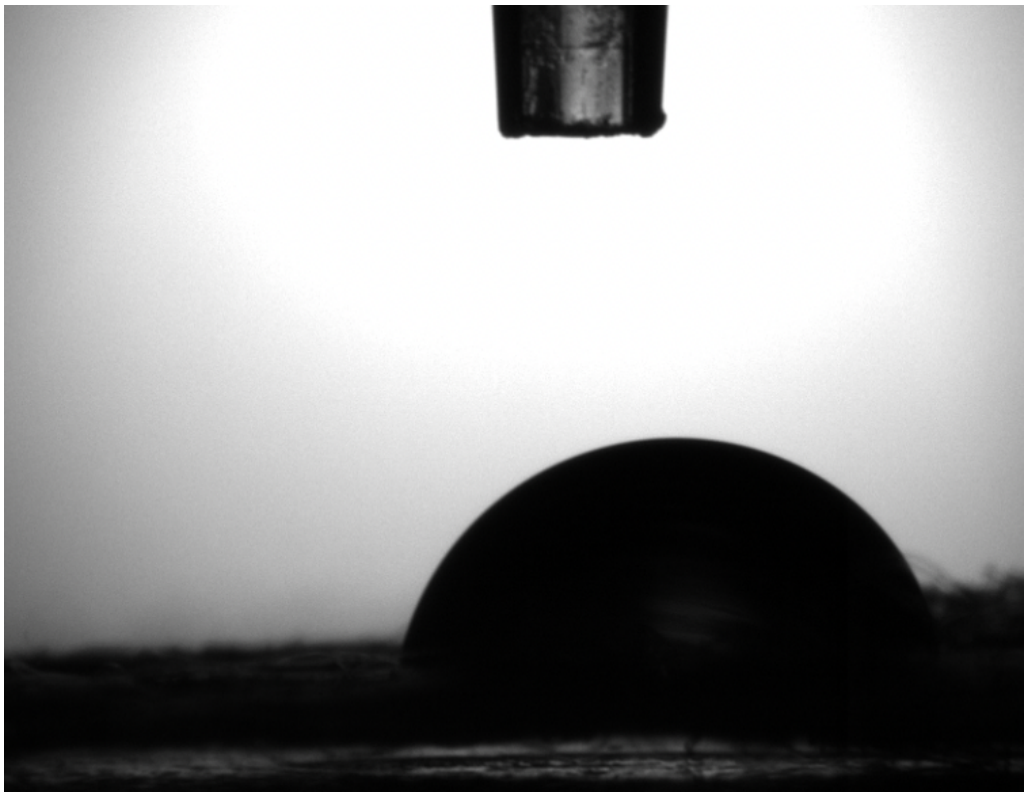

Figure 13.27. ACD 3 with a contact angle of 76.55 °

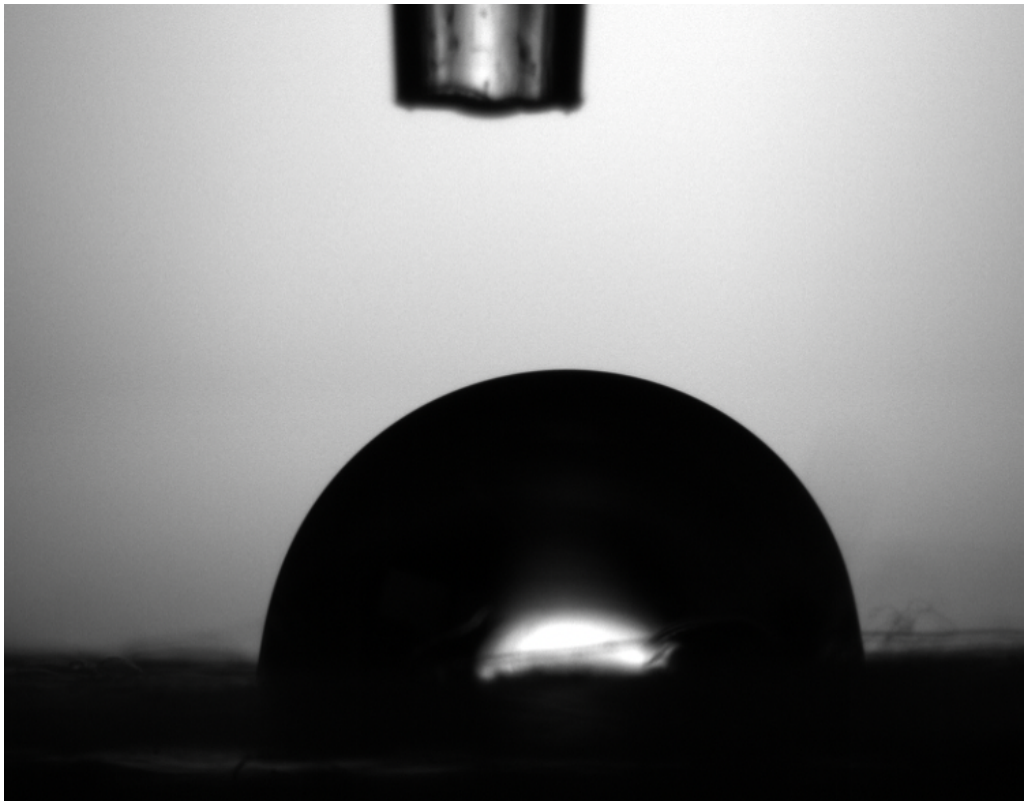

Figure 13.28. ACD 4 with a contact angle of 91.05 °

Figure 13.29. ACD 4 with a contact angle of 94.13 °

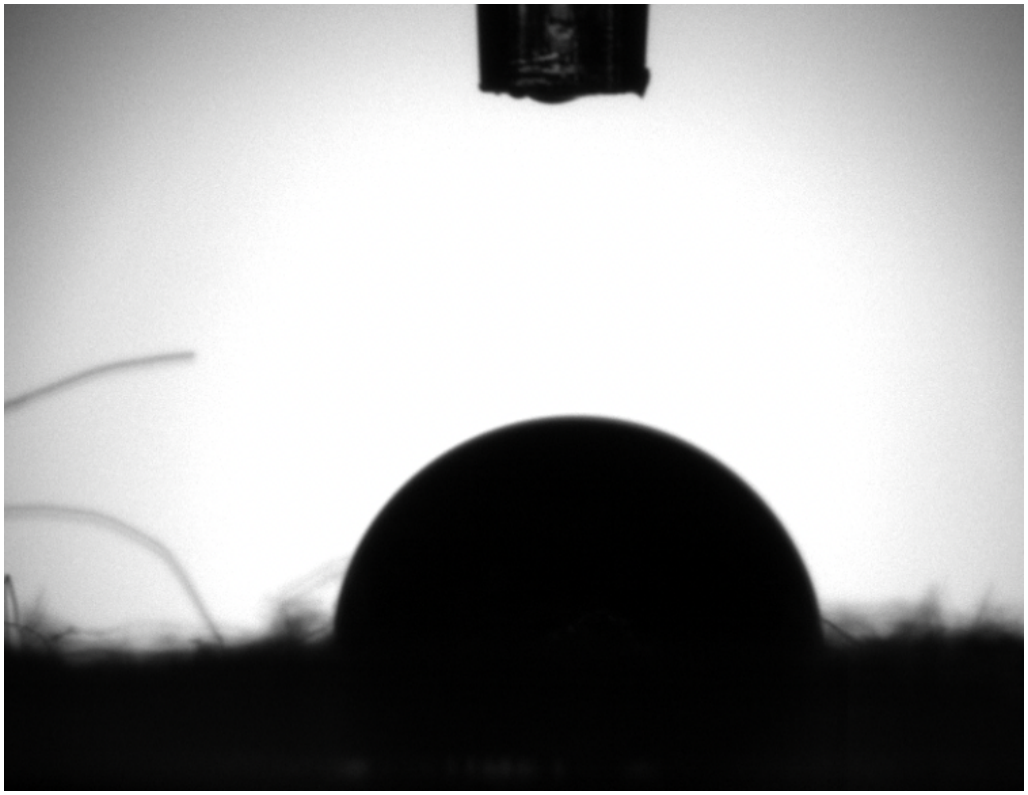

Figure 13.30. ACD 4 with a contact angle of 88.36 °

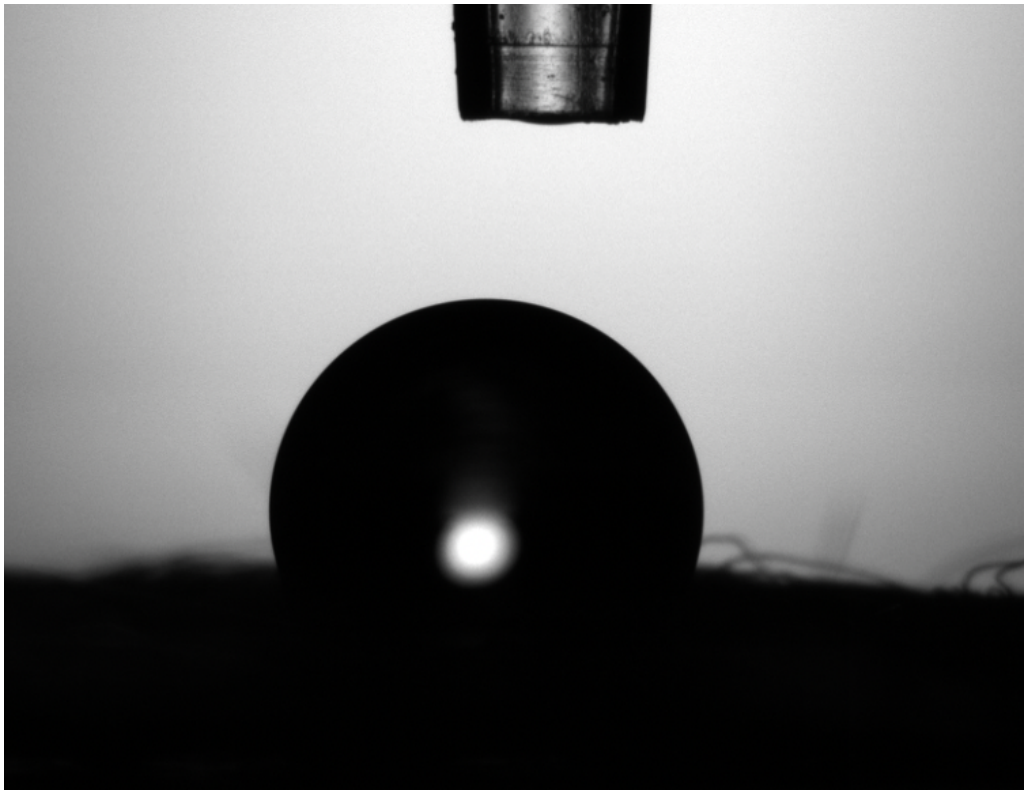

Figure 13.31. ACD 5 with a contact angle of 109.23 °

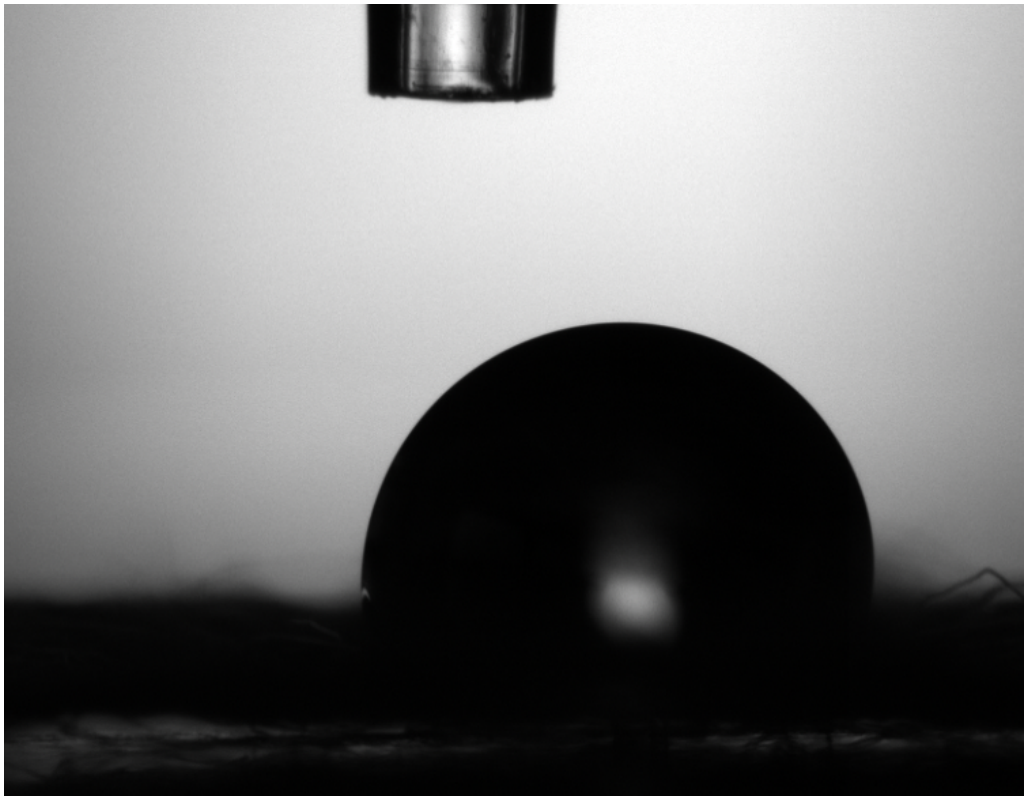

Figure 13.32. ACD 5 with a contact angle of 104.1 °

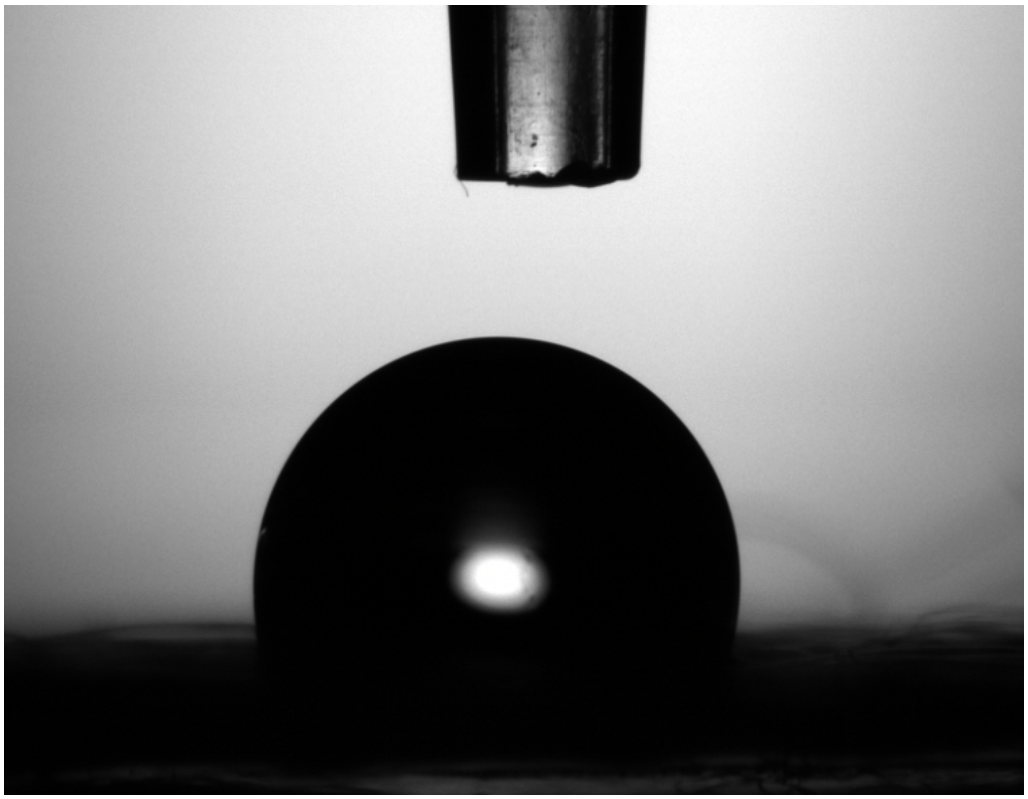

Figure 13.33. ACD 5 with a contact angle of 104.7 °

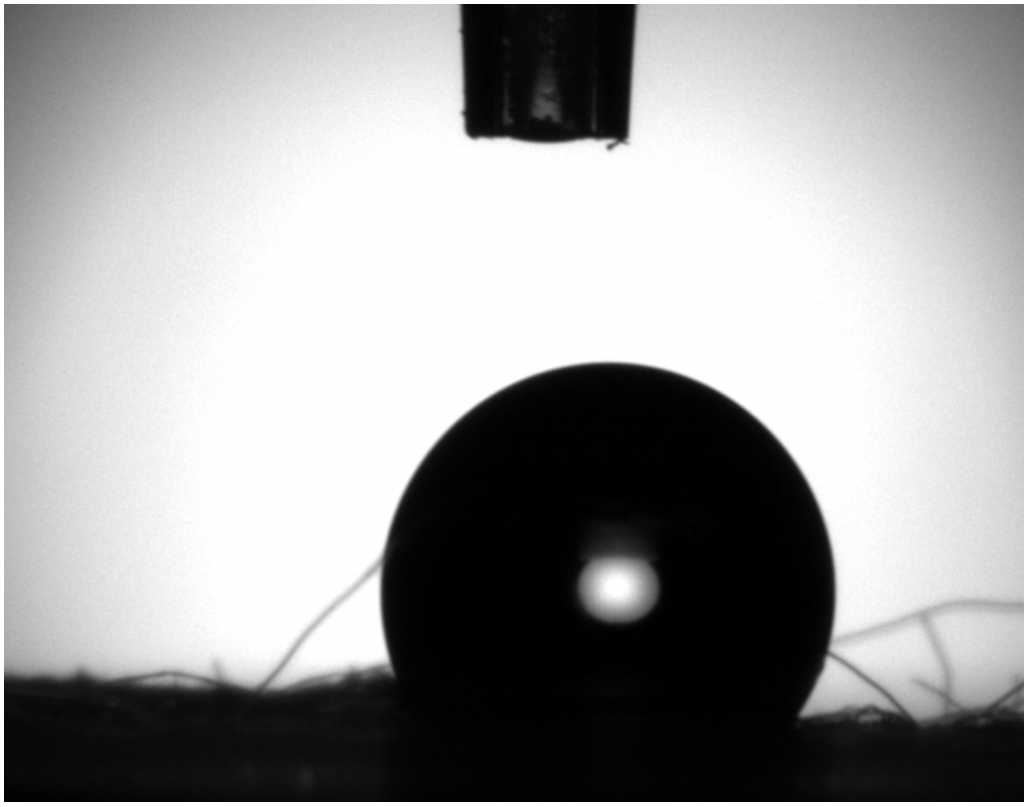

Figure 13.34. Reference with a contact angle of 120.91 °

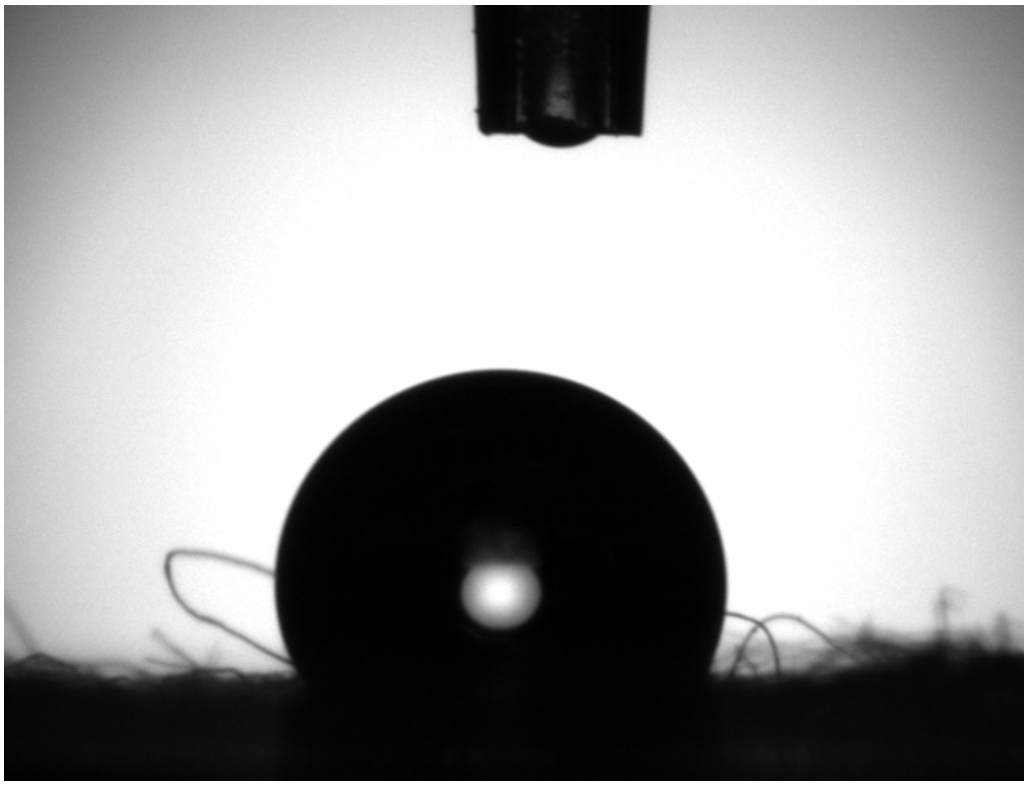

Figure 13.35. Reference with a contact angle of 115.25 °

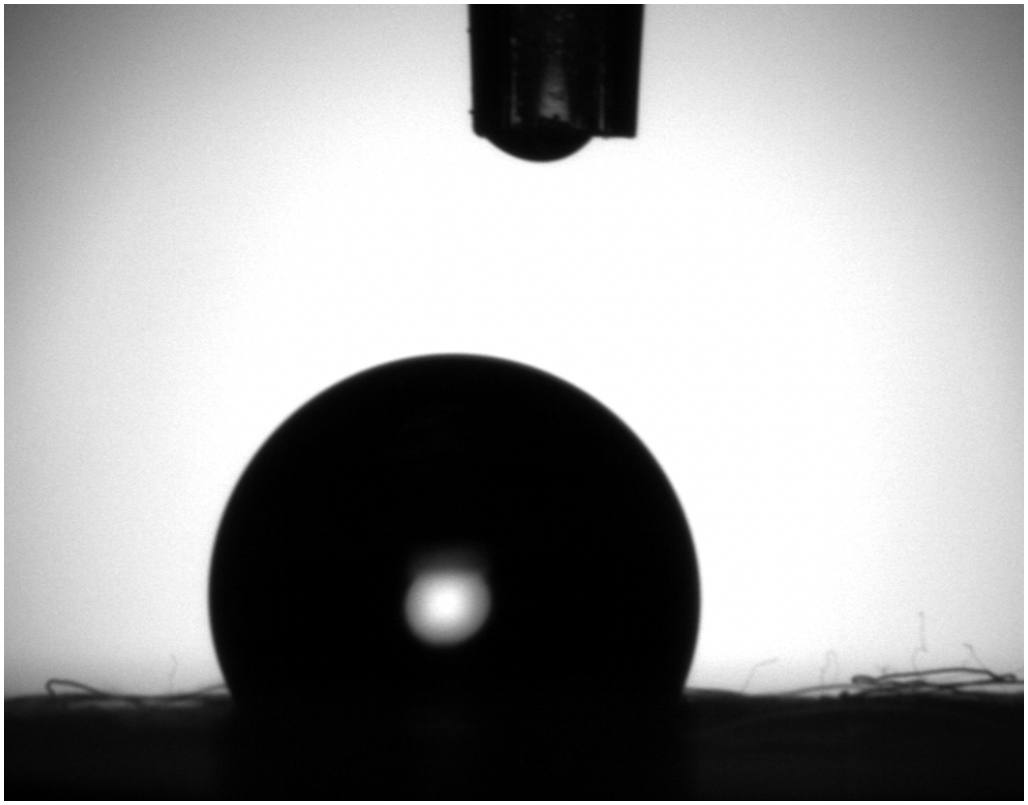

Figure 13.36. Reference with a contact angle of 117.79 °

13.3 PP coated at 20 g/m^2

Figure 13.37. ACD 1 with a contact angle of 51.3 °

Figure 13.38. ACD 1 with a contact angle of 50.28 °

Figure 13.39. ACD 2 with a contact angle of 50.1 °

Figure 13.40. ACD 2 with a contact angle of 48.39 °

Figure 13.41. ACD 3 with a contact angle of 78.88 °

Figure 13.42. ACD 3 with a contact angle of 64.66 °

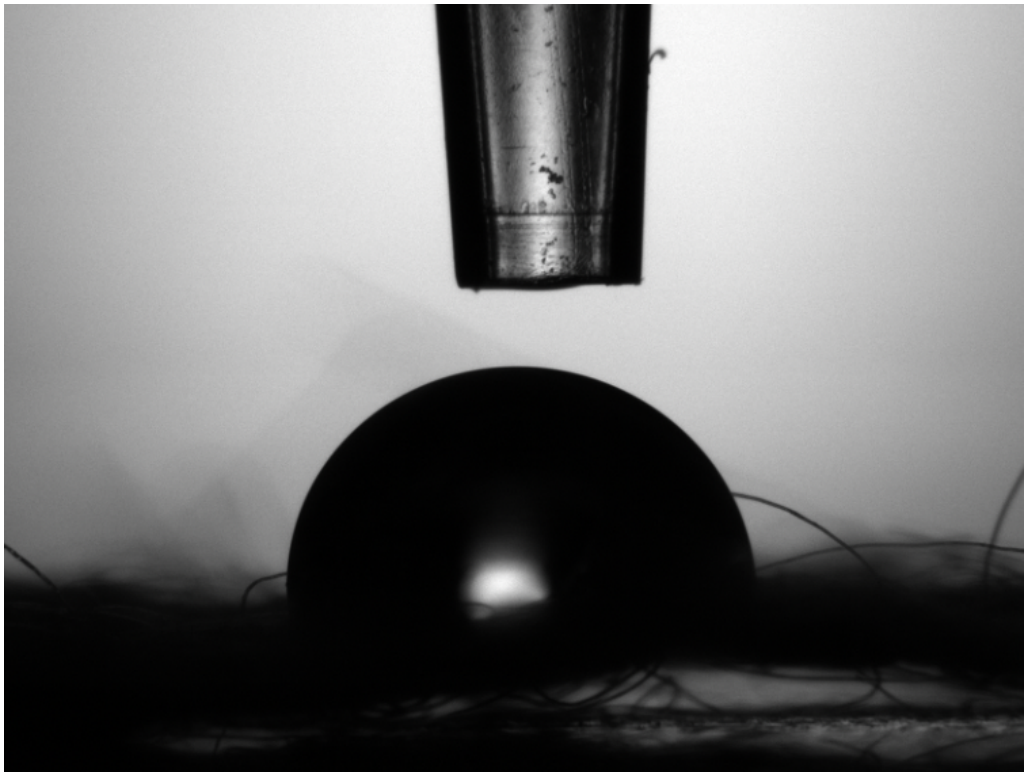

Figure 13.43. ACD 4 with a contact angle of 93.03 °

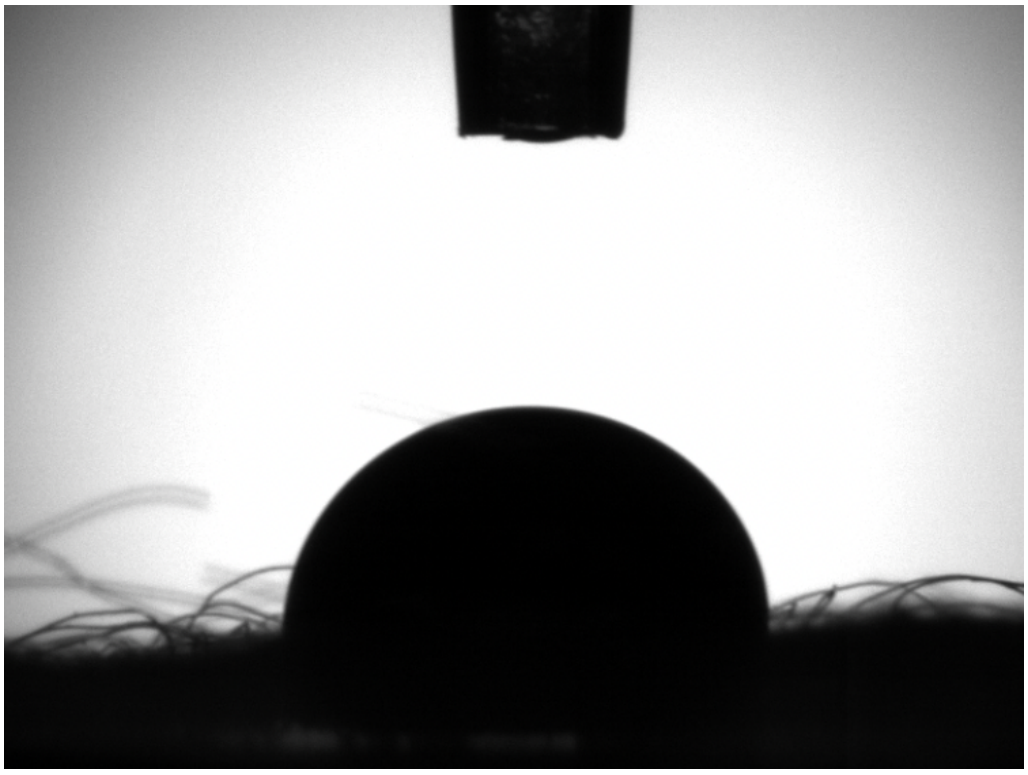

Figure 13.44. ACD 4 with a contact angle of 91.85 °

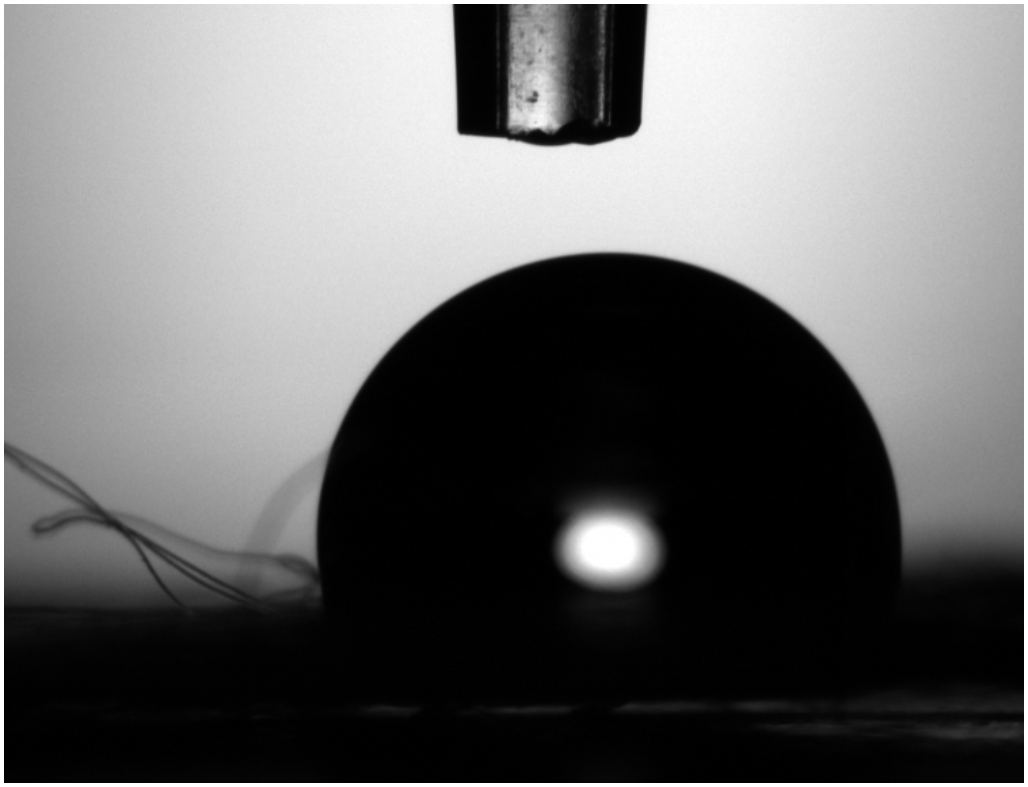

Figure 13.45. ACD 5 with a contact angle of 101.57 °

Figure 13.46. ACD 5 with a contact angle of 107.24 °

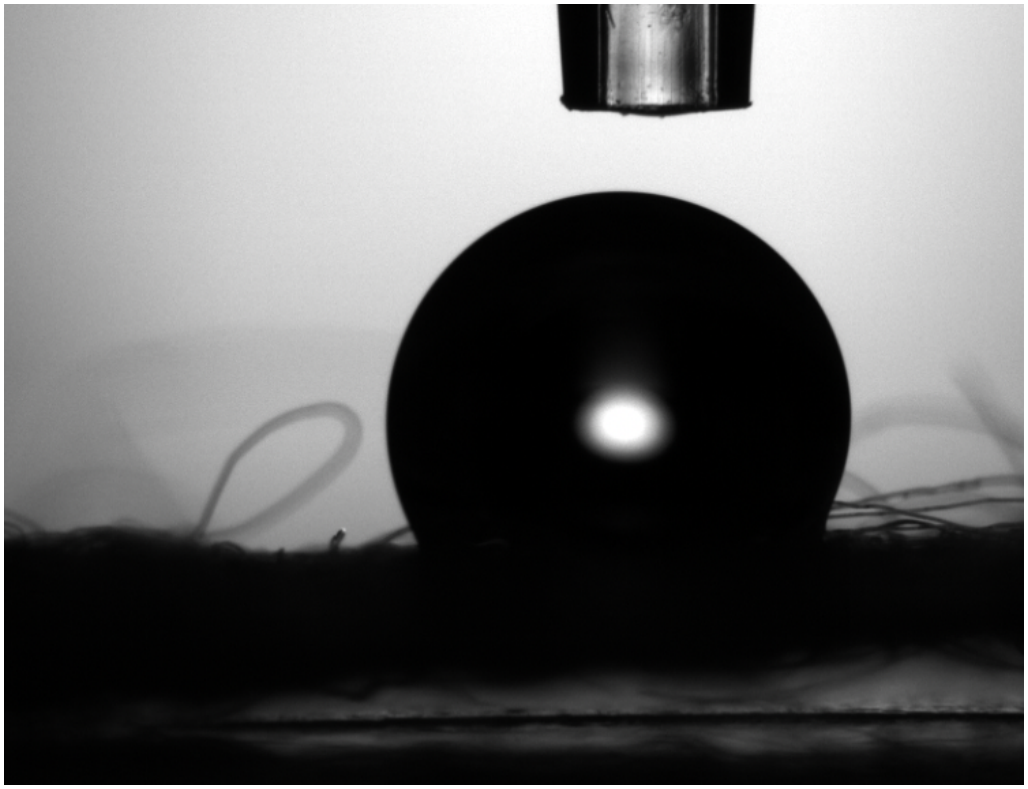

Figure 13.47. Reference with a contact angle of 122.96 °

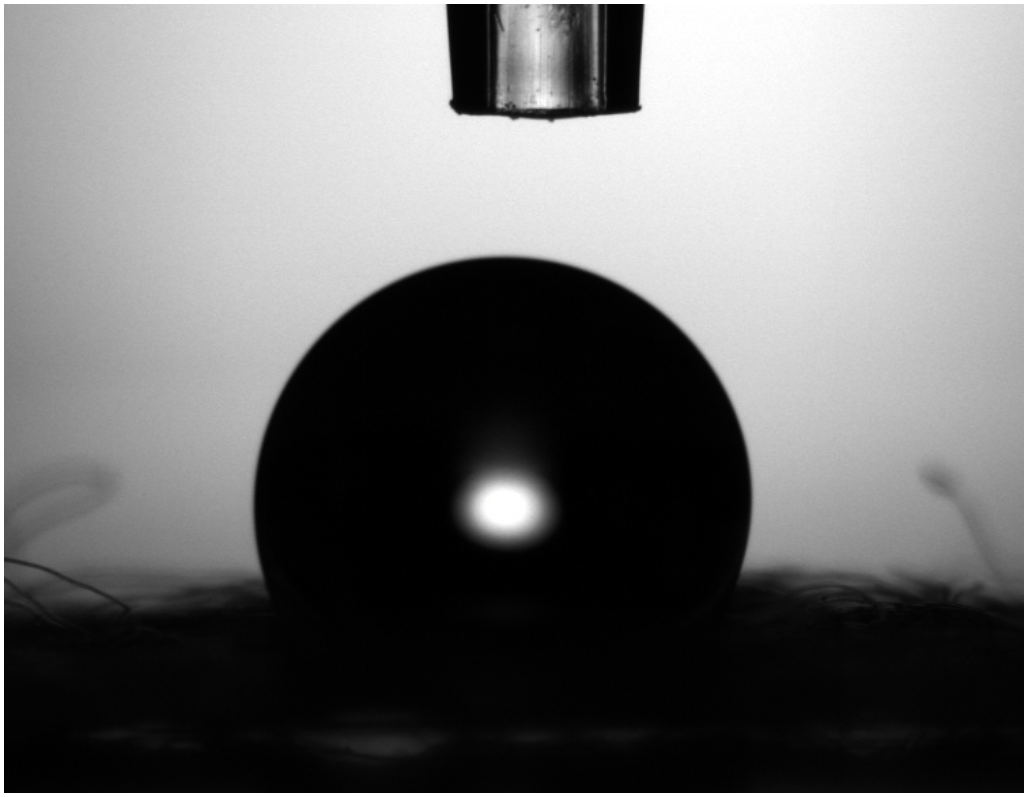

Figure 13.48. Reference with a contact angle of 121.4 °

ludeap

NMR and MS spectra of discarded ACDs. E/W ratios of ACDs containing salt and the detection test can also be seen

14

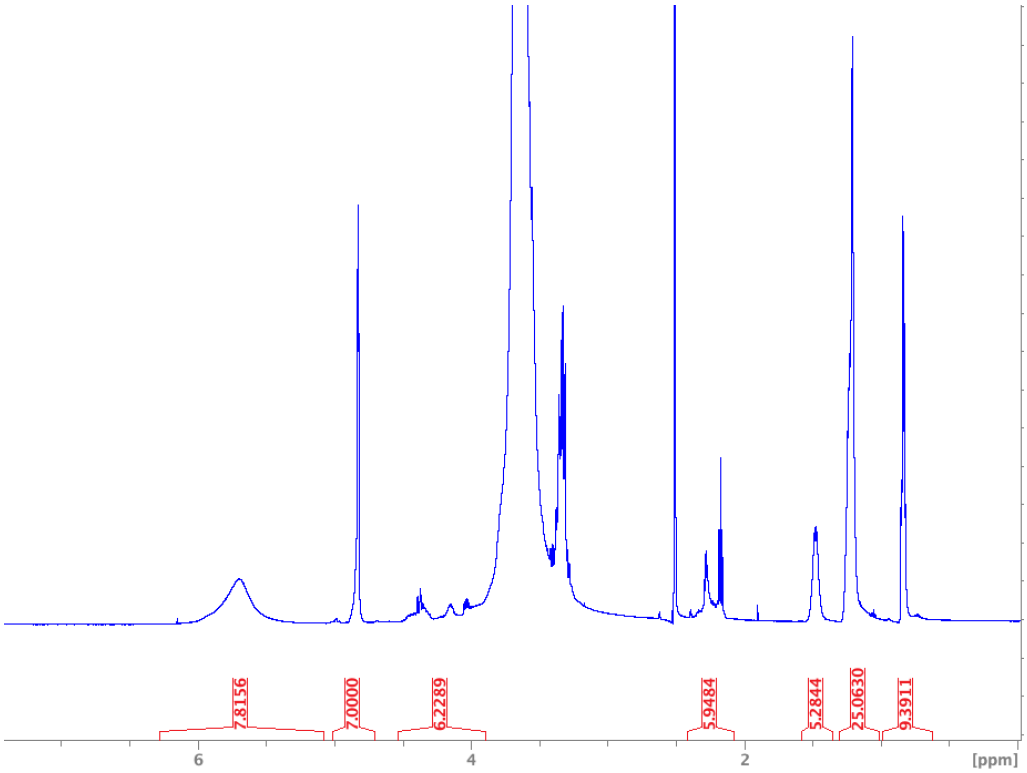

Figure 14.1. ^{1}H-NMR spectrum of an unused ACD

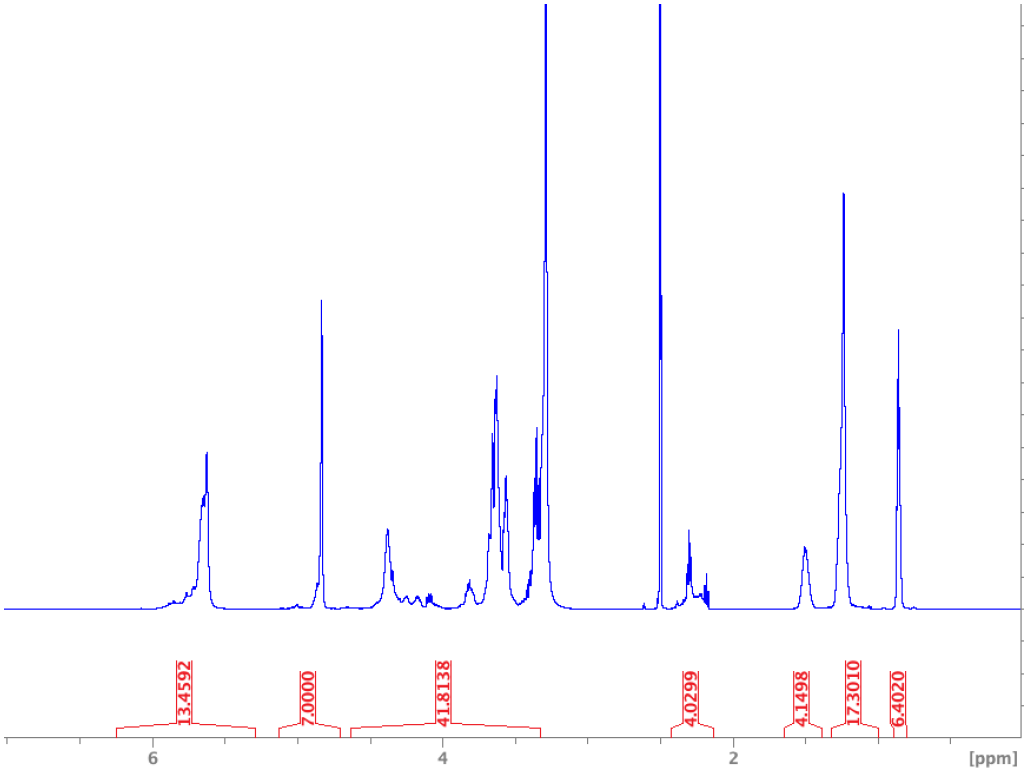

Figure 14.2. ^{1}H-NMR spectrum of an unused ACD

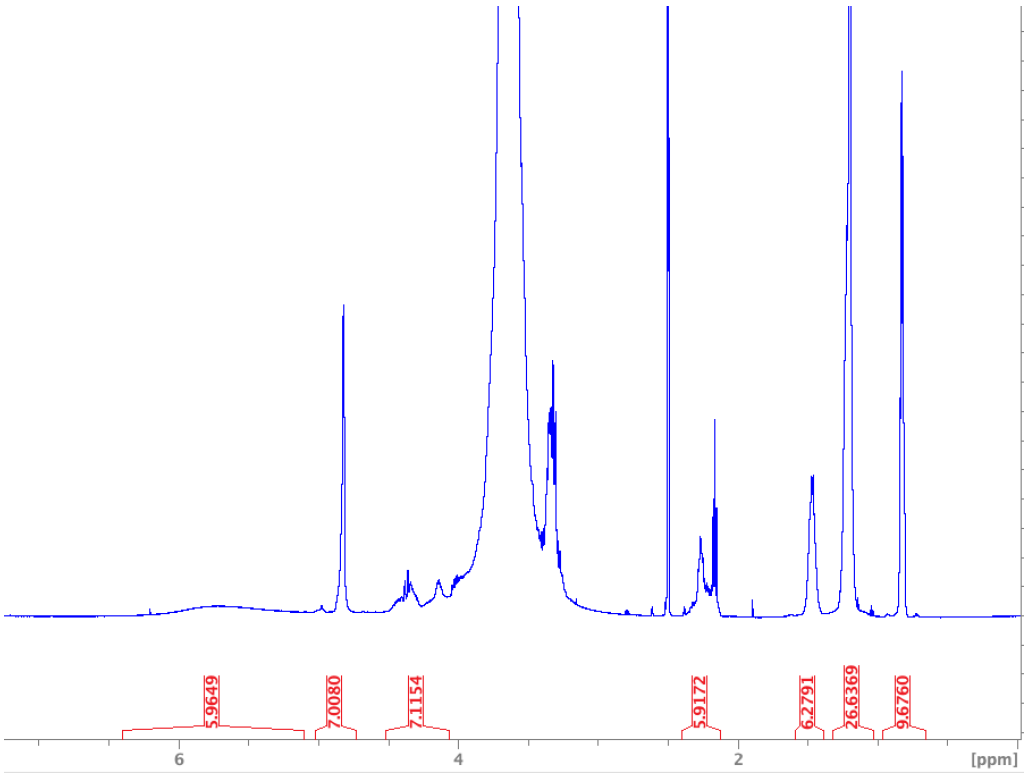

Figure 14.3. ^{1}H-NMR spectrum of an unused ACD

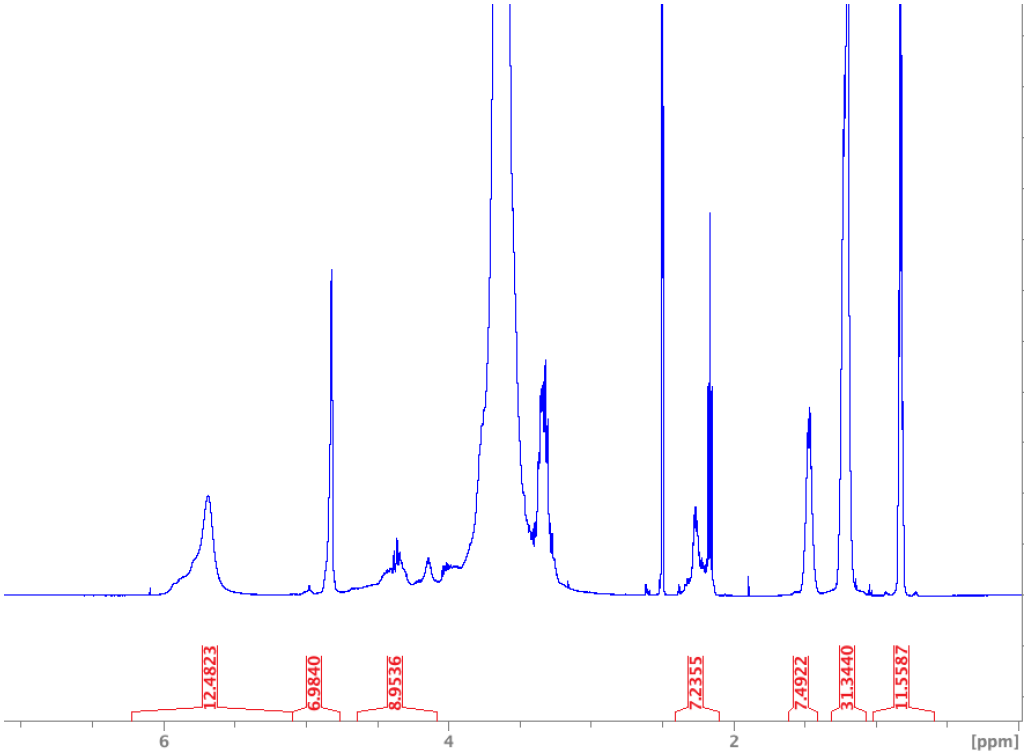

Figure 14.4. ^{1}H-NMR spectrum of an unused ACD

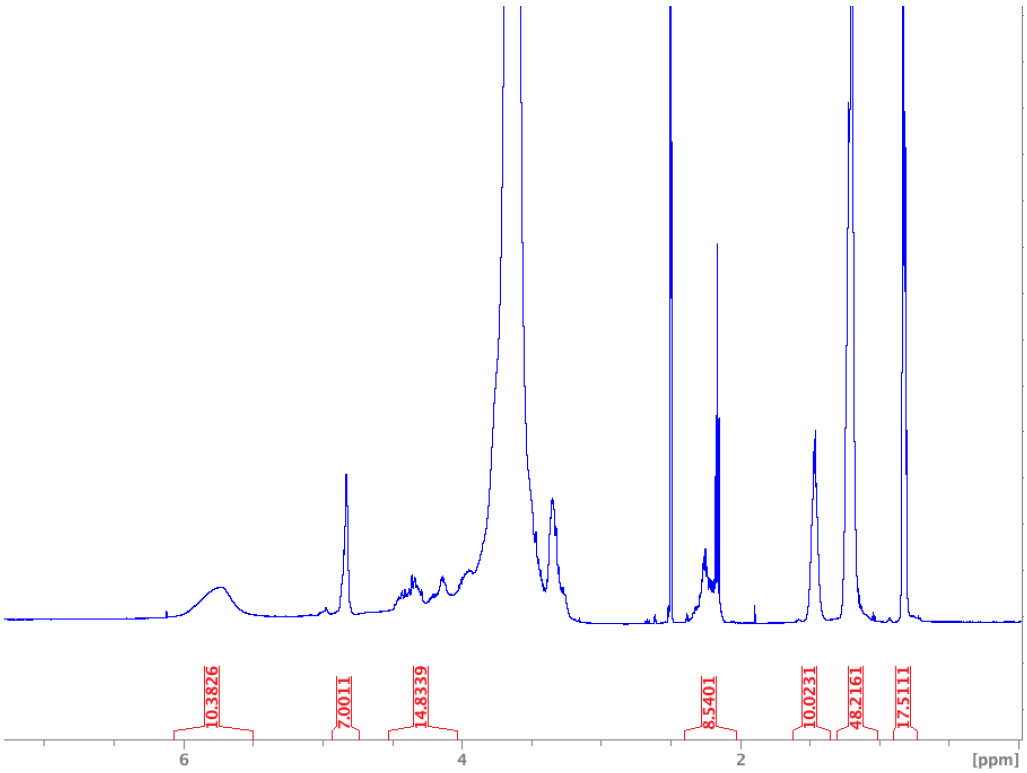

Figure 14.5. ^{1}H-NMR spectrum of an unused ACD

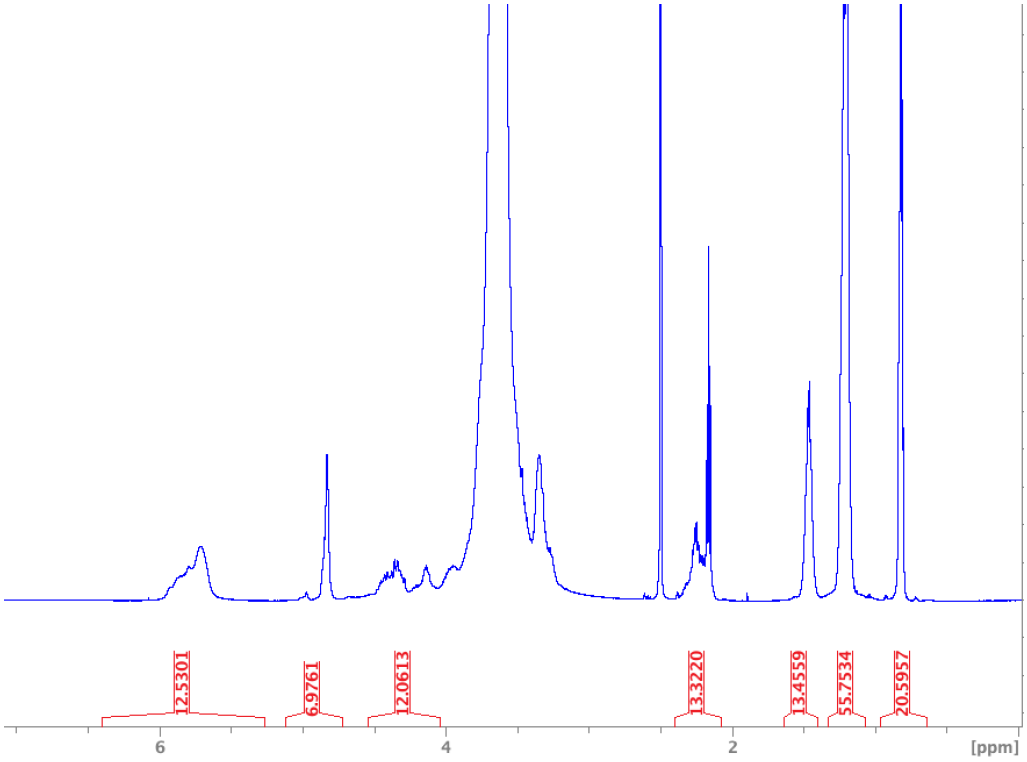

Figure 14.6. ^{1}H-NMR spectrum of an unused ACD

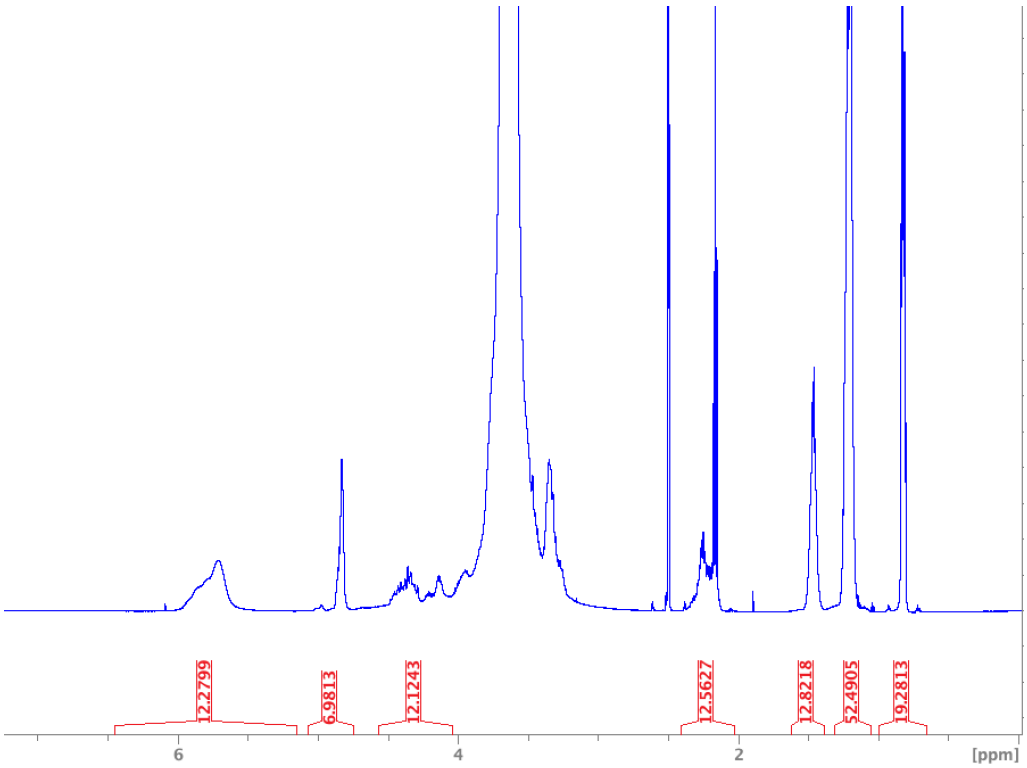

Figure 14.7. ^{1}H-NMR spectrum of an unused ACD

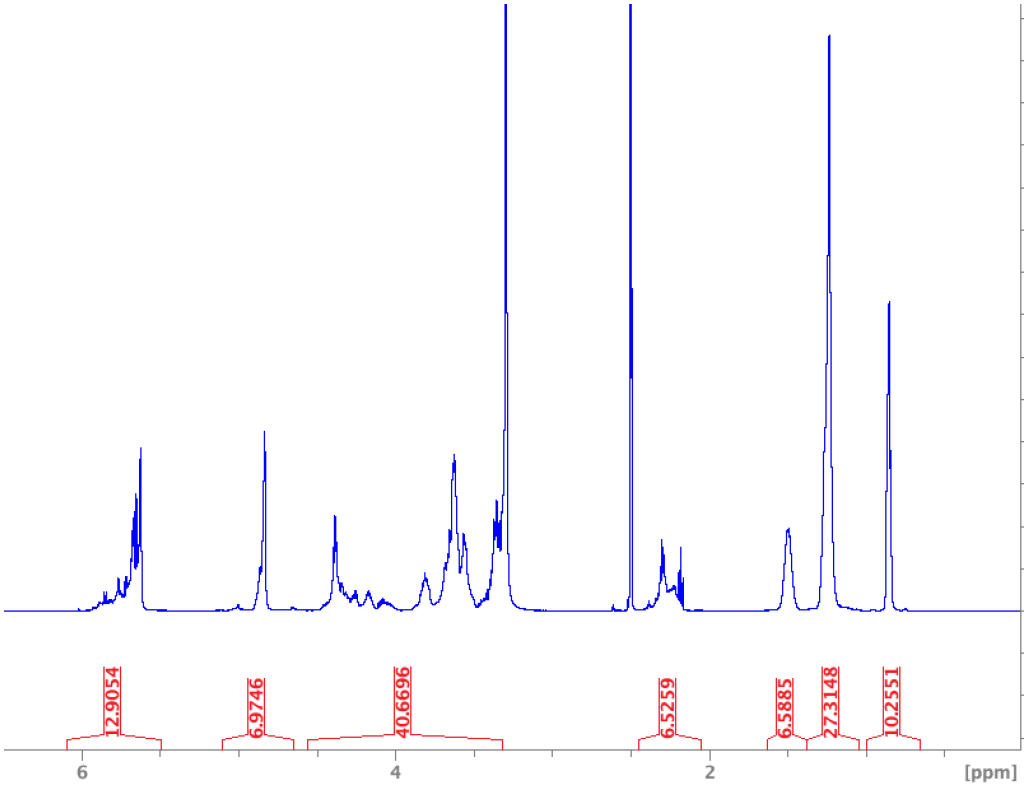

Figure 14.8. ^{1}H-NMR spectrum of an unused ACD

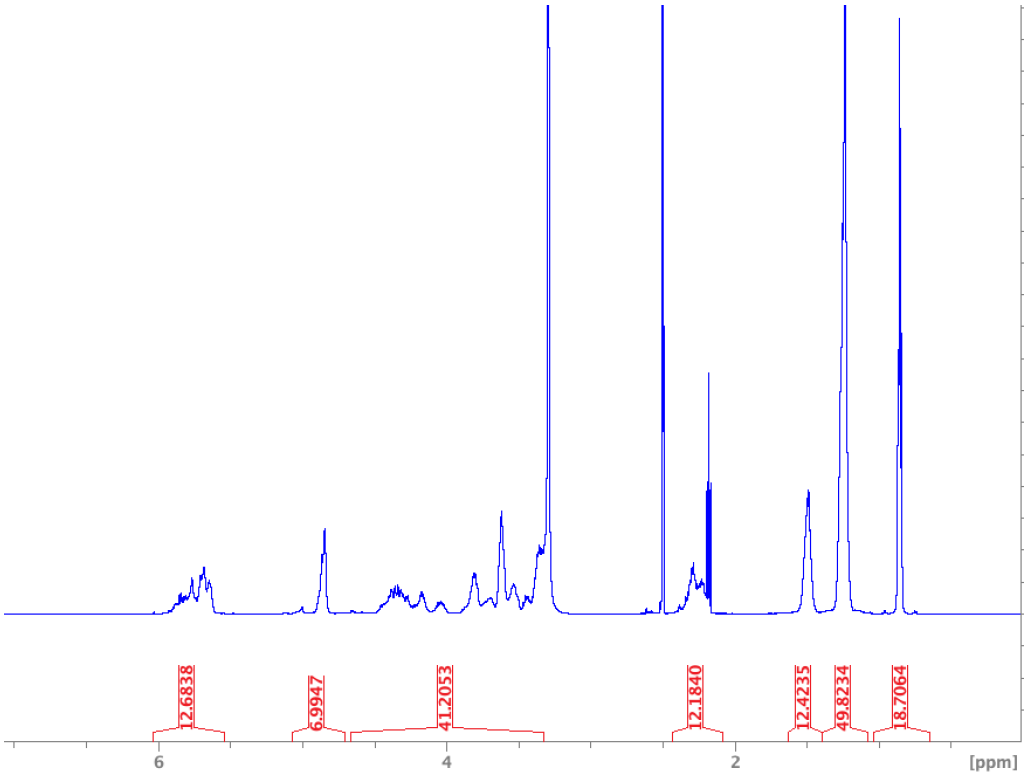

Figure 14.9. ^{1}H-NMR spectrum of an unused ACD

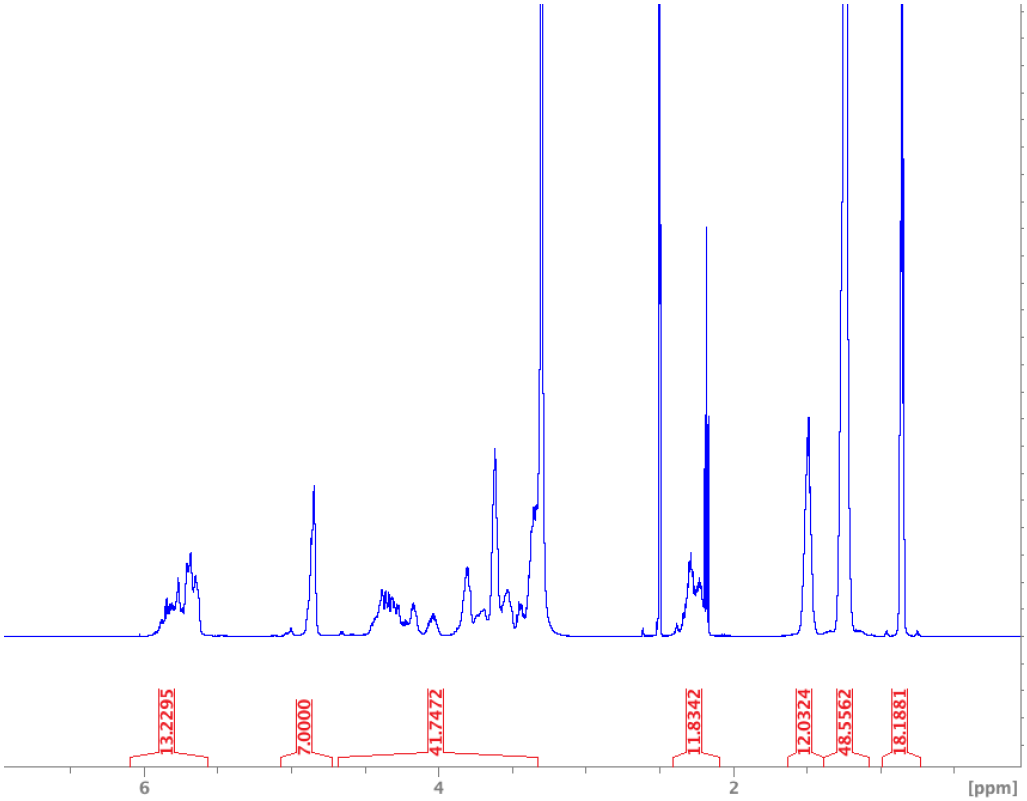

Figure 14.10. ^{1}H-NMR spectrum of an unused ACD

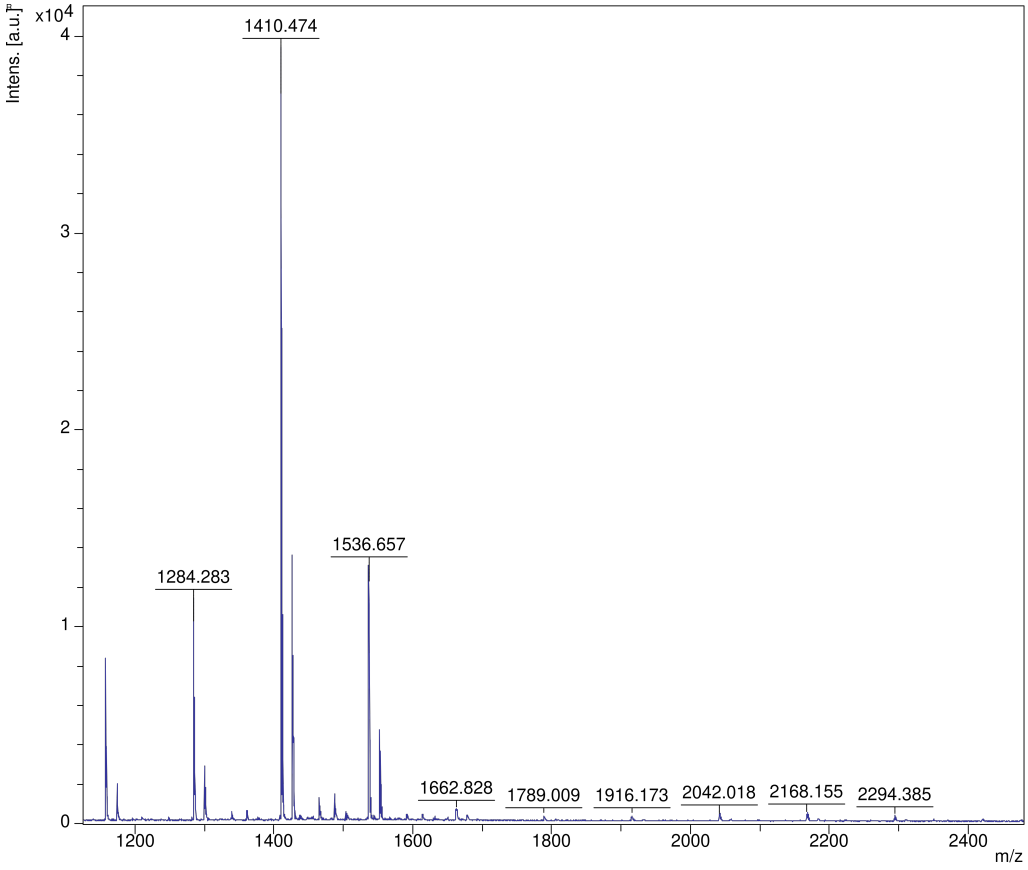

Figure 14.11. MS spectrum of an unused ACD

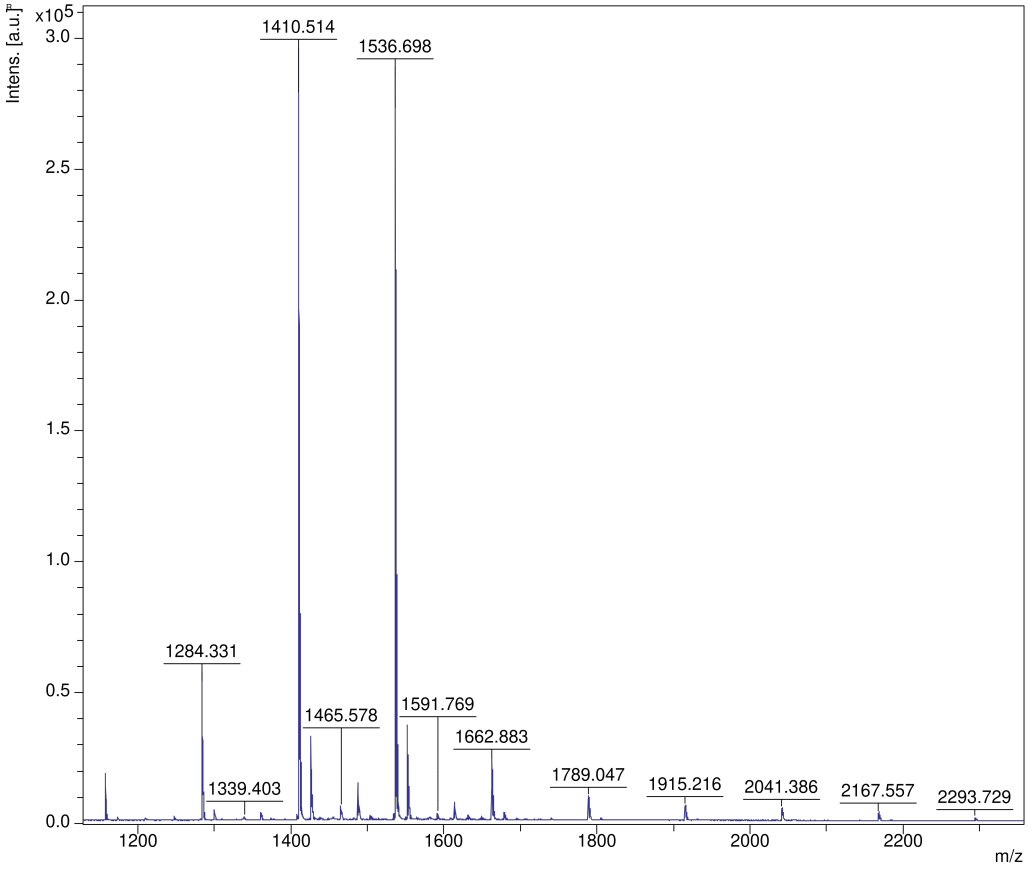

Figure 14.12. MS spectrum of an unused ACD

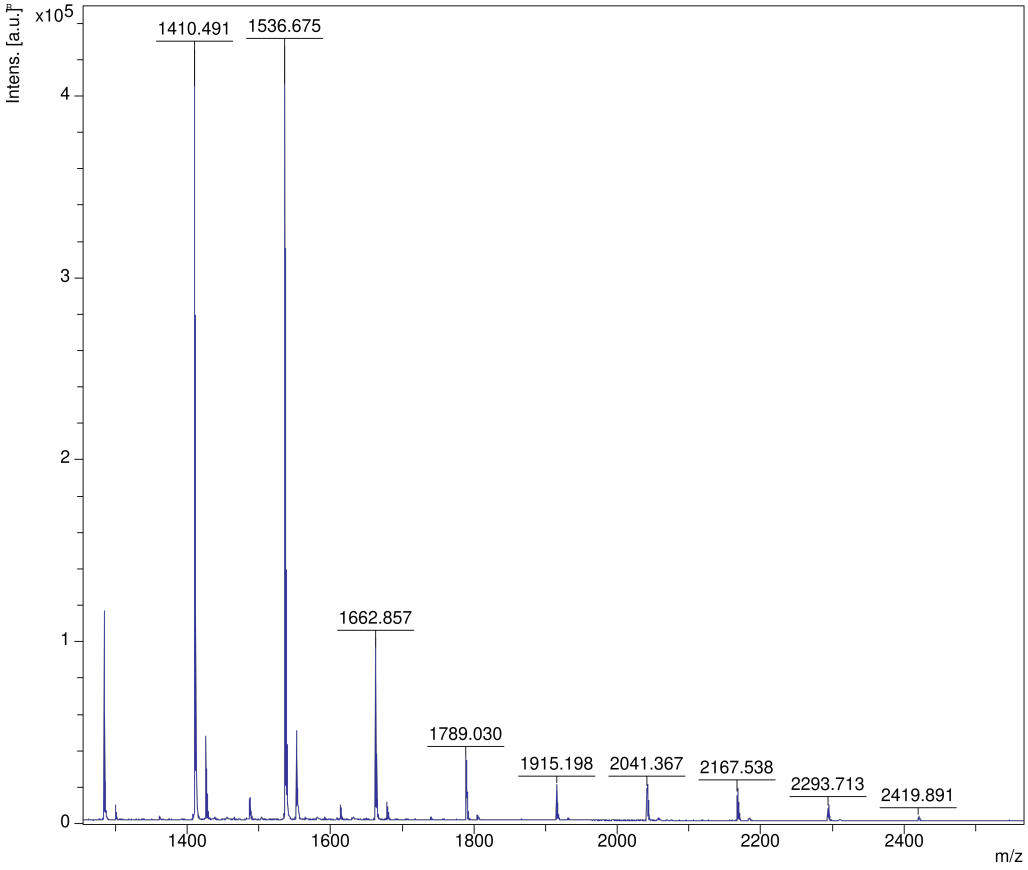

Figure 14.13. MS spectrum of an unused ACD

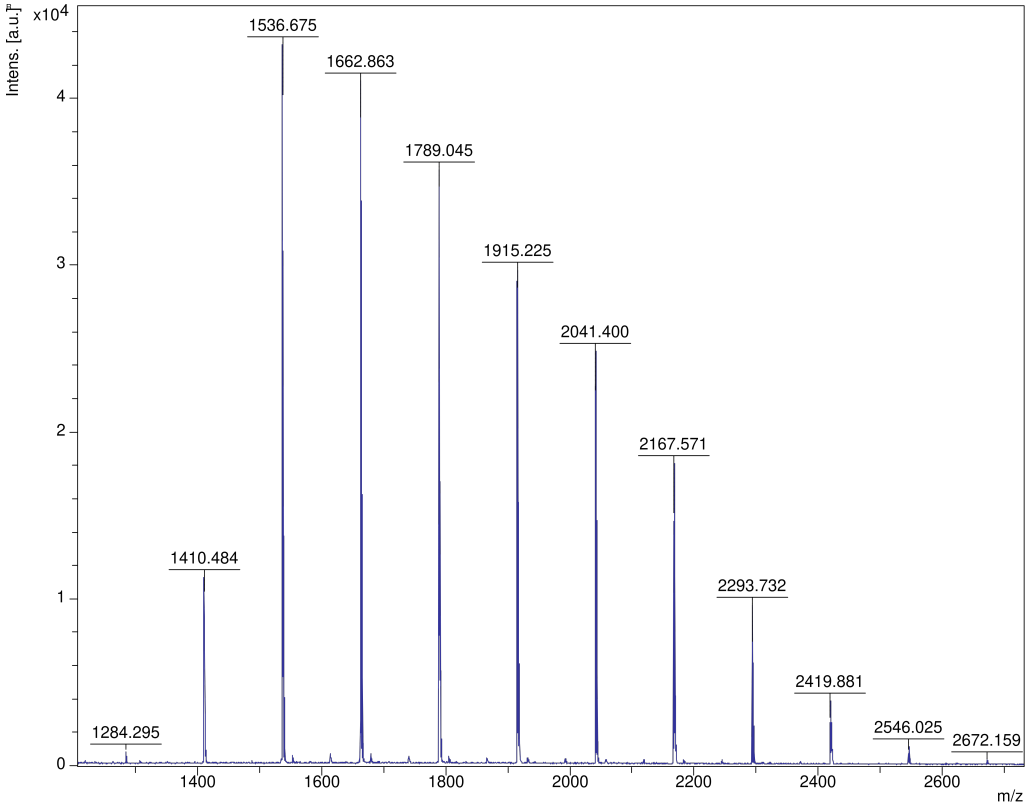

Figure 14.14. MS spectrum of an unused ACD

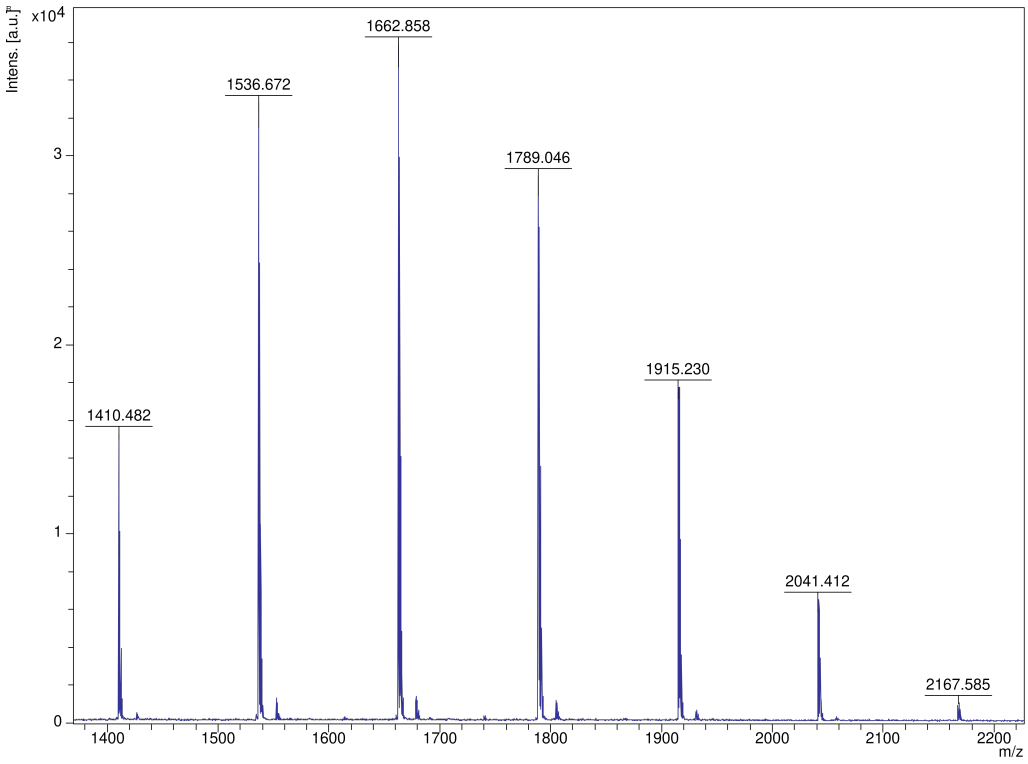

Figure 14.15. MS spectrum of an unused ACD

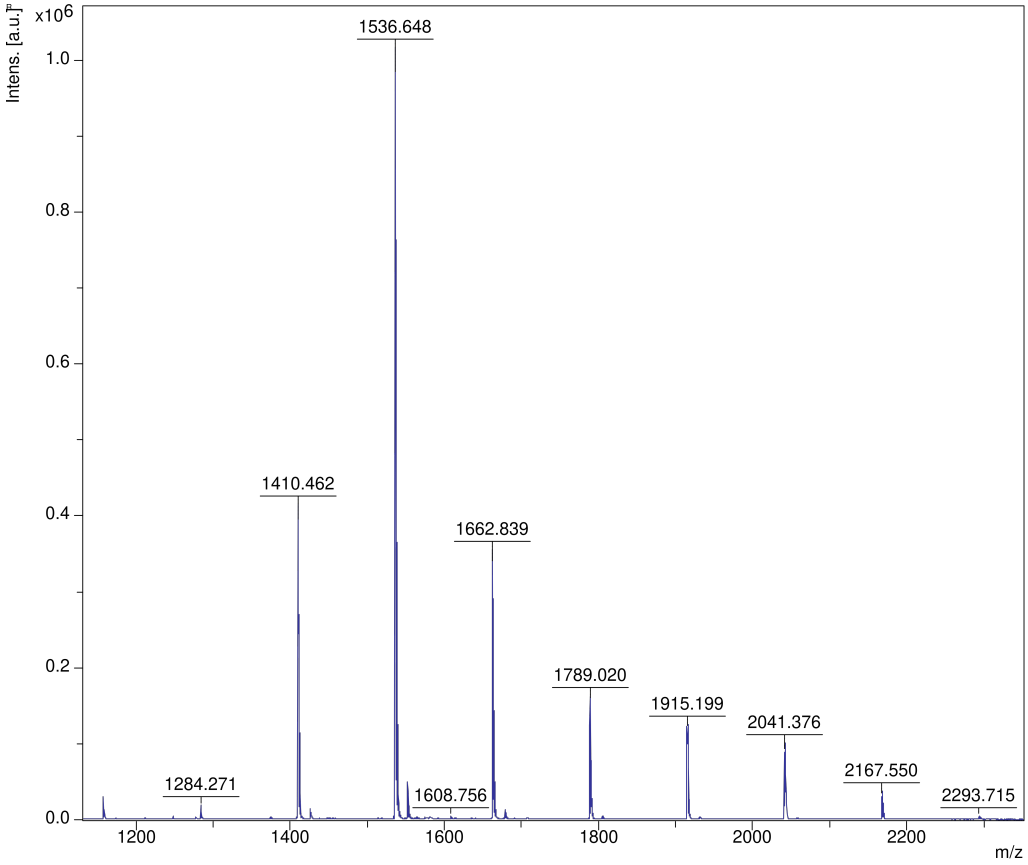

Figure 14.16. MS spectrum of an unused ACD

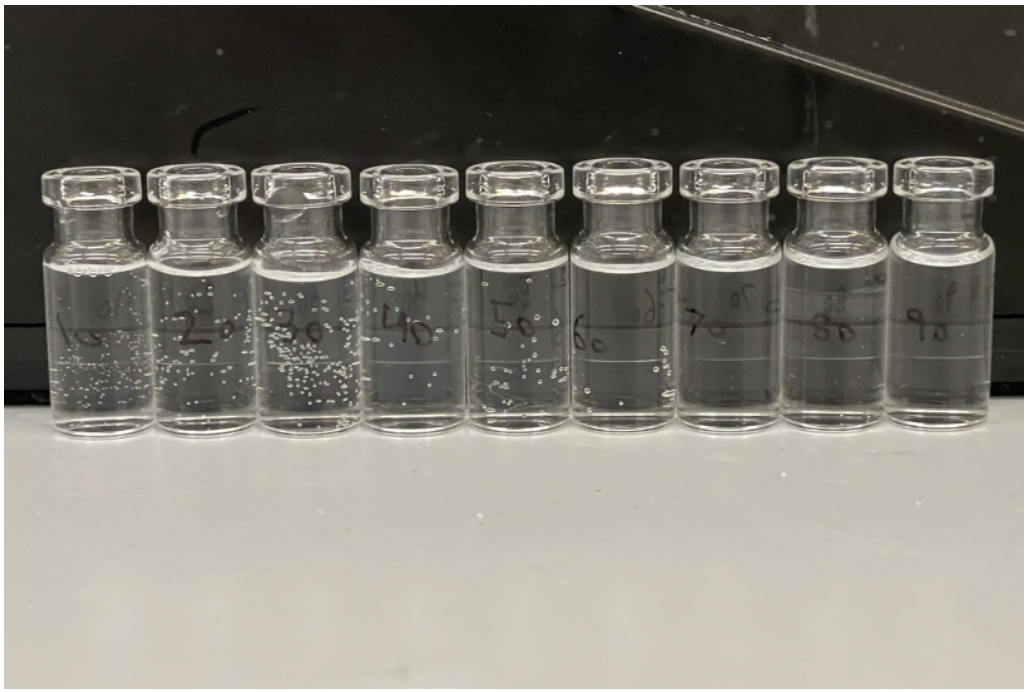

Figure 14.17. E/W ratios of unused an ACD containing salt

Figure 14.18. E/W ratios of unused an ACD containing salt

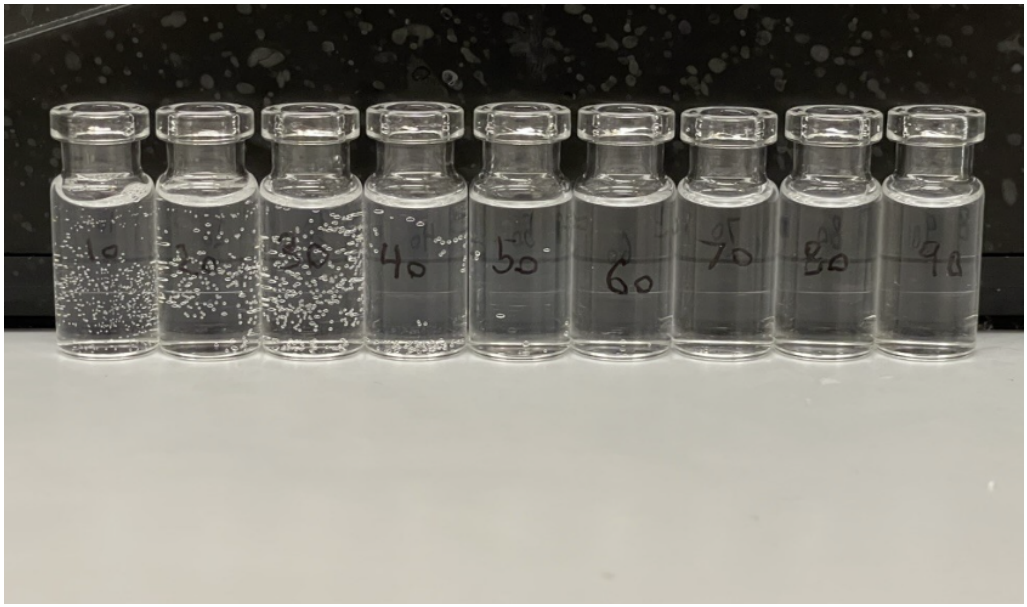

Figure 14.19. E/W ratios of unused an ACD containing salt

Figure 14.20. E/W ratios of unused an ACD containing salt

Figure 14.21. E/W ratios of unused an ACD containing salt

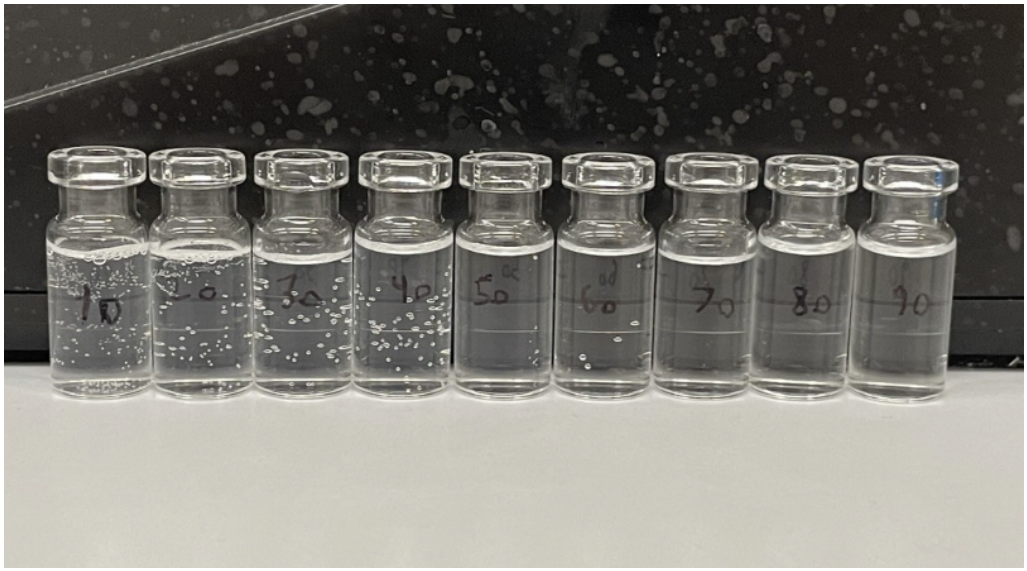

Figure 14.22. E/W ratios of unused an ACD containing salt

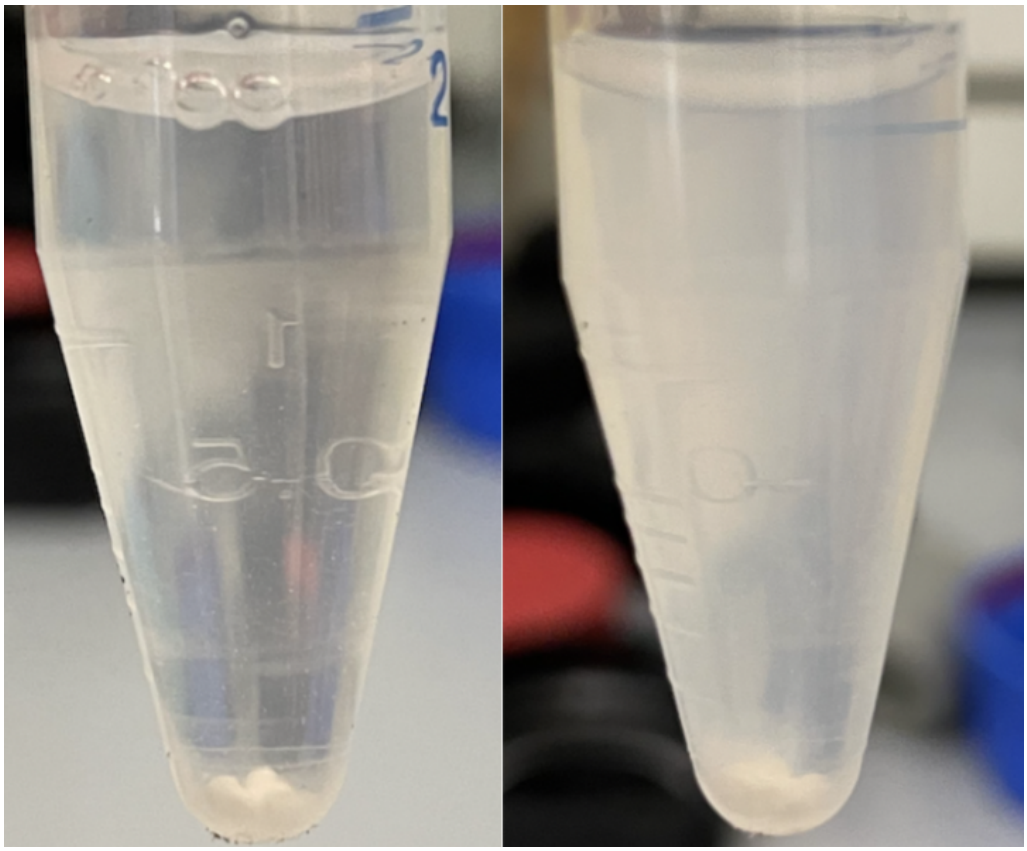

Figure 14.23. Before and after addition of Silver nitrate